Theses and Dissertations   1. Thesis and Dissertation Collection, all items

1985

Interaction of fronts with topography.

Zankofski, Deborah Ann.

Monterey, California. Naval Postgraduate School

http://hdl.handle.net/10945/21389

NAVAL POSTGRADUATE SCHOOL
Monterey, California

THESIS

INTERACTION OF FRONTS WITH TOPOGRAPHY

by

Deborah Ann Zankofski

June 1985

Thesis Advisor: R. T. Williams

REPORT DOCUMENTATION PAGE		READ INSTRUCTIONS BEFORE COMPLETING FORM
1. REPORT NUMBER	2. GOVT ACCESSION NO.	3. RECIPIENT'S CATALOG NUMBER
4. TITLE *(and Subtitle)* Interaction of Fronts with Topography		5. TYPE OF REPORT & PERIOD COVERED Master's Thesis June 1985
		6. PERFORMING ORG. REPORT NUMBER
7. AUTHOR*(s)* Deborah Ann Zankofski		8. CONTRACT OR GRANT NUMBER*(s)*
9. PERFORMING ORGANIZATION NAME AND ADDRESS Naval Postgraduate School Monterey, California 93943-5100		10. PROGRAM ELEMENT, PROJECT, TASK AREA & WORK UNIT NUMBERS
11. CONTROLLING OFFICE NAME AND ADDRESS Naval Postgraduate School Monterey, California 93943-5100		12. REPORT DATE June 1985
		13. NUMBER OF PAGES 95
14. MONITORING AGENCY NAME & ADDRESS*(if different from Controlling Office)*		15. SECURITY CLASS. *(of this report)* Unclassified
		15a. DECLASSIFICATION/DOWNGRADING SCHEDULE

16. DISTRIBUTION STATEMENT *(of this Report)*

Approved for public release; distribution is unlimited

17. DISTRIBUTION STATEMENT *(of the abstract entered in Block 20, if different from Report)*

18. SUPPLEMENTARY NOTES

19. KEY WORDS *(Continue on reverse side if necessary and identify by block number)*

Front; Mountain; Deformation; Frontogenesis; Model;
Boussinesq; Quasi-geostrophic; Finite Difference

20. ABSTRACT *(Continue on reverse side if necessary and identify by block number)*

This study examines the formation of a front over a mountain due to a pre-existing deformation field. The dependent variables are assumed to be independent of x. The hydrostatic Boussinesq equations are used with no diffusion of heat or momentum. A modified coordinate system similar to Phillips' sigma system is used. The model is bounded at the top by a rigid plane and periodic boundary conditions are used in the horizontal. The

#20 - ABSTRACT - (CONTINUED)

solutions show the formation of a front within a finite period of time that tilts toward the cold air. The frontogenesis experiments with a mountain of wavelength 3600 km showed negligible topographic effects.

Interaction of Fronts with Topography

by

Deborah Ann Zankofski
Lieutenant, United States Navy
B.S., John Carroll University, 1977
M.S., The Ohio State University, 1979

Submitted in partial fulfillment of the
requirement for the degree of

MASTER OF SCIENCE IN METEOROLOGY AND OCEANOGRAPHY

from the

NAVAL POSTGRADUATE SCHOOL
June 1985

ABSTRACT

This study examines the formation of a front over a
mountain due to a pre-existing deformation field. The
dependent variables are assumed to be independent of x. The
hydrostatic Boussinesq equations are used with no diffusion
of heat or momentum. A modified coordinate system similar
to Phillips' sigma system is used. The model is bounded at
the top by a rigid plane and periodic boundary conditions are
used in the horizontal. The solutions show the formation of
a front within a finite period of time that tilts toward the
cold air. The frontogenesis experiments with a mountain of
wavelength 3600 km showed negligible topographic effects.

TABLE OF CONTENTS

LIST OF FIGURES

8

LIST OF SYMBOLS

a	One-half total horizontal temperature variation
B	Mountain amplitude
c_p	Specific heat of air at constant temperature
D	Average depth of atmosphere
D_d	Deformation scale
f	Coriolis parameter
g	Acceleration due to gravity
H	θZ
$\hat{k}$	Vertically directed unit vector
L	Domain scale
M_x	uZ
M_y	vZ
p	Pressure
p_0	Reference pressure
R	Gas constant for dry air
t	Time
T	Temperature
U_d	Deformation component in x-direction
u	Velocity component in x-direction
V	Mean flow in the y-direction
V_d	Deformation component in y-direction
v	Velocity component in y-direction
$\vec{v}$	Horizontal wind vector
w	Vertical velocity component in the z-coordinate system

9

x, y	Space coordinates
z	Height above sea level
z_s	Height of lower surface above sea level
Z	Distance from the upper boundary to the lower boundary
θ_0	Constant reference potential temperature
θ	Departure of potential temperature from θ_0
θ_s	Mean θ as a function of z in the undisturbed atmosphere
ζ	$(z - z_s)/(D - z_s)$
$\dot{\zeta}$	Vertical velocity in the ζ-coordinate system
∇	Horizontal gradient operator
$\dfrac{\partial \theta_s}{\partial z}$	Constant lapse rate
Φ	$\theta_0 (c_p (\frac{p}{p_0})^\kappa - \pi_0)$
π_0	$- \dfrac{g}{\theta_0} z + c_p$
κ	$\dfrac{R}{c_p}$
α	$\dfrac{L}{f}(\dfrac{g}{\theta_0} \dfrac{\partial \theta_s}{\partial z})^{1/2}$

ACKNOWLEDGEMENTS

I. INTRODUCTION

Williams and Plotkin (1968) have shown that atmospheric frontogenesis occurs for large time limits using the quasi-geostrophic equation. Their results are unrealistic in the respect that the frontal zone does not tilt with height. A comparison of the linear and nonlinear hydrostatic primitive equations by Williams (1972) shows that the linear solutions are close to the solutions of the quasi-geostrophic equations. The nonlinear solutions are more realistic and show the formation of frontal discontinuities in a finite period of time. Hoskins and Bretherton (1972) showed that dynamic processes in addition to horizontal deformation can produce a front. Bannon (1983) and (1984) investigated quasi-geostrophic and semi-geostrophic frontogenesis over topography. Monotonically sloping topography beneath a deformation leads to the formation of a surface discontinuity in the absence of an initial horizontal thermal gradient. A front associated with a translating deformation field over an isolated orographic feature is affected by the topographically forced divergence field as the front passes over the moutnain. Convergence will increase frontogenesis and divergence will decrease it.

The purpose of this study is to investigate the effect of topography on a front which arises from deformation. Periodic boundary conditions are introduced because they

simplify the mountain flow simulation. The deformation is independent of height. The Boussinesq equations are used in which the dependent variables are independent of x. A coordinate system similar to that of Phillips (1957) is used. The equations are solved numerically and output is shown in the form of vertical cross-sections in the y-ζ plane.

II. BASIC EQUATIONS

The basic equations used in this study are the Boussinesq equations which neglect the compressibility of the atmosphere. The hydrostatic approximation is made and heating and friction are neglected. These equations will be applied to a model in which the flow is bounded above by a rigid horizontal plane.

The Boussinesq equations [Ogura and Phillips, 1962] may be expressed in the z-coordinate system as

$$\frac{\partial \vec{v}}{\partial t} + \vec{v} \cdot \nabla \vec{v} + w \frac{\partial \vec{v}}{\partial z} = -\nabla \phi - f \hat{k} \times \vec{v} , \tag{1}$$

$$\frac{\partial \theta}{\partial t} + \vec{v} \cdot \nabla \theta + w \frac{\partial \theta}{\partial z} = 0 , \tag{2}$$

$$\frac{\partial \phi}{\partial z} = \frac{g}{\theta_0} \theta , \tag{3}$$

$$\nabla \cdot \vec{v} + \frac{\partial w}{\partial z} = 0 , \tag{4}$$

where

$$\theta = T(\frac{p}{p_0})^{\kappa} - \theta_0 , \tag{5}$$

$$\phi = \theta_0 [c_p (\frac{p}{p_0})^{\kappa} - \pi_0] , \tag{6}$$

and

14

$$\pi_0 = -\frac{g}{\theta_0} z + c_p . \tag{7}$$

In this model, the Coriolis parameter is constant, and the only quantity which varies with longitude is Φ.

To simplify the finite differencing of the equations, a modified coordinate system is introduced in which the lower boundary surface becomes a coordinate surface. This system permits the application of the lower boundary condition at the surface of the mountain. The coordinate system is similar to the sigma system introduced by Phillips (1957).

Following Walton (1968) and DeBoer (1970), the vertical coordinate, zeta, is defined as

$$\zeta = \frac{z - z_s}{Z} , \tag{8}$$

where D and z_s are defined in Fig. 1 and $Z = D - z_s$. With these definitions, $\zeta = 0$ at the lower boundary and $\zeta = 1$ at the upper boundary.

Transformation of equations (1) through (4) from the z-coordinate system into the ζ-coordinate system yields

$$\frac{\partial \vec{v}}{\partial t} + \vec{v} \cdot \nabla \vec{v} + \dot{\zeta} \frac{\partial \vec{v}}{\partial \zeta} = -\nabla \Phi - \frac{\partial \Phi}{\partial \zeta} (\frac{\zeta - 1}{Z}) \nabla_h z_s - f \hat{k} \times \vec{v} , \tag{9}$$

$$\frac{\partial \theta}{\partial t} + \vec{v} \cdot \nabla \theta + \dot{\zeta} \frac{\partial \theta}{\partial \zeta} = 0 , \tag{10}$$

$$\frac{\partial \Phi}{\partial \zeta} = \frac{g}{\theta_0} Z \theta , \tag{11}$$

15
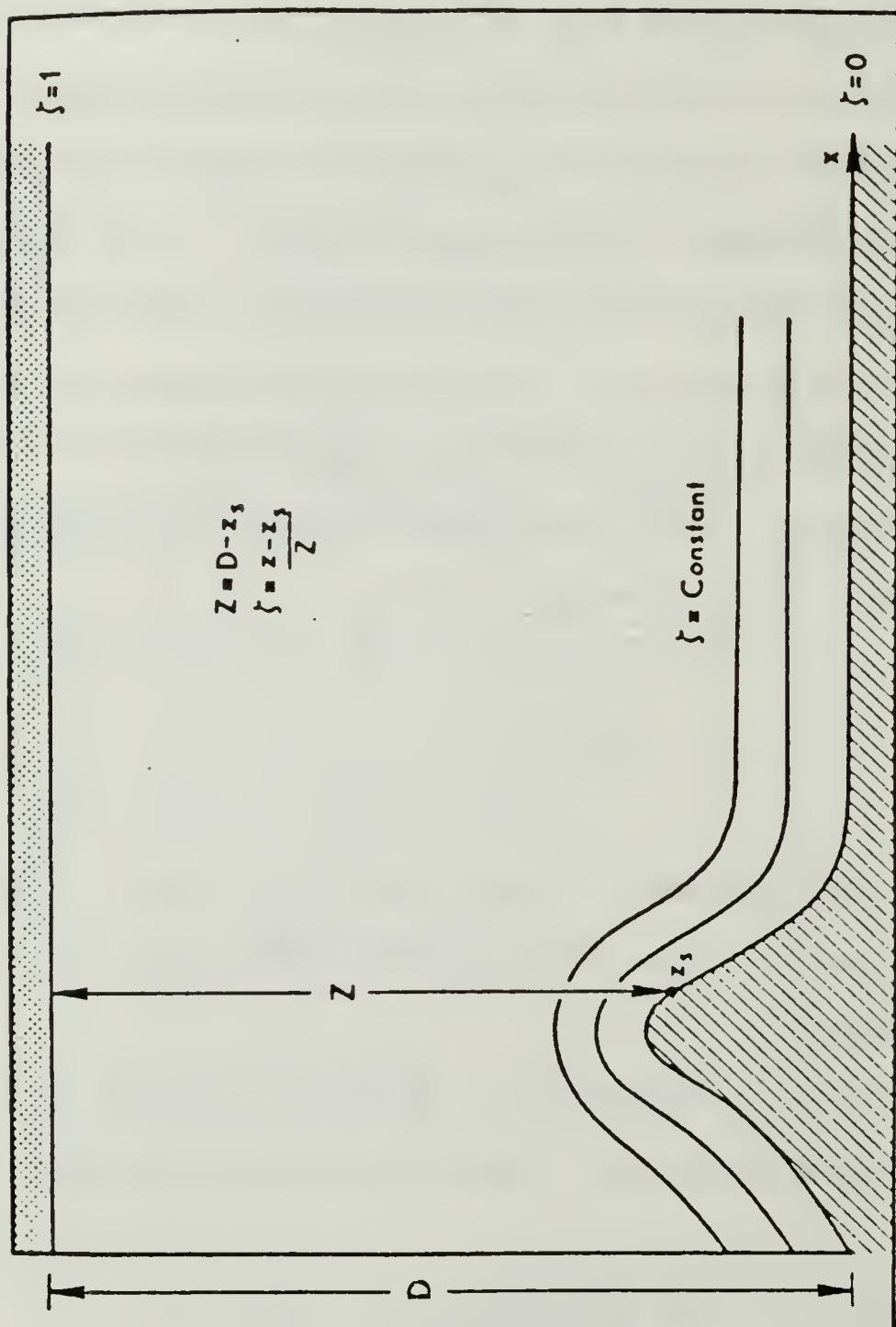
Fig. 1. Schematic diagram of the zeta-coordinate system

$$\nabla \cdot (Z\vec{v}) + Z \frac{\partial \dot{\zeta}}{\partial \zeta} = 0 \; . \tag{12}$$

In equations (9) through (12), ∇ is the horizontal gradient operator on zeta surfaces.

It is desirable to put the equations in flux form in order to satisfy certain computational properties. Equations (9) through (12) become

$$\frac{\partial (M_x)}{\partial t} + \frac{\partial}{\partial y}(M_y u) + \frac{\partial}{\partial \zeta}(\dot{\zeta} u Z) = -Z \frac{\partial \Phi}{\partial x} + f M_y \; , \tag{13}$$

$$\frac{\partial (M_y)}{\partial t} + \frac{\partial}{\partial y}(M_y v) + \frac{\partial}{\partial \zeta}(\dot{\zeta} v Z) = -Z \frac{\partial \Phi}{\partial y} + \frac{g}{\theta_0} Z \theta (\zeta-1) \cdot \frac{\partial Z}{\partial y} - F M_x \; , \tag{14}$$

$$\frac{\partial H}{\partial t} + \frac{\partial}{\partial y}(M_y \theta) + \frac{\partial}{\partial \zeta}(\dot{\zeta} \theta Z) = 0 \; , \tag{15}$$

$$\frac{\partial \Phi}{\partial \zeta} = \frac{g}{\theta_0} Z \theta \; , \tag{16}$$

$$\frac{\partial M_y}{\partial y} + Z \frac{\partial \dot{\zeta}}{\partial \zeta} = 0 \tag{17}$$

where $M_x = uZ$, $M_y = vZ$ and $H = \theta Z$.

The boundary conditions are

$$\dot{\zeta} = 0 \quad \text{at} \quad \zeta = 0 \; , \tag{18}$$

and

$$\dot{\zeta} = 0 \quad \text{at} \quad \zeta = 1 \; . \tag{19}$$

For this study, the flow will be independent of x and periodic in y. Φ is the only variable allowed to vary in the x-direction, so $\frac{\partial}{\partial x} = 0$ for all other variables.

In order to obtain an expression for Φ, equation (16) may be integrated with respect to ζ giving

$$\Phi = \int_0^\zeta \frac{g}{\theta_0} \theta Z \, d\zeta + C .\tag{20}$$

The constant of integration, C, can be eliminated by taking the vertical average of equation (20) and subtracting from equation (20) which gives the following

$$\Phi = \frac{g}{\theta_0} \int_0^\zeta \theta Z \, d\zeta - \overline{\int_0^\zeta \theta Z \, d\zeta}) + \overline{\Phi} .\tag{21}$$

In the above equation, $\overline{}$ represents the vertical average of a given variable.

A value for $\overline{\Phi}$ must be found before a solution for Φ can be determined. First, take the vertical average of (17) and apply the boundary conditions (18) and (19) which gives

$$\frac{\partial}{\partial y} \overline{M_y} = - Z \dot{\zeta} \Big|_0^1 = 0 .\tag{22}$$

This equation shows that $\overline{M_y}$ must be a constant in order to satisfy the boundary conditions. Next, take the vertical

18

average of equation (14) and differentiate with respect to y which yields

$$\frac{\partial^2}{\partial t \partial y}(\overline{M_y}) + \frac{\partial^2}{\partial y^2}(\overline{M_y v}) = \frac{\partial}{\partial y}(-Z\frac{\overline{\partial \Phi}}{\partial y} + \frac{g}{\theta_0}\overline{(Z\theta)(\zeta-1)\frac{\partial Z}{\partial y}} - \overline{fM_x}) . \quad (23)$$

The first term in equation (23) is identically zero from (22) and the resulting equation becomes

$$\frac{\partial}{\partial y}(Z\frac{\overline{\partial \Phi}}{\partial y}) = \frac{\partial}{\partial y}(-\frac{\partial}{\partial y}\overline{(M_y v)} + \frac{g}{\theta_0}\overline{(Z\theta)(\zeta-1)\frac{\partial Z}{\partial y}} - f\overline{Zu}) . \quad (24)$$

This equation can be solved diagnostically for $\overline{\Phi}$. This equation must be applied in order to satisfy the boundary conditions (18) and (19).

To obtain an expression for $\frac{\partial \Phi}{\partial x}$, which is a constant, equation (21) is differentiated with respect to x which yields

$$\frac{\partial \Phi}{\partial x} = \frac{g}{\theta_0}Z(\int_0^\zeta \frac{\partial \theta}{\partial x}\,d\zeta - \overline{\int_0^\zeta \frac{\partial \theta}{\partial x}\,d\zeta}) + \frac{\overline{\partial \Phi}}{\partial x} . \quad (25)$$

Since $\frac{\partial \theta}{\partial x} = 0$ in this study,

$$\frac{\partial \Phi}{\partial x} = \frac{\overline{\partial \Phi}}{\partial x} \quad (26)$$

and this quantity is assumed to be independent of y.

Consider the domain averages of equations (13) and (14) which are

$$\frac{d}{dt}(\overline{\overline{M_x}}) = -\overline{Z}\,\frac{\overline{\partial \Phi'}}{\partial x} + f\,\overline{\overline{M_y}} \,, \tag{27}$$

$$\frac{d}{dt}(\overline{\overline{M_y}}) = -\overline{Z}\,\frac{\overline{\partial \Phi'}}{\partial y} + \overline{\frac{g}{\theta_0}(Z\theta)(\zeta-1)\frac{\partial Z'}{\partial y}} - f\,\overline{\overline{M_x}} \,, \tag{28}$$

where —— represents the y average. Initially, $\frac{\partial \Phi}{\partial x}$ is computed geostrophically as

$$\frac{\overline{\partial \Phi'}}{\partial x} = \frac{f}{\overline{Z}}\,\overline{\overline{M_y}}_{\,t=0} \,. \tag{29}$$

If this relationship is used for all time and if the mass flux in the x-direction is zero initially, then $\overline{\overline{M_x}}$ will be zero for all time. The first two terms on the right side of equation (28) represent the mountain drag. The sum of these two terms for mid-latitude flow has been shown to be negative in the mean. This will lead to a continual loss of y-momentum. This kind of loss would make a quasi-steady final state impossible. An artificial source of momentum is required to maintain the mean meridional flow. This artificial source of momentum is provided by holding $\frac{\overline{\partial \Phi'}}{\partial x}$ constant as obtained in equation (29). In this case, if $\overline{\overline{M_y}}$ is decreased below the initial geostrophic value, $\overline{\overline{M_x}}$ will increase and restore the momentum loss. Thus, in the long term mean, the mountain

20

terms are balanced by the mean Coriolis force. However, for the horizontal scales to be considered in this study, this momentum source may not be needed since synoptic scale mountains cause very little wave drag.

The dependent variables are to be divided as follows:

$$u(x,y,\zeta,t) = U_d(x,y) + u'(y,\zeta,t) ,$$

$$v(x,y,\zeta,t) = V_d(x,y) + v'(y,\zeta,t) ,$$

$$\dot{\zeta}(y,\zeta,t) = \zeta'(y,\zeta,t) , \qquad (30)$$

$$\theta(y,\zeta,t) = \theta'(y,\zeta,t) ,$$

$$\Phi(x,y,\zeta,t) = \Phi(x,y) + \phi'(y,\zeta,t) .$$

The basic wind deformation field is chosen to be periodic in y and to have zero vorticity and divergence. Thus, the deformation field is given by

$$U_d(x,y) = -D_d L \sinh\left(\frac{x}{L}\right) \sin\left(\frac{y}{L}\right) , \qquad (31)$$

$$V_d(x,y) = -D_d L \cosh\left(\frac{x}{L}\right) \cos\left(\frac{y}{L}\right) , \qquad (32)$$

where D_d and L are constants. This deformation field was used by Stone (1966) in his study of quasi-geostrophic

frontogenesis. Since the flow is assumed to be independent

of x in this study, equations (31) and (32) are evaluated at

x = 0 resulting in

$$U_d(0,y) \;=\; 0 \;,\tag{33}$$

$$V_d(0,y) \;=\; -D_d\, L\cos\left(\tfrac{y}{L}\right)\;.\tag{34}$$

Substituting the expressions in equations (30) through (34)

into equations (13) through (15) and dropping the prime

notation yields

$$Z\,\frac{\partial u}{\partial t} \;+\; V_d\, Z\,\frac{\partial u}{\partial y} \;+\; u\,\frac{\partial(V_d Z)}{\partial y} \;+\; \frac{\partial}{\partial y}(vZu) \;+\; \frac{\partial}{\partial \zeta}(\dot{\zeta}uZ)$$

$$=\; -\,Z\,\frac{\partial \phi}{\partial x} \;+\; f\,vZ\;,\tag{35}$$

$$Z\,\frac{\partial v}{\partial t} \;+\; \frac{\partial}{\partial y}(vZv) \;+\; v\,\frac{\partial(V_d Z)}{\partial y} \;+\; V_d\, Z\,\frac{\partial v}{\partial y} \;+\; \frac{\partial}{\partial \zeta}(\dot{\zeta}uZ)$$

$$=\; -\,Z\,\frac{\partial \phi}{\partial y} \;+\; \frac{g}{\theta_0}\,\theta\,Z(\zeta-1)\,\frac{\partial Z}{\partial y} \;-\; fuZ\;,\tag{36}$$

$$Z\,\frac{\partial \theta}{\partial t} \;+\; \frac{\partial}{\partial y}(vZ\theta) \;+\; \frac{\partial}{\partial \zeta}(\dot{\zeta}\theta Z) \;=\; 0\;,\tag{37}$$

where $V_d = -D_d\, L\cos\left(\tfrac{y}{L}\right)$. This last set of equations is the

set that needs to be solved for u, v and θ. In this study,

equation (24) does not have to be solved if $\overline{M_y'}$ is restored

to the initial constant value at every timestep.

III.   FINITE DIFFERENCE FORMULATIONS

Staggered grids are used in both the horizontal and vertical. The vertical grid is divided into K-1 levels of constant $\Delta\zeta$ (Fig. 2). Quantities defined for the layers will be denoted by integer subscripts and the ζ coordinate value will be denoted by ζI_k. The quantities θ, u, v and ϕ are all defined on the integer levels. The vertical motion, $\dot{\zeta}$, on the other hand, is defined on the top, bottom and interface levels. These levels will be denoted with half-integer subscripts and the vertical coordinate will be identified by $\zeta_{k+1/2}$. The horizontal grid is divided into J-1 sections of constant resolution (Fig. 3). Momentum variables are defined on the integer subscripted points denoted by Y_j. The momentum variables include u, v, M_x, M_y and V_d. The mass variables, θ, ϕ, Z and $\dot{\zeta}$, are defined on the half-integer subscripted points. These points will be denoted as $YI_{j+1/2}$. Values needed off their respective grid points will be identified by a caret and will be defined as

$$\hat{S}_j = \frac{(Y_{j+1}-Y_j)S_{j+1/2} + (Y_j-Y_{j-1})S_{j-1/2}}{2[YI_{j+1/2}-YI_{j-1/2}]} ,$$ (38)

for quantities defined on the half-integer points and as

$$\zeta_{K1+1/2} \quad \square \ \dot{\zeta}$$

$$\zeta l_{K1} \qquad \square \ u, v, \theta, \phi$$

$$\zeta_{K1-1/2} \quad \square \ \dot{\zeta}$$

$$\zeta_{k+1/2} \quad \square \ \dot{\zeta}$$

$$\zeta l_{k} \qquad \square \ u, v, \theta, \phi$$

$$\zeta_{k-1/2} \quad \square \ \dot{\zeta}$$

$$\zeta_{3/2} \qquad \square \ \dot{\zeta}$$

$$\zeta l_{1} \qquad \square \ u, v, \theta, \phi$$

$$\zeta_{1/2} \qquad \square \ \dot{\zeta}$$

Fig. 2.   The vertical grid, showing the indexing
convention and staggering of the variables

24

ζ̇ φ Z θ ▫ $Yl_{j+\frac{1}{2}}$

$M_{x,y}$ V_d $\hat{Z}$ $\hat{v}$ ▫ Y_j

ζ̇ φ Z θ ▫ $Yl_{j-\frac{1}{2}}$

Fig. 3. The horizontal grid, showing the indexing convention and staggering of the variables

$$\hat{S}_{j+1/2} = \frac{(YI_{j+3/2} - YI_{j+1/2})S_{j+1} + (YI_{j+1/2} - YI_{j-1/2})S_j}{2[Y_{j+1} - Y_j]} , \quad (39)$$

for quantities at the integer points. Periodic boundary conditions are used in this study for all quantities.

Equations (11), (13) through (15) and (17) are solved by using finite differences in y, ζ and t. The finite differencing scheme is chosen to conserve the sum of kinetic energy and potential energy.

The time differencing scheme uses a leapfrog scheme with a periodic use of the Euler backward scheme. The Euler backward scheme is used to eliminate the computational mode arising with the leapfrog scheme [Haltiner and Williams, 1980].

Equations (11), (17) and (13) through (15) may be written in finite difference form as

$$\hat{Z}_j \frac{\partial u_{j,k}}{\partial t} + \frac{(\frac{M_{Y_{j+1,k}} + M_{Y_{j,k}}}{2})(\frac{u_{j+1,k} + u_{j,k}}{2}) - (\frac{M_{Y_{j,k}} + M_{Y_{j-1,k}}}{2})(\frac{u_{j,k} + u_{j-1,k}}{2})}{YI_{j+1/2} - YI_{j-1/2}}$$

$$+ \frac{(\dot{\zeta Z})_{j,k+1/2}(\frac{u_{j,k+1} + u_{j,k}}{2}) - (\dot{\zeta Z})_{j,k-1/2}(\frac{u_{j,k} + u_{k,k-1}}{2})}{\zeta_{k+1/2} - \zeta_{k-1/2}}$$

$$= - \hat{Z}_j \frac{\partial \phi}{\partial x} + f v_{j,k} \hat{Z}_j , \quad (40)$$

26

$$\hat{Z}_j \, \frac{\partial v_{j,k}}{\partial t} + \frac{\left(\frac{M_{Y_{j+1,k}}+M_{Y_{j,k}}}{2}\right)\left(\frac{v_{j+1,k}+v_{j,k}}{2}\right) - \left(\frac{M_{Y_{j,k}}+M_{Y_{j-1,k}}}{2}\right)\left(\frac{v_{j,k}+v_{j-1,k}}{2}\right)}{YI_{j+1/2} - YI_{j-1/2}}$$

$$+ \; \frac{(\dot{\zeta}\hat{Z})_{j,k+1/2}\left(\frac{v_{j,k+1}+v_{j,k}}{2}\right) - (\dot{\zeta}\hat{Z})_{j,k-1/2}\left(\frac{v_{j,k}+v_{j,k-1}}{2}\right)}{\zeta_{k+1/2} - \zeta_{k-1/2}}$$

$$= \; - \hat{Z}_j \, \frac{\phi_{j+1/2,k}-\phi_{j-1/2,k}}{YI_{j+1/2} - YI_{j-1/2}} + \frac{g}{\theta_0}(\hat{\theta}\hat{Z})_{j,k}(\zeta-1)_{j,k} \, \frac{Z_{j+1/2}-Z_{j-1/2}}{YI_{j+1/2}-YI_{j-1/2}}$$

$$- \; fu_{j,k} \, \hat{Z}_{j,k} \; , \tag{41}$$

$$Z_{j+1/2} \, \frac{\partial \theta_{j+1/2,k}}{\partial t} + \frac{M_{Y_{j+1,k}}\left(\frac{\theta_{j+3/2,k}+\theta_{j+1/2,k}}{2}\right) - M_{Y_{j,k}}\left(\frac{\theta_{j+1/2,k}+\theta_{j-1/2,k}}{2}\right)}{Y_{j+1} - Y_j}$$

$$+ \; \frac{(\dot{\zeta}Z)_{j+1/2,k+1/2}\left(\frac{\theta_{j+1/2,k+1}+\theta_{j+1/2,k}}{2}\right) - (\dot{\zeta}Z)_{j+1/2,k-1/2}\left(\frac{\theta_{j+1/2,k}+\theta_{j+1/2,k-1}}{2}\right)}{\zeta_{k+1/2} - \zeta_{k-1/2}}$$

$$= \; 0 \; , \tag{42}$$

$$\frac{\phi_{j+1/2,k+1} - \phi_{j+1/2,k}}{\zeta_{k+1} - \zeta_k} \; = \; \frac{g}{\theta_0} \, Z_{j+1/2} \, \frac{\theta_{j+1/2,k+1}+\theta_{j+1/2,k}}{2} \; , \tag{43}$$

and

$$\frac{M_{Y_{j+1,k}} - M_{Y_{j,k}}}{Y_{j+1} - Y_j} \; = \; -Z_{j+1/2}\left(\frac{\dot{\zeta}_{j+1/2,k+1/2}-\dot{\zeta}_{j+1/2,k-1/2}}{\zeta_{k+1/2} - \zeta_{k-1/2}}\right) . \tag{44}$$

27

IV. RESULTS

All numerical results to be shown use the following
numerical values for the constants:

$$a = 12 \text{ K}$$

$$B = 375 \text{ m}$$

$$D = 9 \text{ km}$$

$$D_d = 10^{-5} \text{ sec}^{-1}$$

$$f = 10^{-4} \text{ sec}^{-1} \tag{45}$$

$$g = 9.81 \text{ m/sec}^2$$

$$L = 3600 \text{ km}$$

$$\theta_0 = 300 \text{ K}$$

$$\frac{\partial \theta_s}{\partial z} = 4 \text{ K/km}$$

The following finite-difference increments are used.

$$\Delta t = 180 \text{ sec}$$

$$\Delta y = 40 \text{ km} \tag{46}$$

$$\Delta \zeta = 1/27$$

A. MOUNTAIN WITH NO DEFORMATION FLOW

The initial conditions are obtained from the quasi-
geostrophic equations for steady state flow over topography
[Walton, 1968; DeBoer, 1970]. The initial potential
temperature field is given by

28

$$\theta(y,z,0) = \theta_s + B \frac{\partial \theta_s}{\partial z} \frac{\sinh[\alpha(z-D)]}{\sinh(\alpha D)} \cos\left(\frac{y}{L}\right) - \frac{2a}{\pi} \cos\left(\frac{y}{L}\right) . \quad (47)$$

The quantity $\frac{\partial \theta_s}{\partial z}$ is the constant initial lapse rate and

$$\alpha = \frac{1}{fL}\left(\frac{g}{\theta_0} \frac{\partial \theta_s}{\partial z}\right)^{1/2} . \quad (48)$$

Substituting equation (47) into the thermal wind equation yields

$$\frac{\partial u}{\partial z} = \frac{1}{f} \frac{g}{\theta_0} \frac{1}{L}\left[B\frac{\partial \theta_s}{\partial z} \frac{\sinh[\alpha(z-D)]}{\sinh(\alpha D)} \sin\left(\frac{y}{L}\right) - \frac{2a}{\pi} \sin\left(\frac{y}{L}\right)\right] . \quad (49)$$

This equation can be integrated with respect to z to give

$$u(y,z,0) = B\left(\frac{g}{\theta_0} \frac{\partial \theta_s}{\partial z}\right)^{1/2} \frac{\cosh[\alpha(z-D)]}{\sinh(\alpha D)} \sin\left(\frac{y}{L}\right)$$

$$- \frac{2a}{\pi} \sin\left(\frac{y}{L}\right)\left(Z - \frac{D}{2}\right) . \quad (50)$$

The initial v field can be shown to be

$$v(y,z,0) = V + \alpha VB \frac{\cosh[\alpha(z-D)]}{\sinh(\alpha D)} \cos\left(\frac{y}{L}\right) . \quad (51)$$

The initial w and ϕ are obtained from equations (4) and (3).

It is necessary to rewrite the initial conditions in the zeta-coordinate system. From equation (6), equations (47), (50), and (51) can be rewritten as

$$\theta(y,\zeta,0) \;=\; \theta_s + B\,\frac{\partial\theta_s}{\partial z}\,\frac{\sinh[\alpha Z(\zeta-1)]}{\sinh(\alpha D)}\,\sin\!\left(\tfrac{y}{L}\right) - \frac{2a}{\pi}\,\sin\!\left(\tfrac{y}{L}\right),\quad (52)$$

$$u(y,\zeta,0) \;=\; B\!\left(\frac{g}{\theta_0}\frac{\partial\theta_s}{\partial z}\right)^{1/2}\frac{\cosh[\alpha Z(\zeta-1)]}{\sinh(\alpha D)}\,\sin\!\left(\tfrac{y}{L}\right)$$

$$-\frac{2a}{\pi}\,\sin\!\left(\tfrac{y}{L}\right)\left(\zeta-\tfrac{1}{2}\right)D,\qquad (53)$$

and

$$v(y,\zeta,0) \;=\; V + \alpha VB\,\frac{\cosh[\alpha Z(\zeta-1)]}{\sinh(\alpha D)}\,\cos\!\left(\tfrac{y}{L}\right).\qquad (54)$$

These initial conditions are shown in Figs. 4-7. ζ and ϕ are given by equations (10) and (9).

The value of θ_s was computed using the formula

$$\theta_s \;=\; \frac{\partial\theta_s}{\partial z}\left[\tfrac{D}{2} + Z(\zeta-1)\right].\qquad (55)$$

The profile of the mountain used in this study is given by

$$z_s \;=\; B\,\cos\!\left(\tfrac{y}{L}\right).\qquad (56)$$

and is shown in Fig. 8.

The initial conditions show anticyclonic vorticity over the ridge and cyclonic vorticity over the valley. There is divergence on the upslope and convergence on the downslope. These perturbations die off with height above the surface.
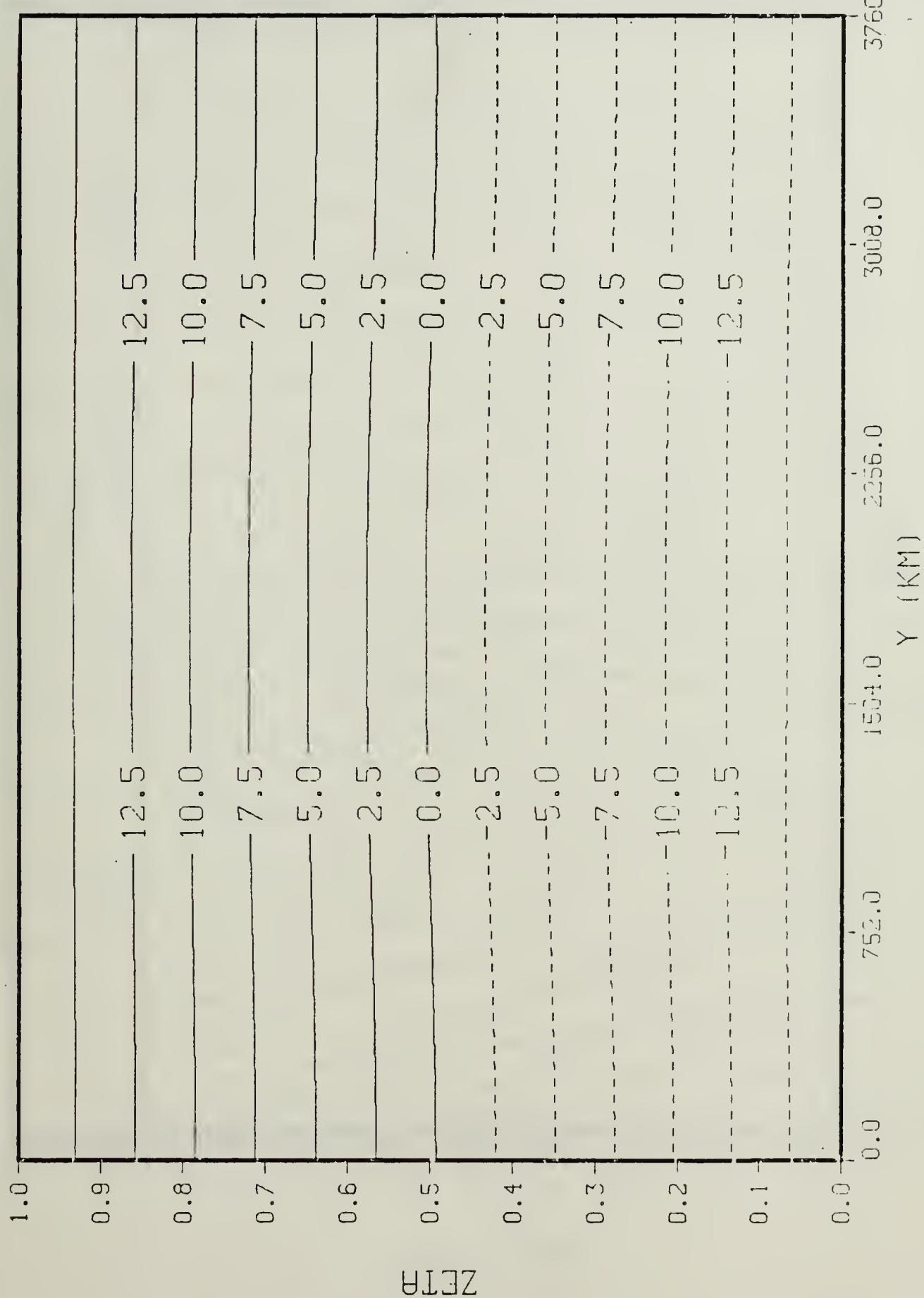
Fig. 4. θ(K). Initial. Mountain only
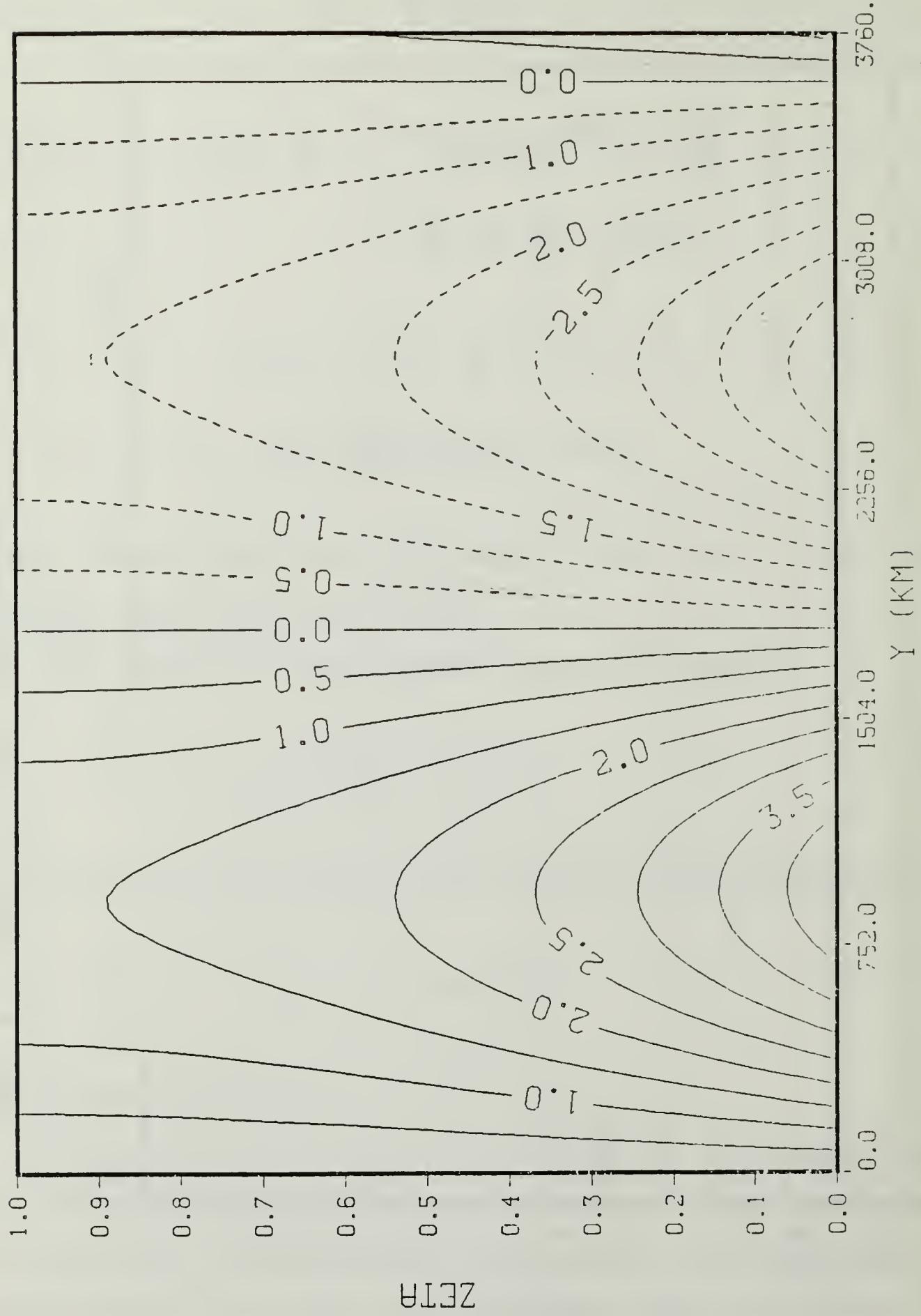
Fig. 5. u (m/sec). Initial. Mountain only

32
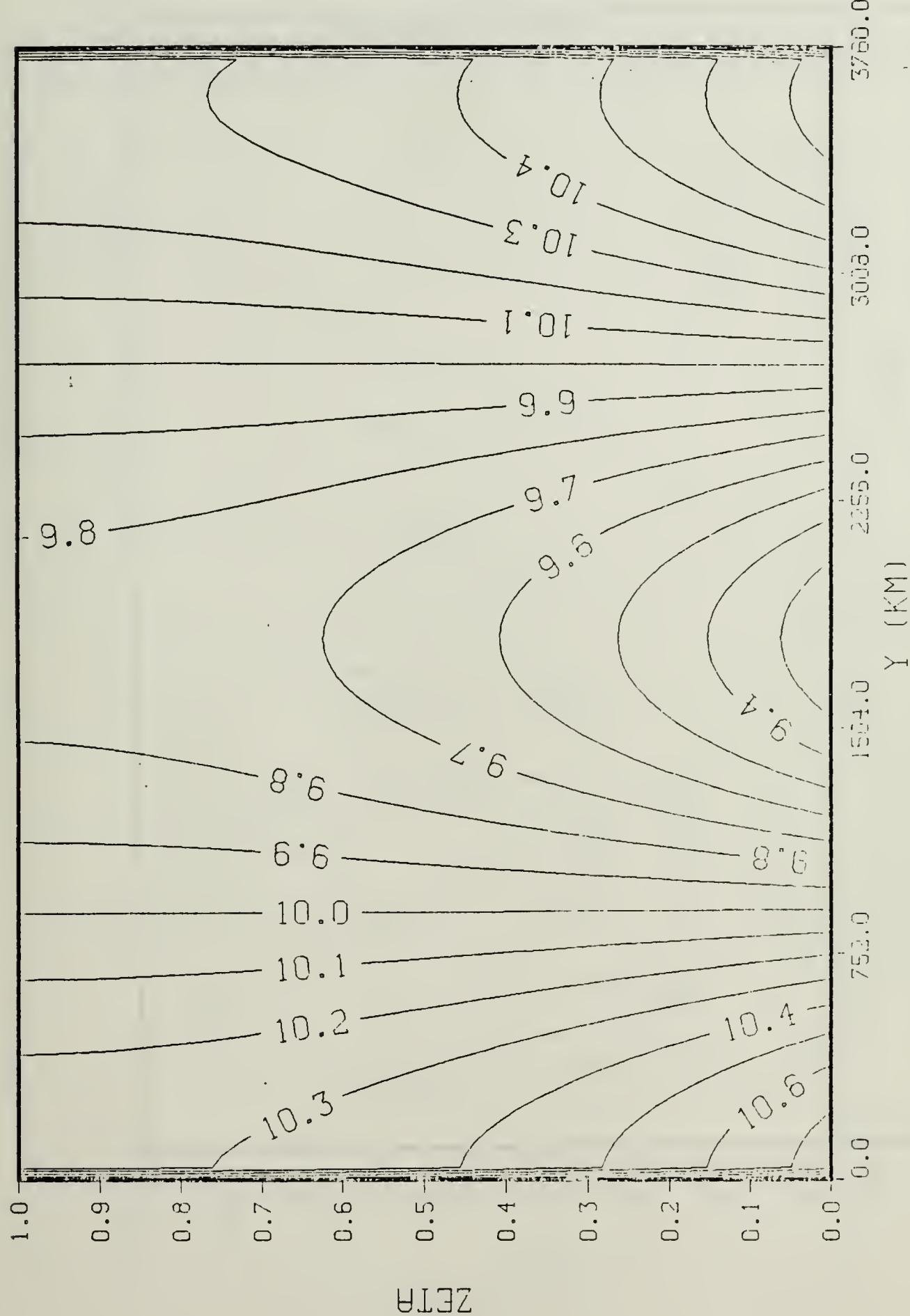
Fig. 6. v (m/sec). Initial. Mountain only
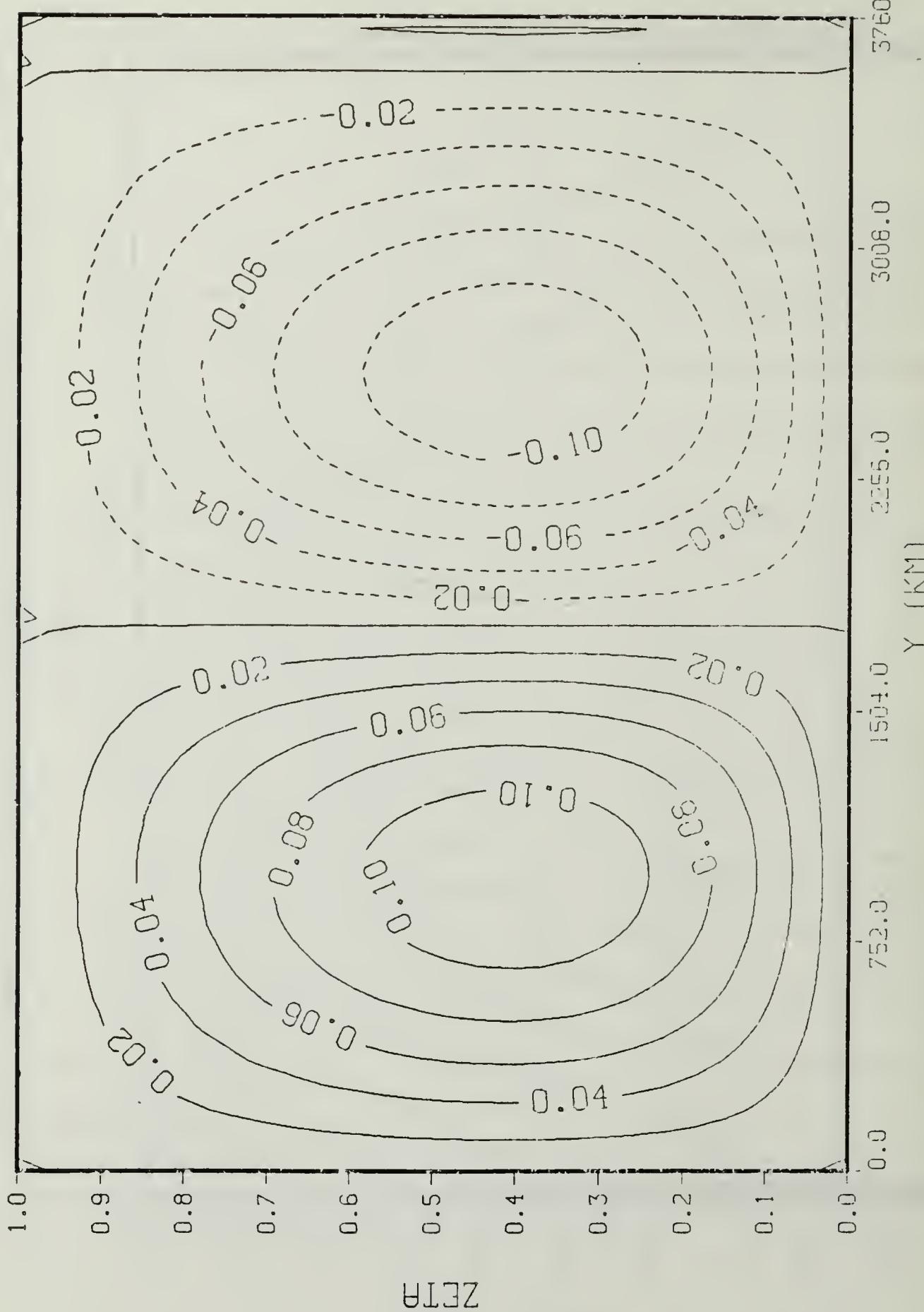
Fig. 7. $\dot{\zeta}$ ($\times 10^{-6}$ sec^{-1}). Initial. Mountain only

34
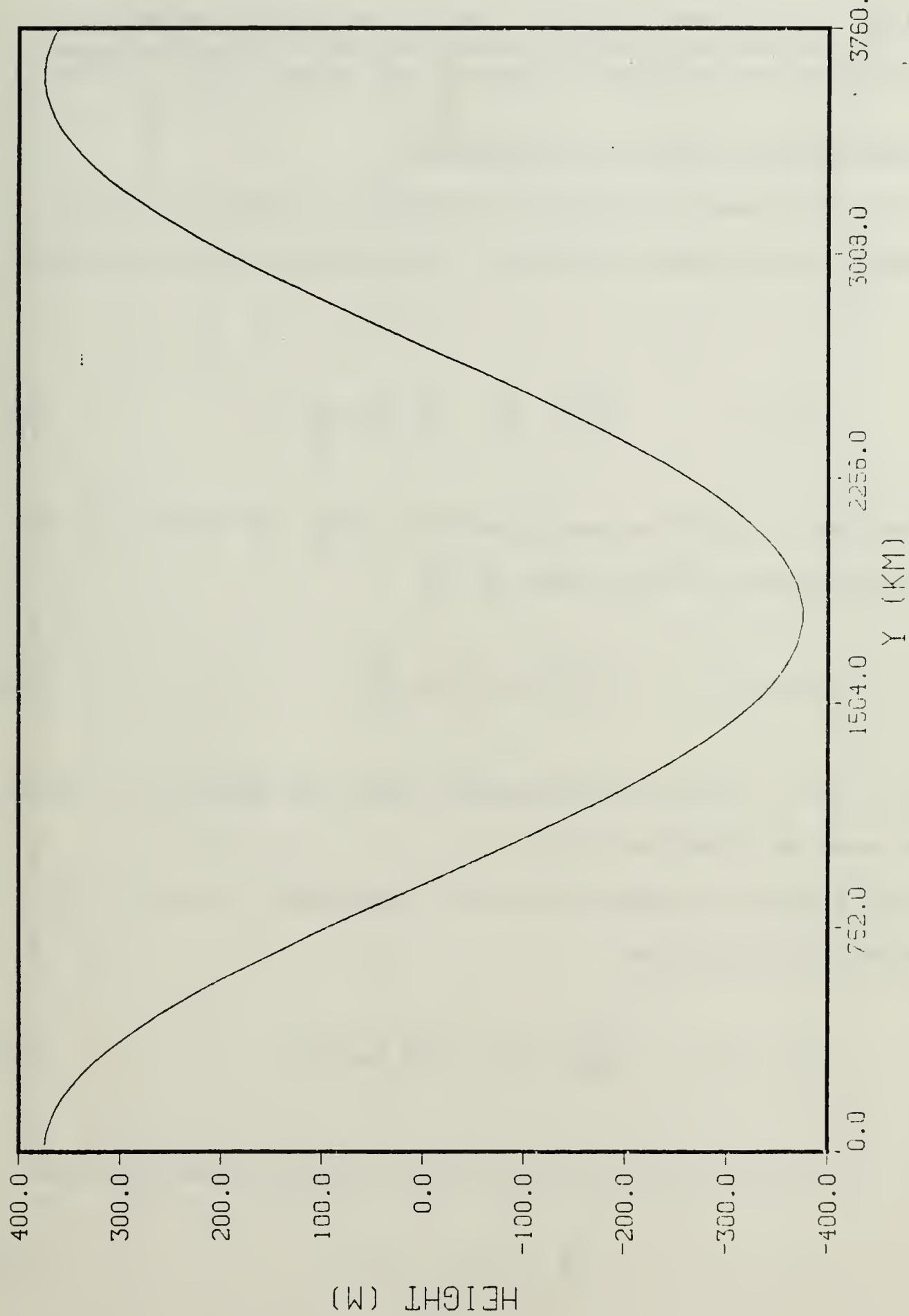
Fig. 8. Profile of the mountain with maximum height 375 m

Figs. 9-12 show the results at t = 72 hours. Since the original fields were analytic, only a slight adjustment to the mountain can be seen in the v, and hence, the $\dot{\zeta}$ fields.

B. DEFORMATION OVER FLAT TOPOGRAPHY

For this case, the initial potential temperature field contains a horizontal variation. The initial field is given by

$$\theta(y,z,0) \;=\; \frac{\partial \theta_s}{\partial z}(z - \frac{D}{2}) \;-\; \frac{2a}{\pi} \cos\left(\frac{y}{L}\right) \,. \tag{57}$$

The initial u field is again derived using the thermal wind relationship and can be shown to be

$$u(y,z,0) \;=\; -\,\frac{2a}{\pi} \sin\left(\frac{y}{L}\right)(z - \frac{D}{2}) \,. \tag{58}$$

The initial v field is identically zero and thus, w is forced to be zero by equation (3).

It is again necessary to write equations (48) and (49) in zeta-coordinates as

$$\theta(y,\zeta,0) \;=\; \frac{\partial \theta_s}{\partial z}(\zeta-1)D \;-\; \frac{2a}{\pi} \cos\left(\frac{y}{L}\right) \,, \tag{59}$$

and

$$u(y,\zeta,0) \;=\; -\,\frac{2a}{\pi} \sin\left(\frac{y}{L}\right)(\zeta - \frac{1}{2})D \,. \tag{60}$$

36
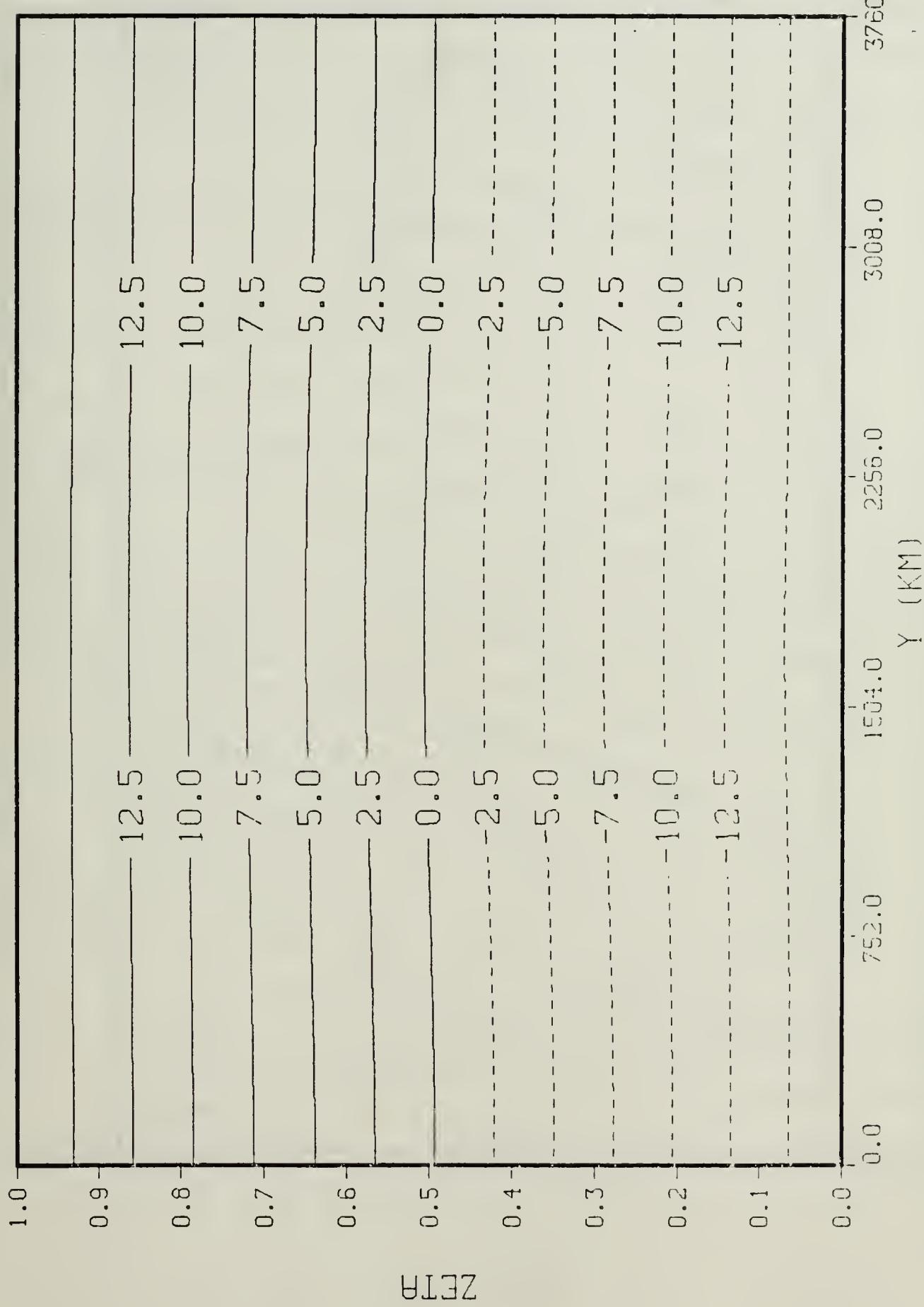
Fig. 9. θ(K). 72 hours. Mountain only

37
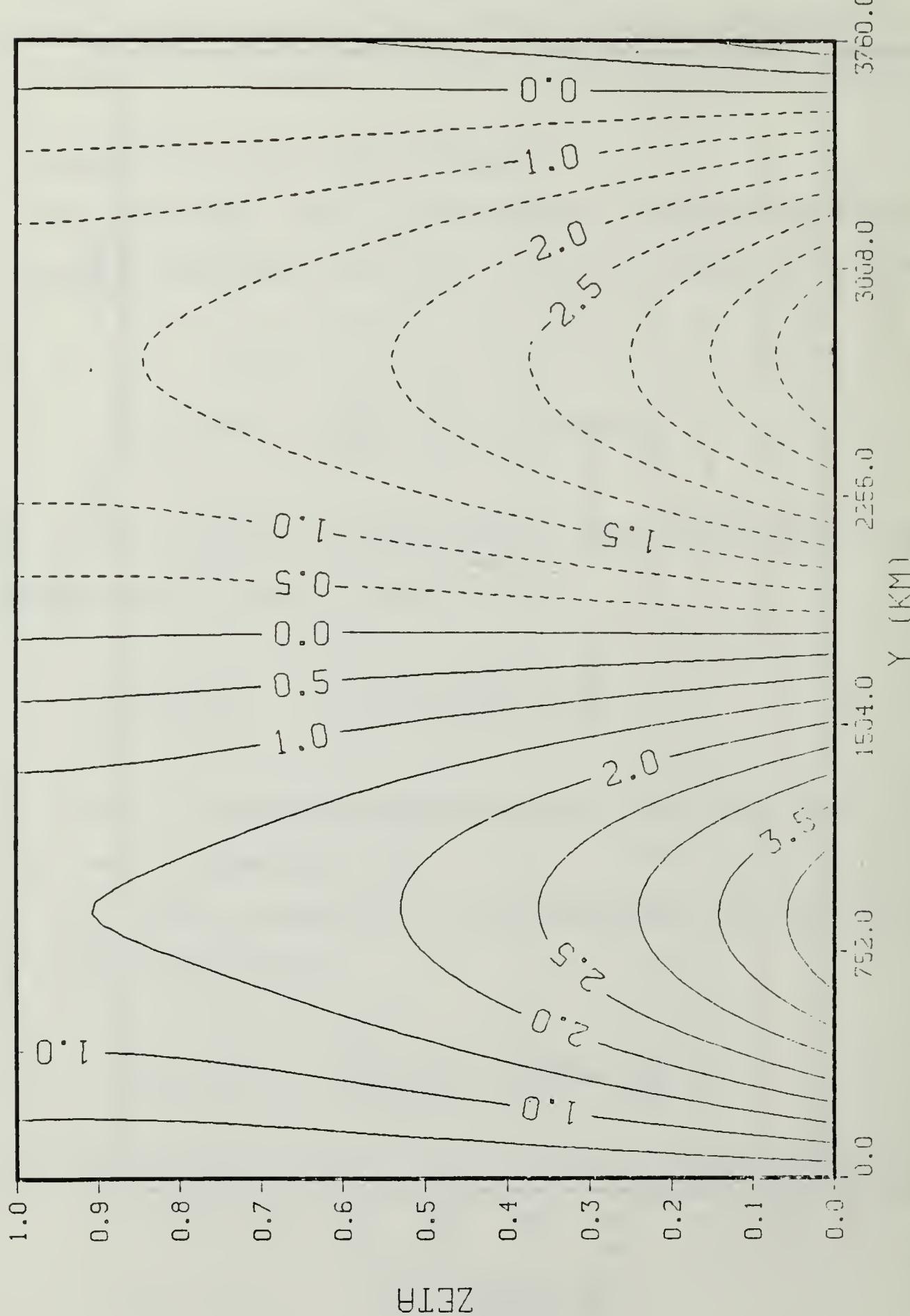
Fig. 10. u (m/sec). 72 hours. Mountain only

38
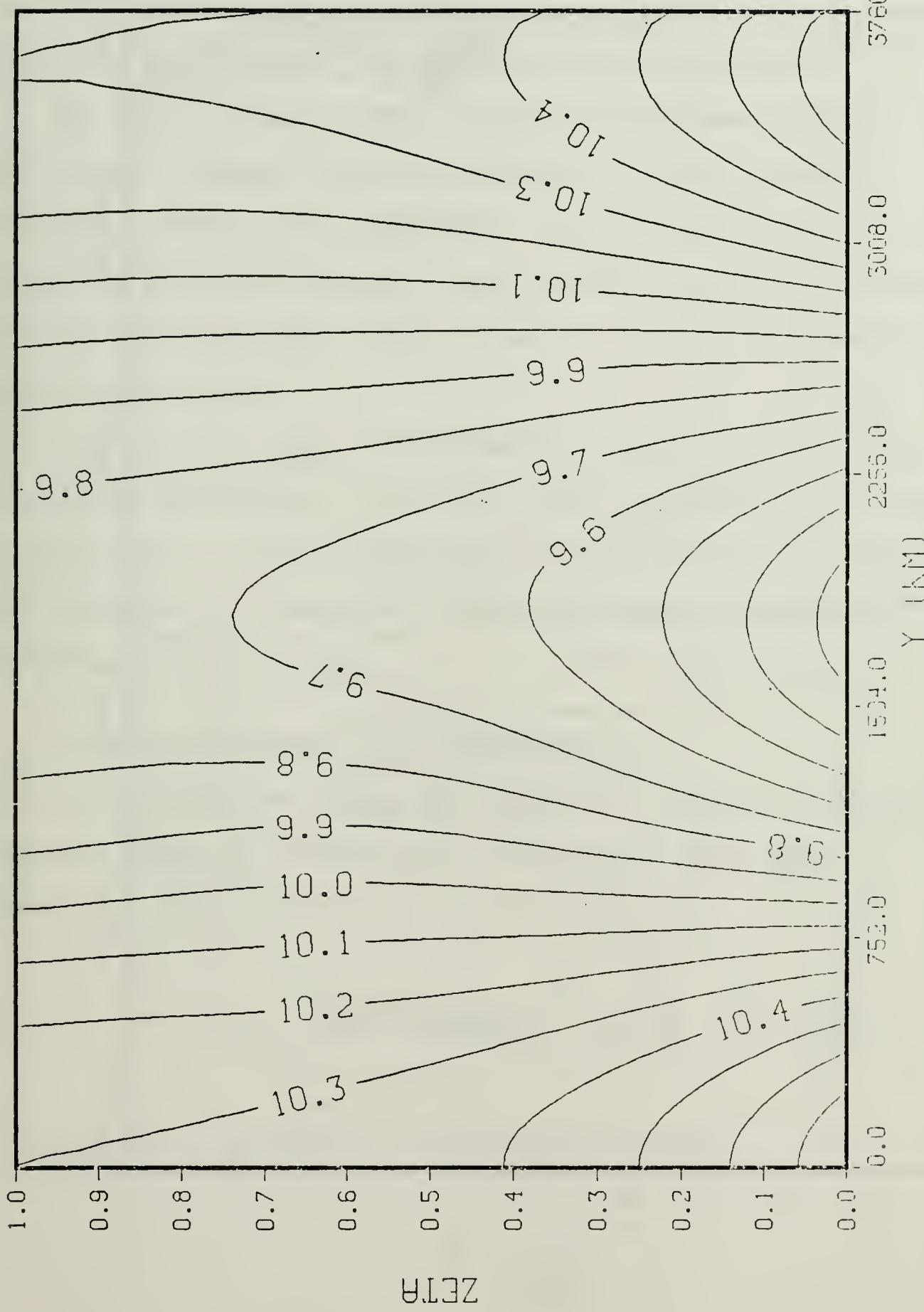
Fig. 11. v (m/sec). 72 hours. Mountain only
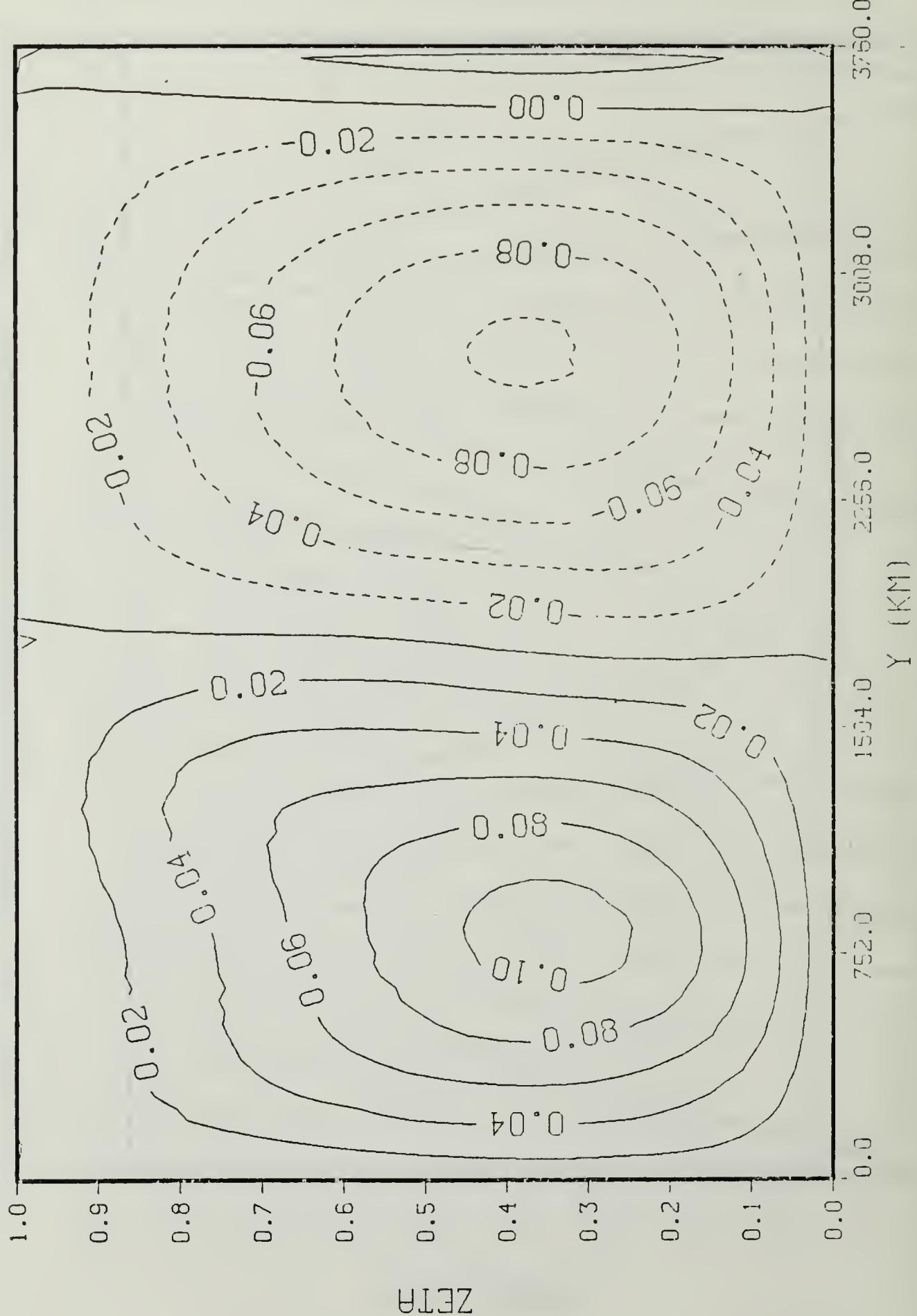
Fig. 12. $\dot{\zeta}$ ($\times 10^{-6}$ sec^{-1}). 72 hours. Mountain only

40

v and $\dot{\zeta}$ are zero initially and ϕ is given by equation (9).
Figures 13 and 14 show the initial conditions and Fig. 15
shows the deformation flow given by equation (34).

The front is developed by 24 hours as shown in Figs. 16-19.
The frontal discontinuity forms along the point where v = 0
and tilts toward the colder air. Cyclonic shear can be seen
along the frontal boundary. The relative vorticity is less
than zero on the north side of the front and is greater than
zero to the south.

By 48 hours, Figs. 20-23 show the strengthening of the
frontal discontinuity. The tilt remains the same as at the
24 hour point. On the other side of the domain, the tempera-
ture gradient is weakening, which indicates frontolysis
occurring in that region.

C. MOUNTAIN WITH NON-MOVING DEFORMATION

The previous two cases are combined in order to investi-
gate the combined effects of a deformation flow and a
mountain. The initial fields are given by

$$\theta(y,\zeta,0) = \theta_s + B \frac{\partial \theta_s}{\partial z} \frac{\sinh[\alpha Z(\zeta-1)]}{\sinh(\alpha D)} \sin\left(\frac{y}{L}\right) - \frac{2a}{\pi} \cos\left(\frac{y}{L}\right) , \quad (61)$$

$$u(y,\zeta,0) = B\left(\frac{g}{\theta_0} \frac{\partial \theta_s}{\partial z}\right)^{1/2} \frac{\cosh[\alpha Z(\zeta-1)]}{\sinh(\alpha D)} \sin\left(\frac{y}{L}\right)$$

$$- \frac{2a}{\pi} \sin\left(\frac{y}{L}\right) , \quad (62)$$

Fig. 13. θ(K). Initial. Deformation only

42
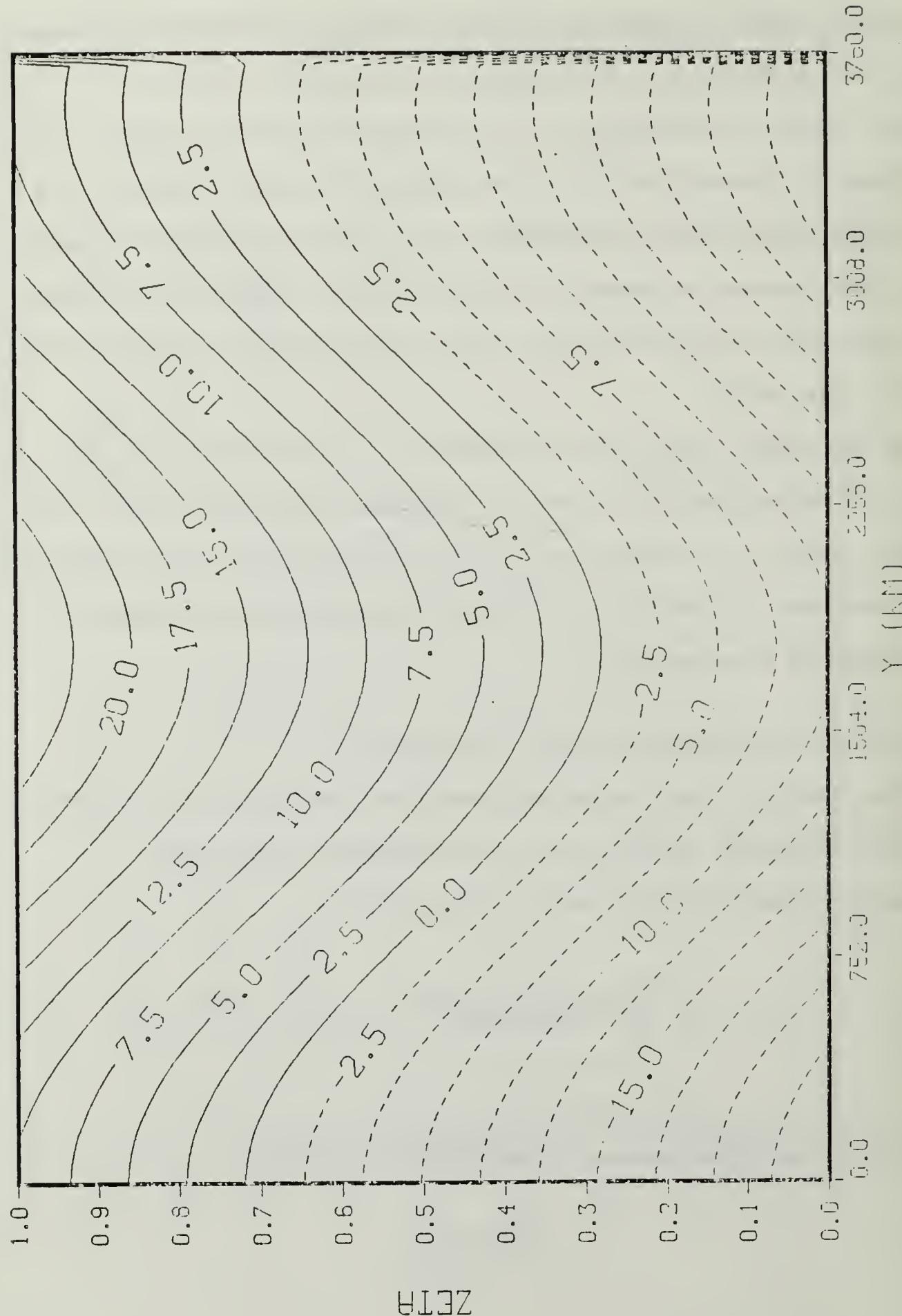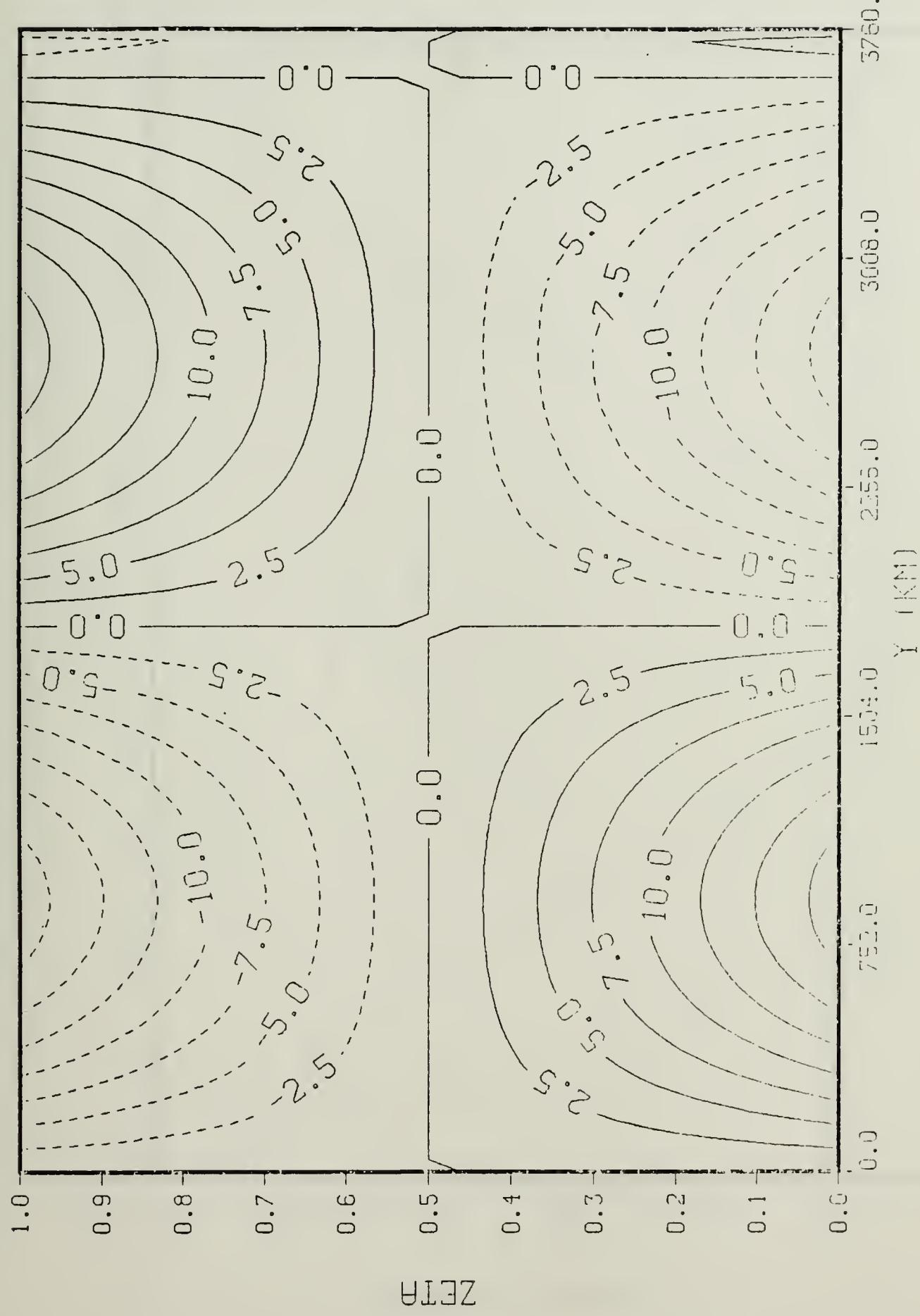
Fig. 14. u (m/sec). Initial. Deformation only

43
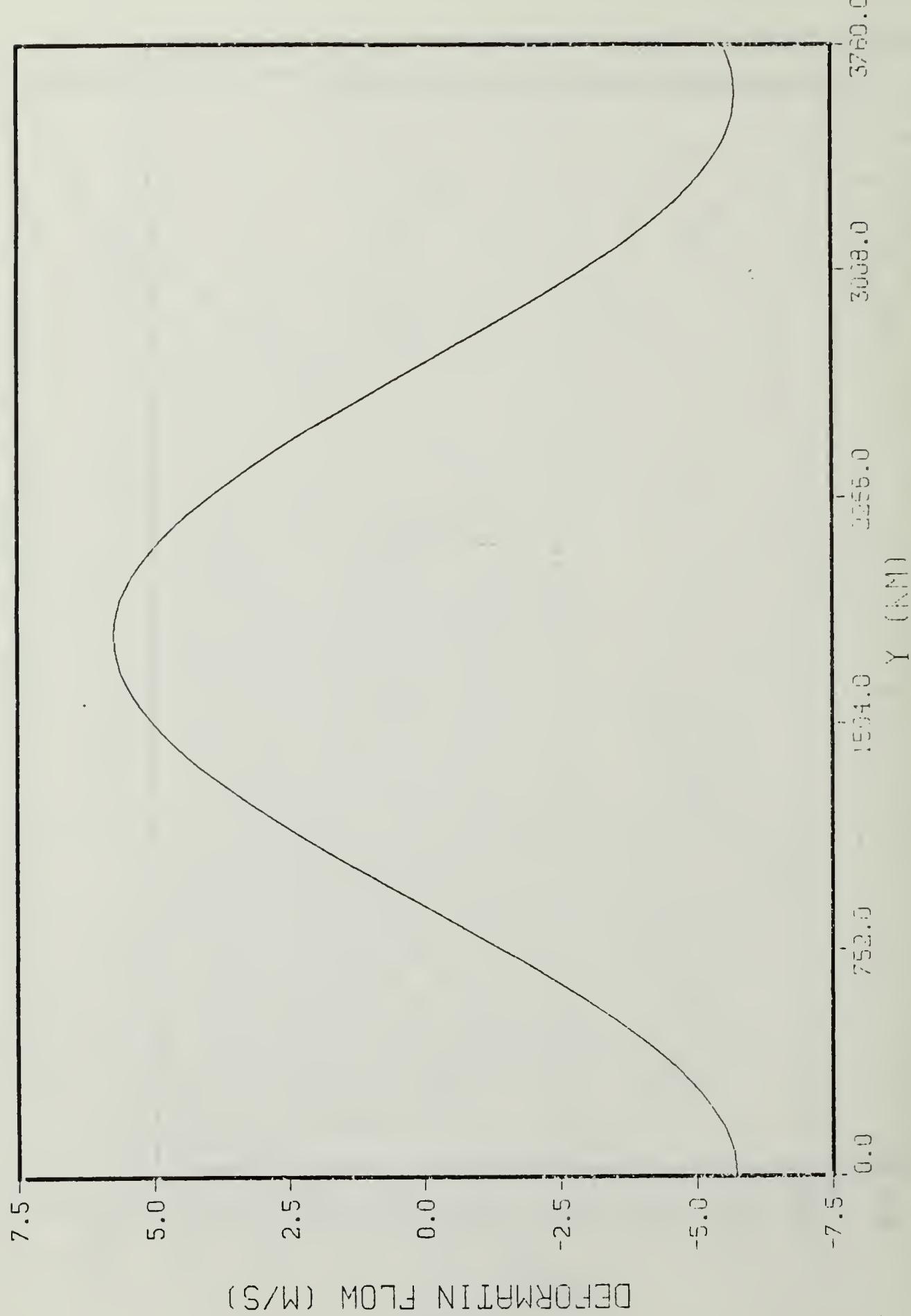
Fig. 15. Deformation flow

44

Fig. 16. θ(K). 24 hours. Deformation only

45
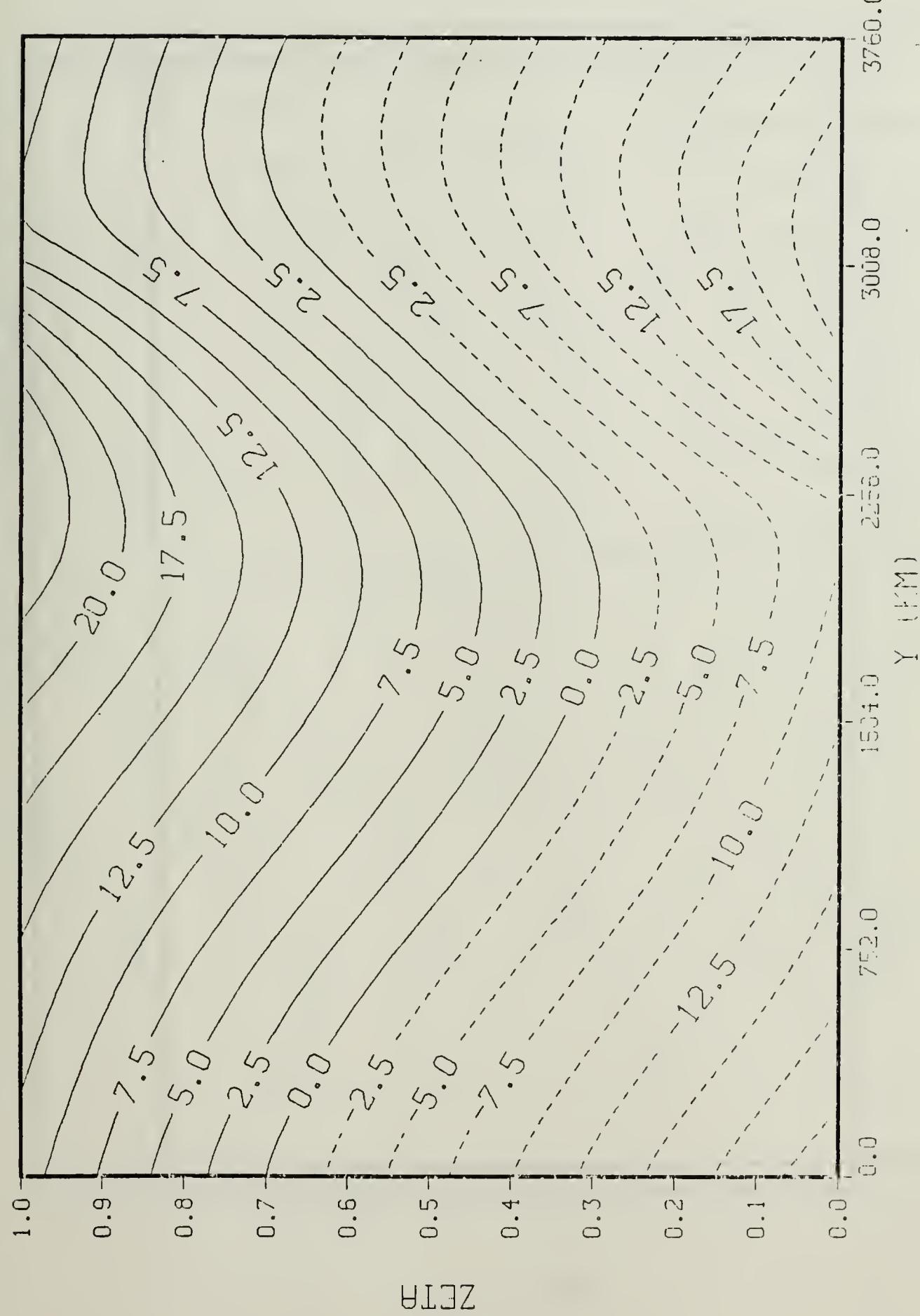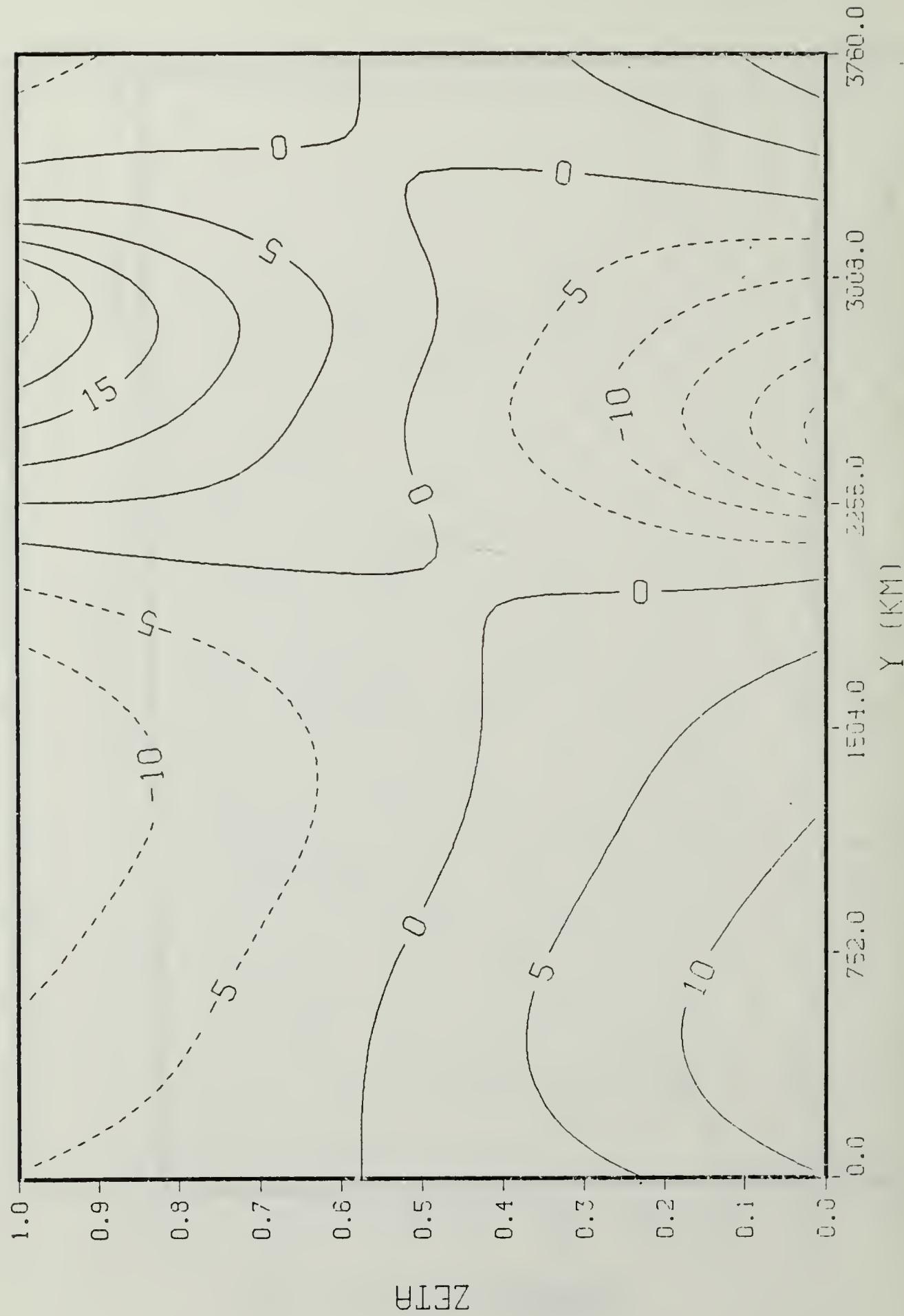
Fig. 17. u (m/sec). 24 hours. Deformation only

46
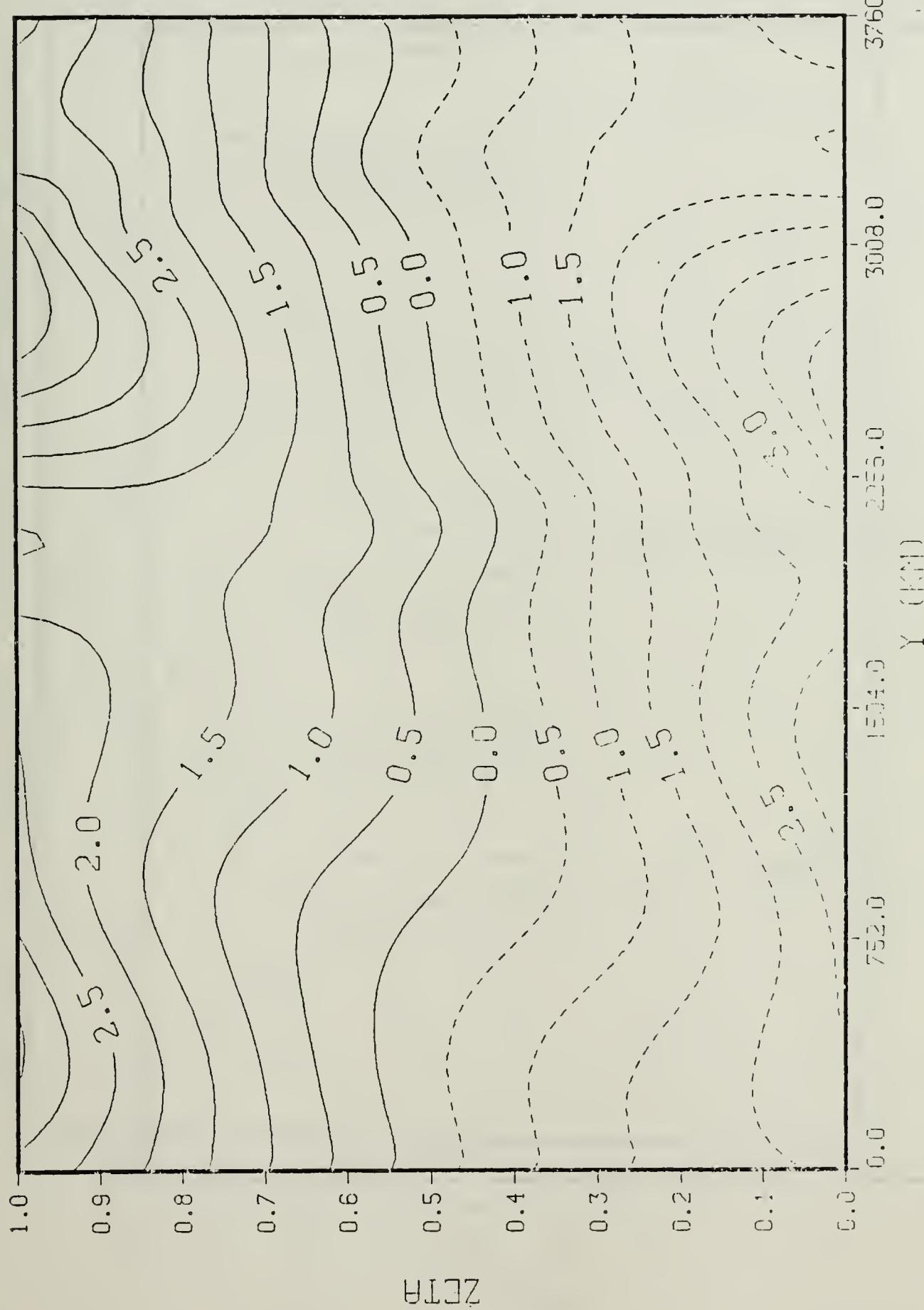
Fig. 18. v (m/sec). 24 hours. Deformation only

47
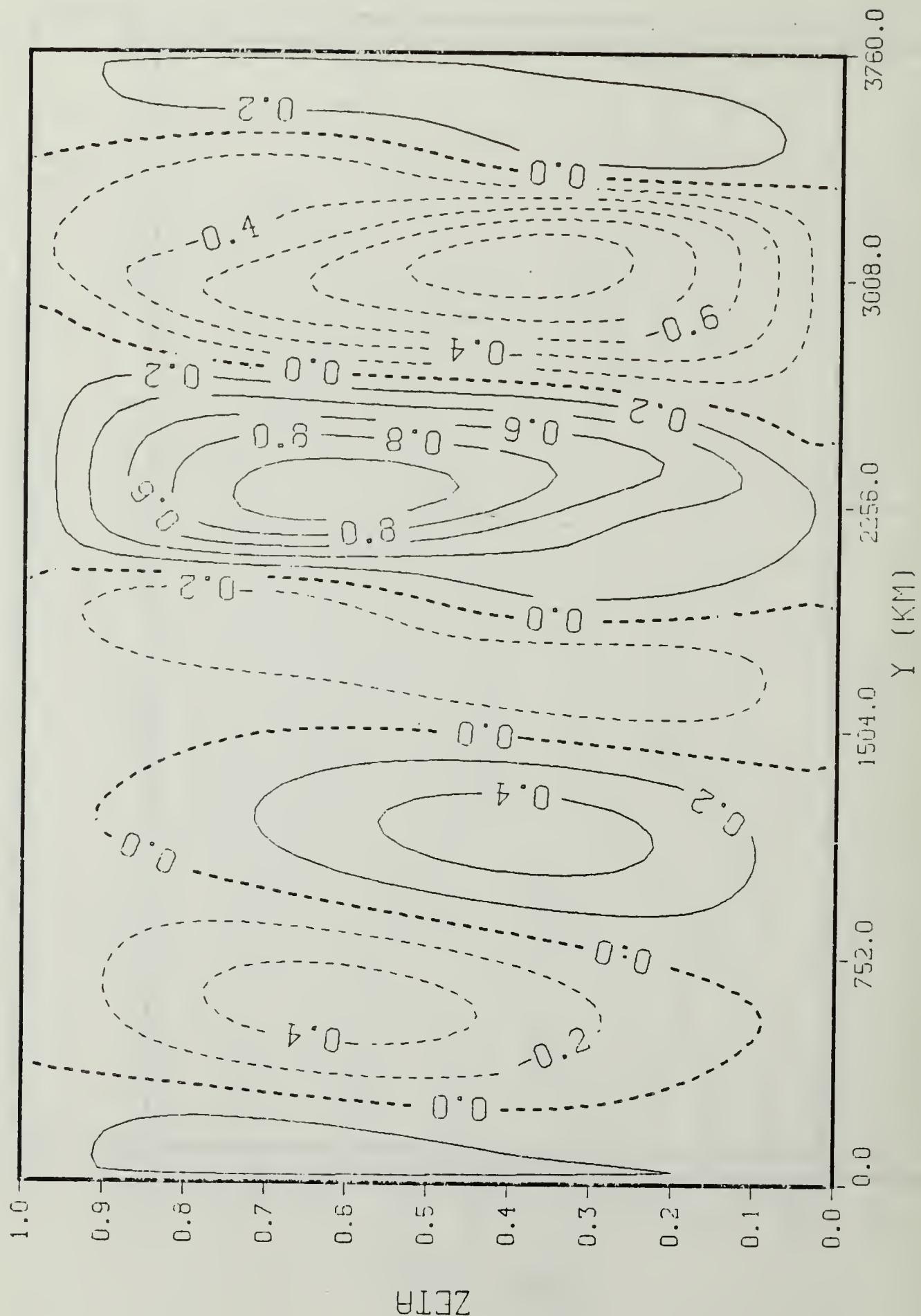
Fig. 19. $\dot{\zeta}$ ($\times 10^{-6}$ sec^{-1}). 24 hours. Deformation only

48

Fig. 20. θ(K). 48 hours. Deformation only

49
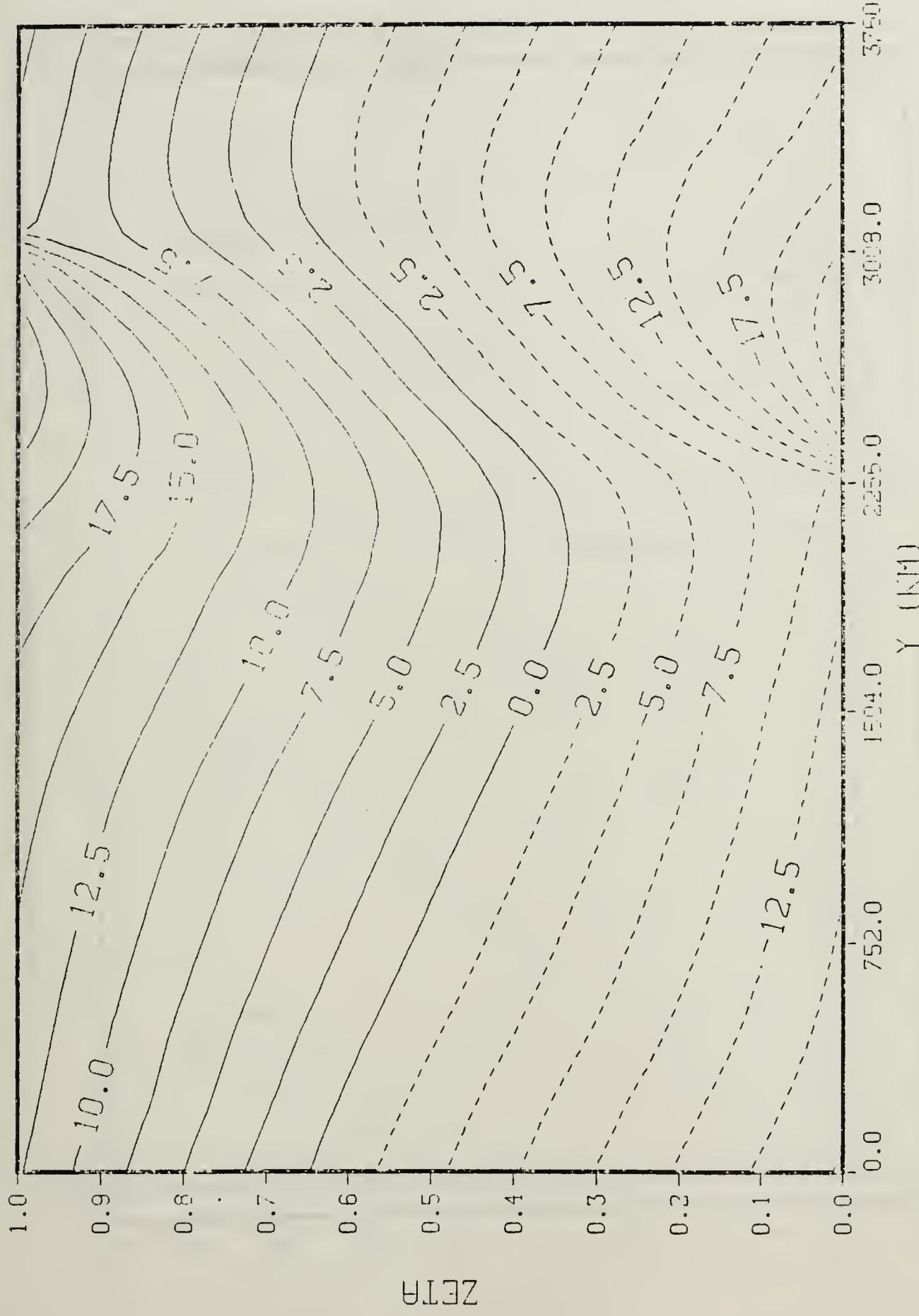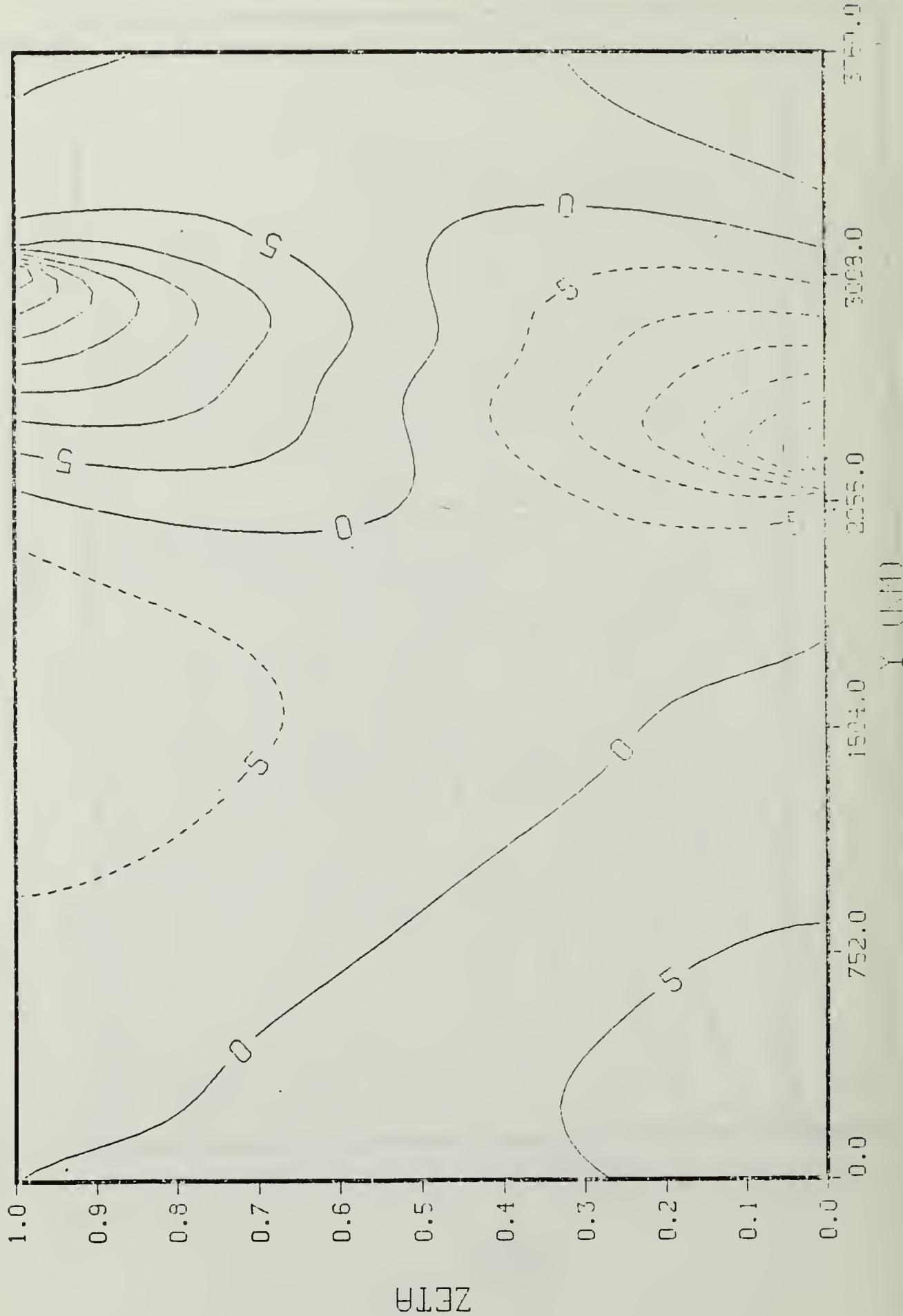
Fig. 21. u (m/sec). 48 hours. Deformation only

50
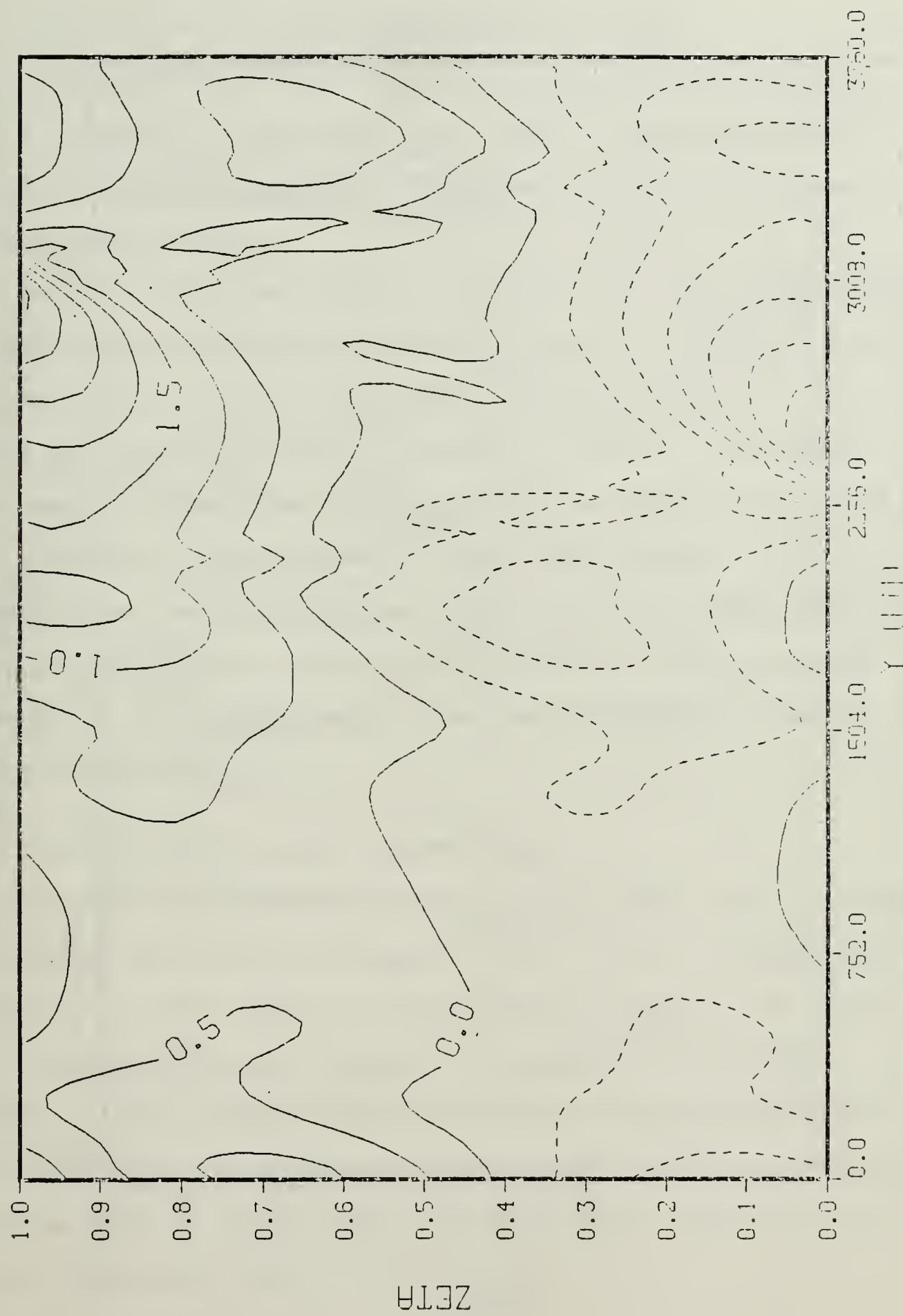
Fig. 22.   v (m/sec).   48 hours.   Deformation only

51
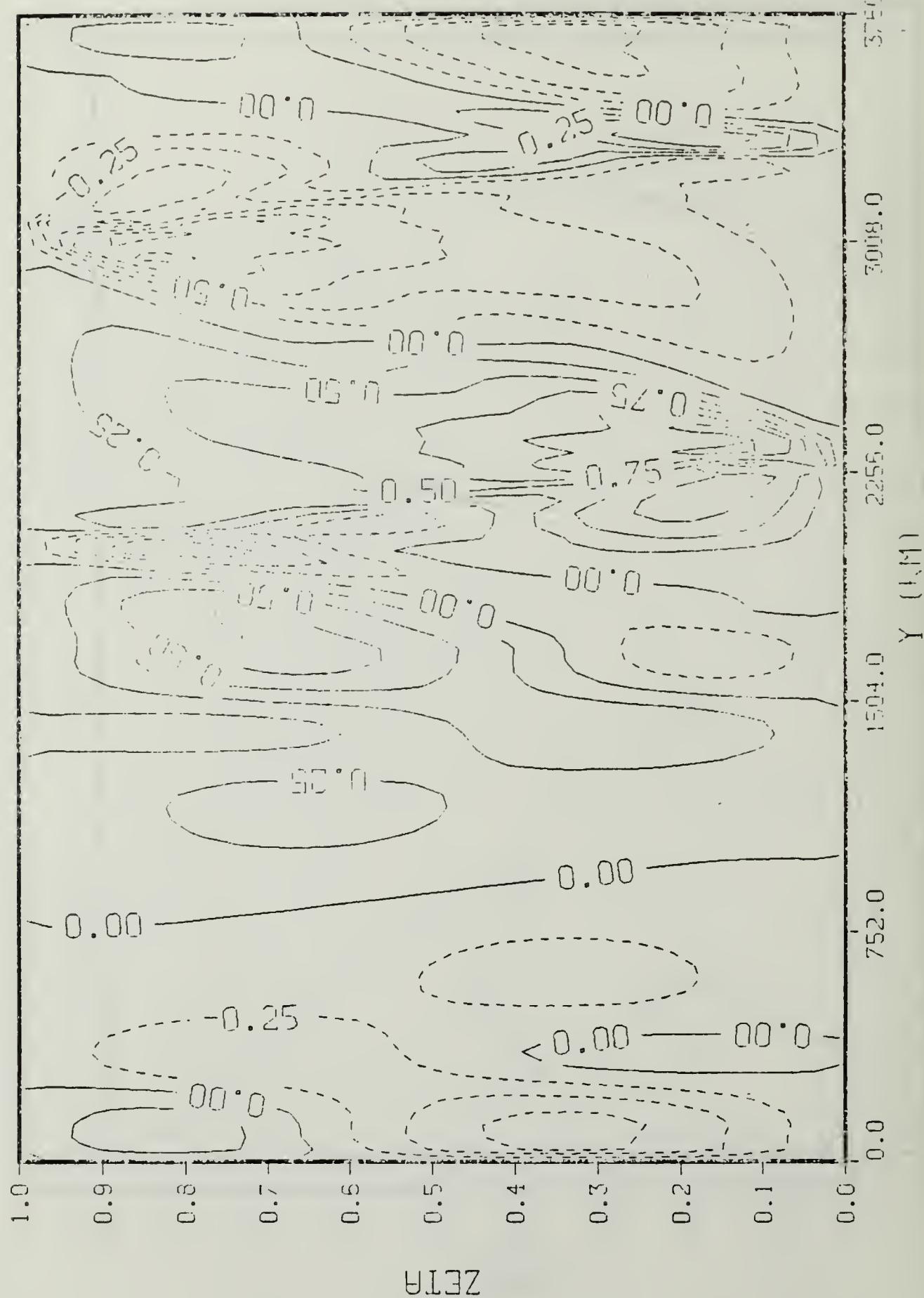
Fig. 23. $\dot{\zeta}$ ($\times 10^{-6}$ sec^{-1}). 48 hours. Deformation only

52

$$v(y,\zeta,0) \;\; = \;\; V + \alpha VB \; \frac{\cosh[\alpha Z(\zeta-1)]}{\sinh(\alpha D)} \; \cos\left(\frac{y}{L}\right) \; , \qquad\qquad (63)$$

and $\dot\zeta$ is given by equation (10). These fields can be seen
in Figs. 24, 25, 26 and 27. The deformation is the same as
in the previous case.

As in the previous case, a tightening of the temperature
gradient has occurred by the 24 hour point, although not as
strong (Figs. 26-29). The front has moved farther to the
north and the tilt is smaller than in Case B. Throughout
the next 24 hours, the front continues to move to the north
and passes over the mountain ridge (Figs. 30-33). The
gradient weakens as the front passes over the ridge and the
tilt is negligible. In this experiment, the front weakens
because it is advected away from the frontogenetic part of
the deformation field.

D. MOUNTAIN WITH MOVING DEFORMATION

The next four cases to be considered start with the same
initial conditions as in Case C (Figs. 24, 25, 26 and 27).
However, in these cases, the deformation moves to the north
at a speed of 10 m/sec. Each case examines a different
starting place for the maximum northward deformation flow.
The cases have the maximum flow over the valley, on the
upslope side of the mountain, directly over the ridge, and
on the downslope side of the mountain.

Fig. 24. θ(K). Initial. Deformation and mountain

54
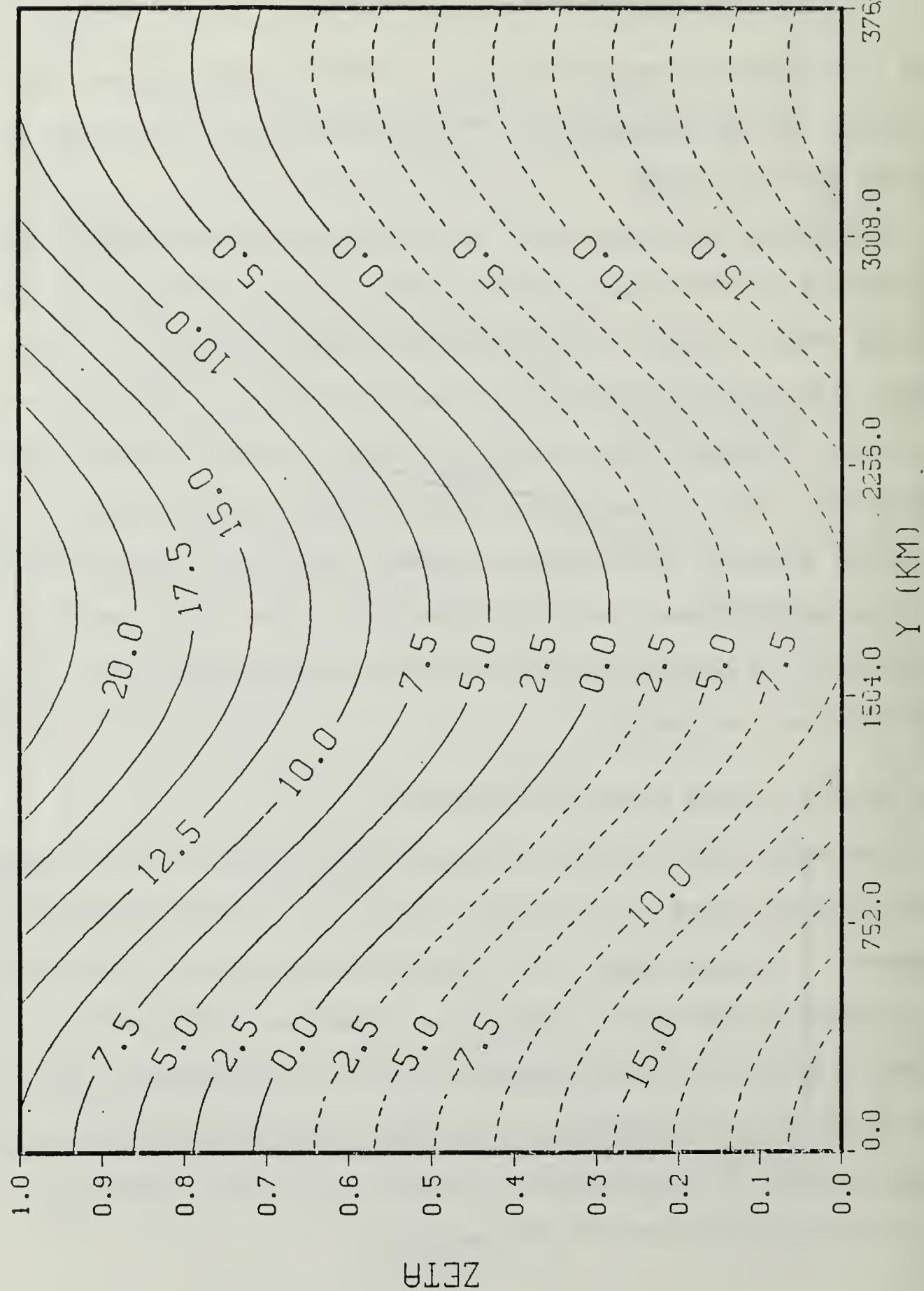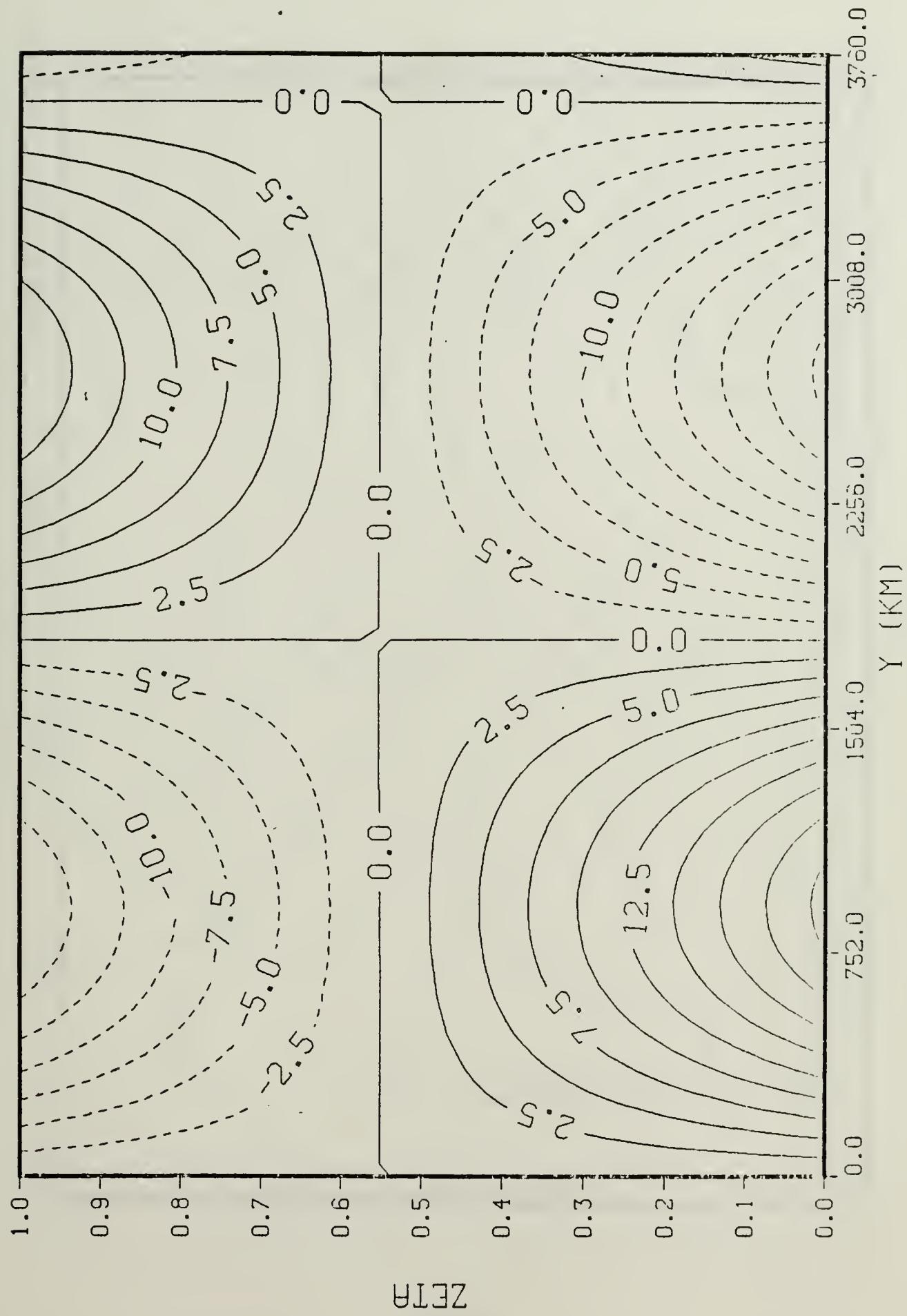
Fig. 25. u (m/sec). Initial. Deformation and mountain

55

Fig. 26. θ(K). 24 hours. Deformation and mountain

56
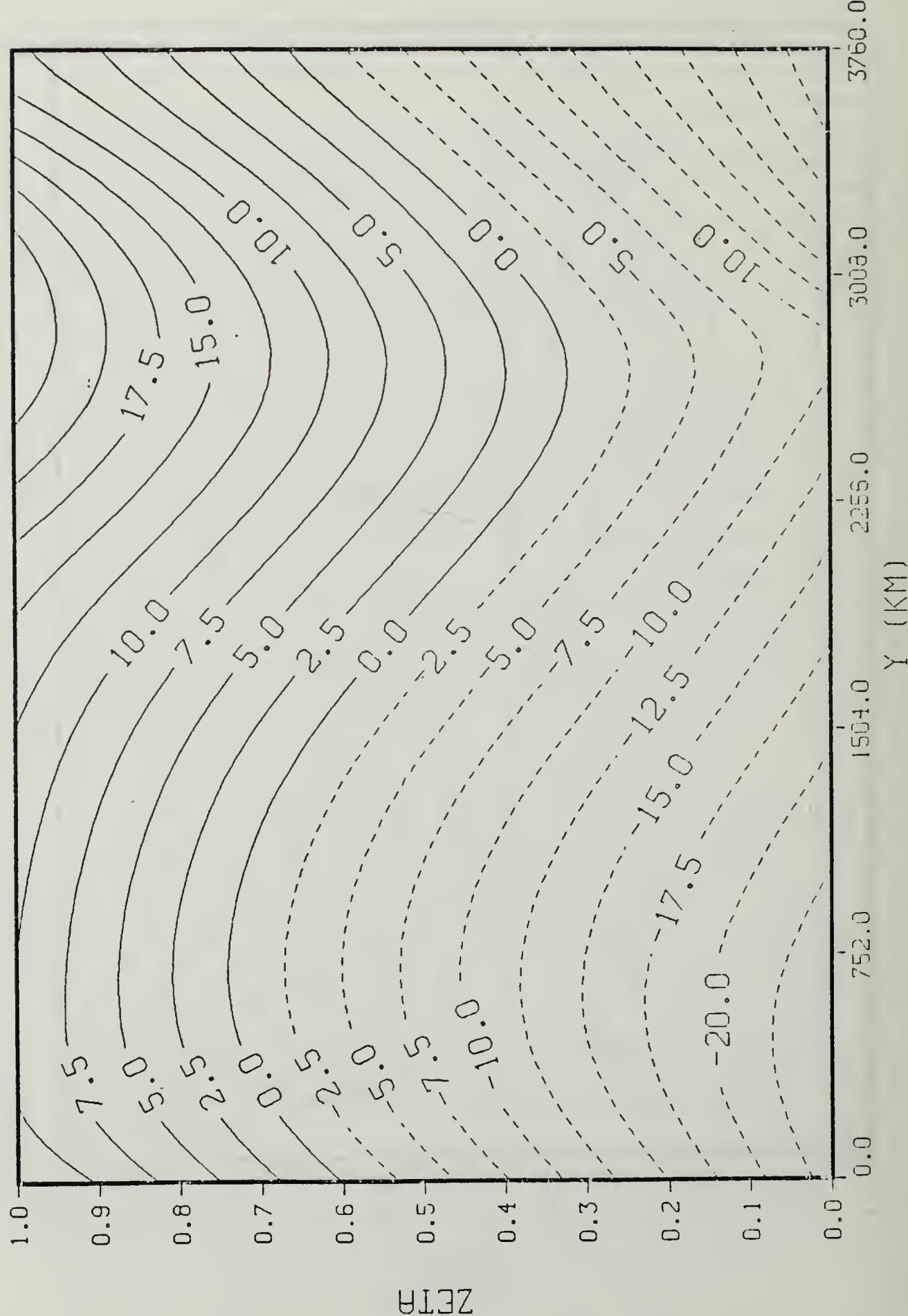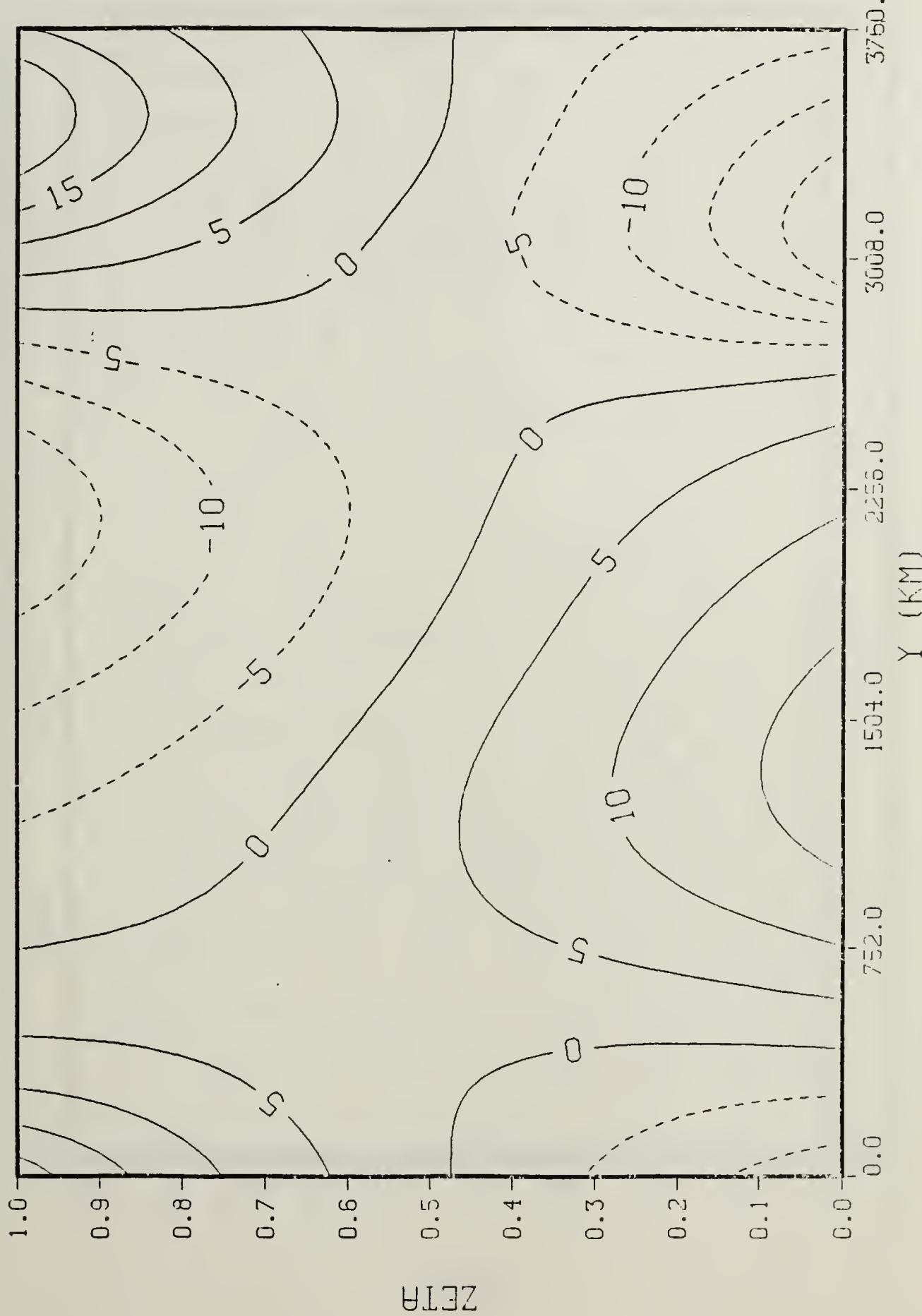
Fig. 27. u (m/sec). 24 hours. Deformation and mountain

57
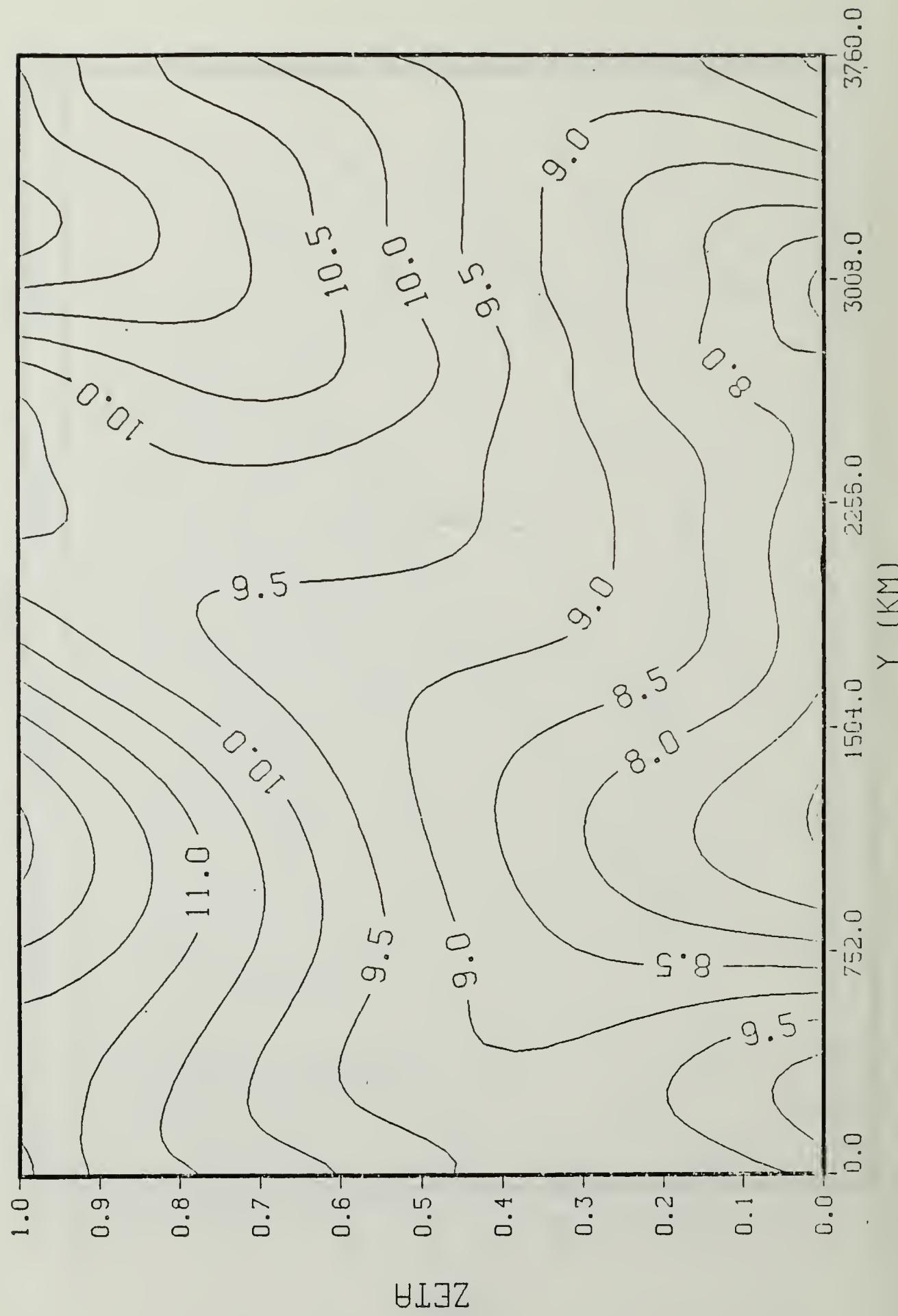
Fig. 28. v (m/sec). 24 hours. Deformation and mountain

58
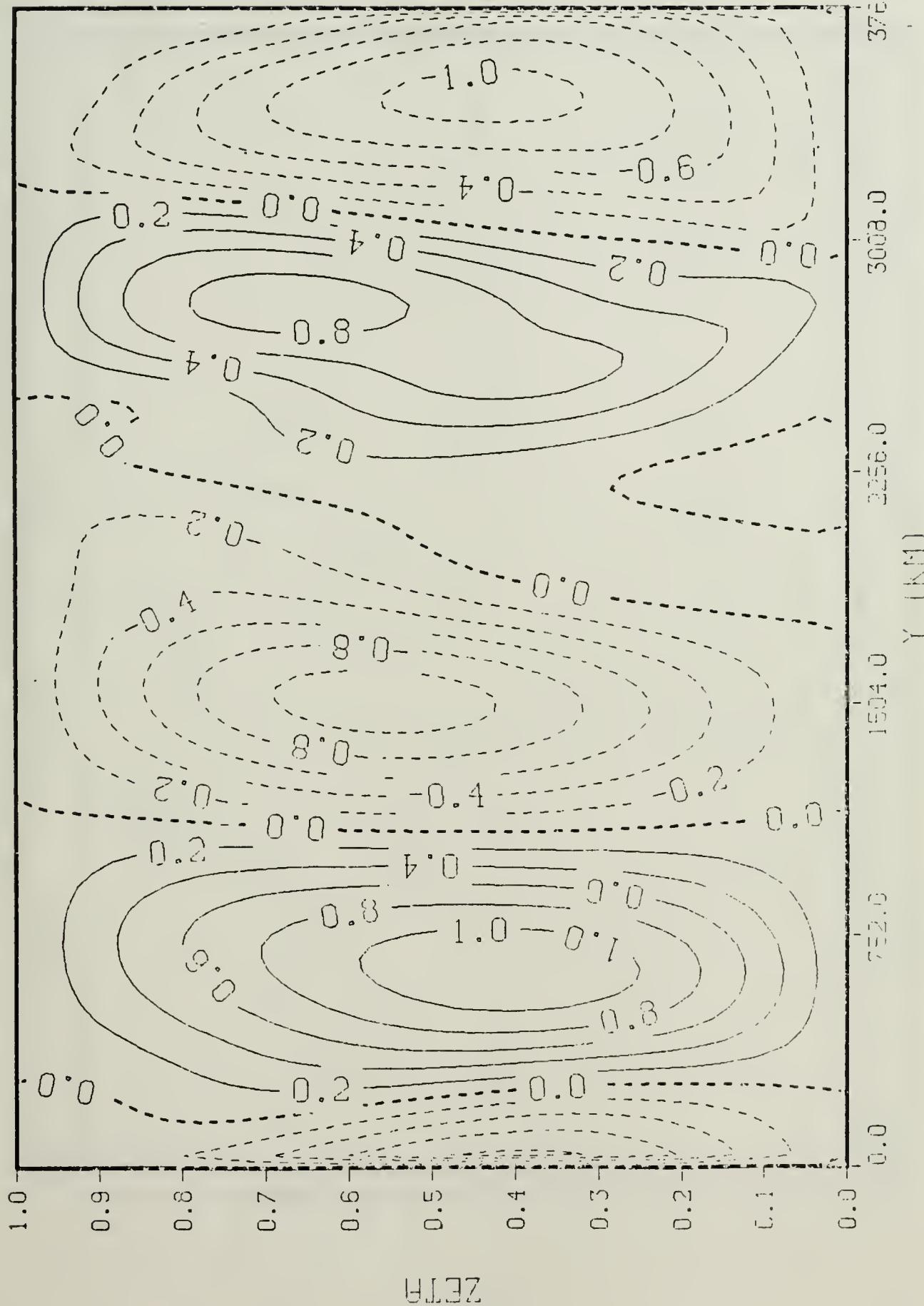
Fig. 29. $\dot{\zeta}$ ($\times 10^{-6}$ sec^{-1}). 24 hours. Deformation and mountain.

Fig. 30. θ(K). 48 hours. Deformation and mountain

60
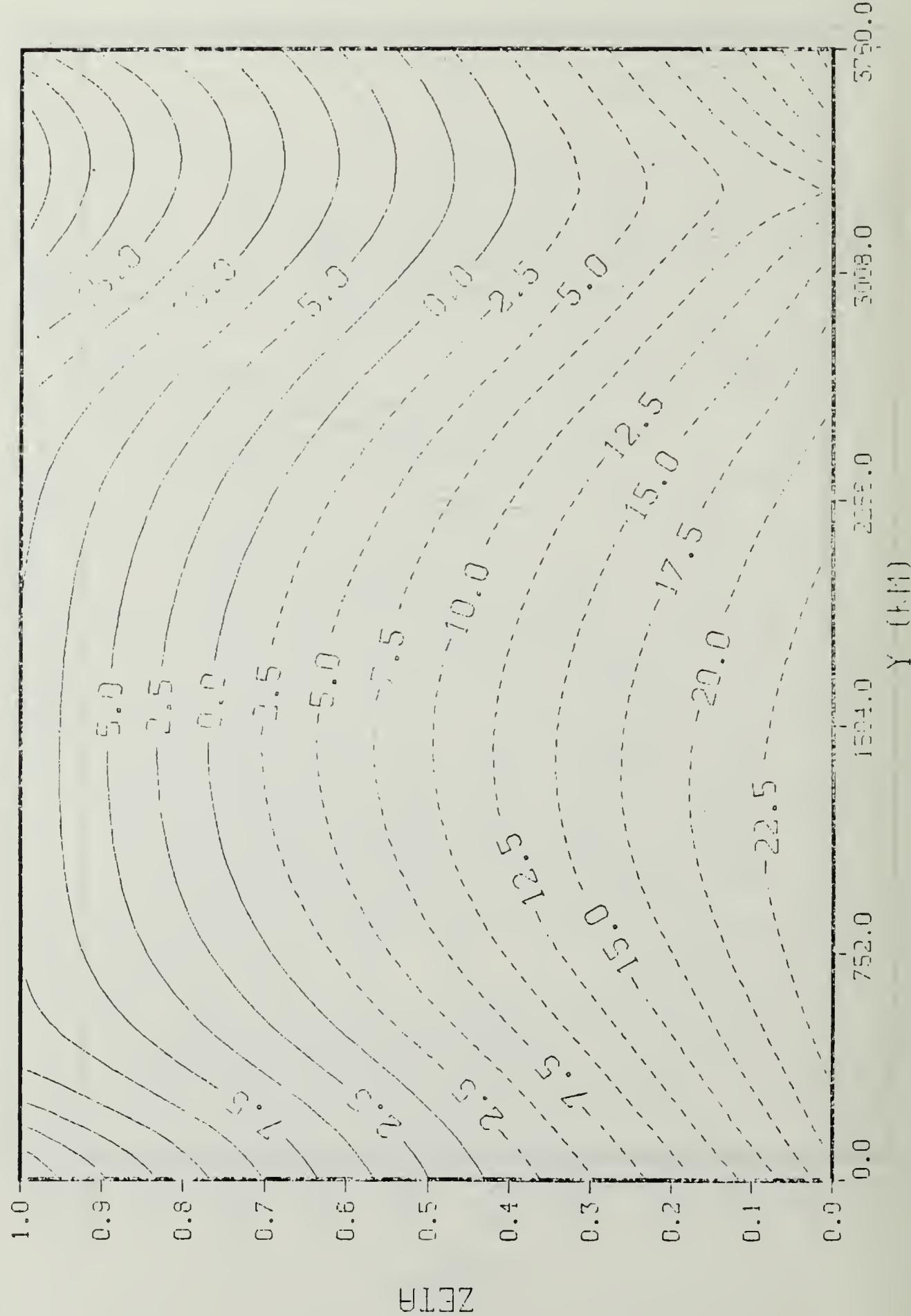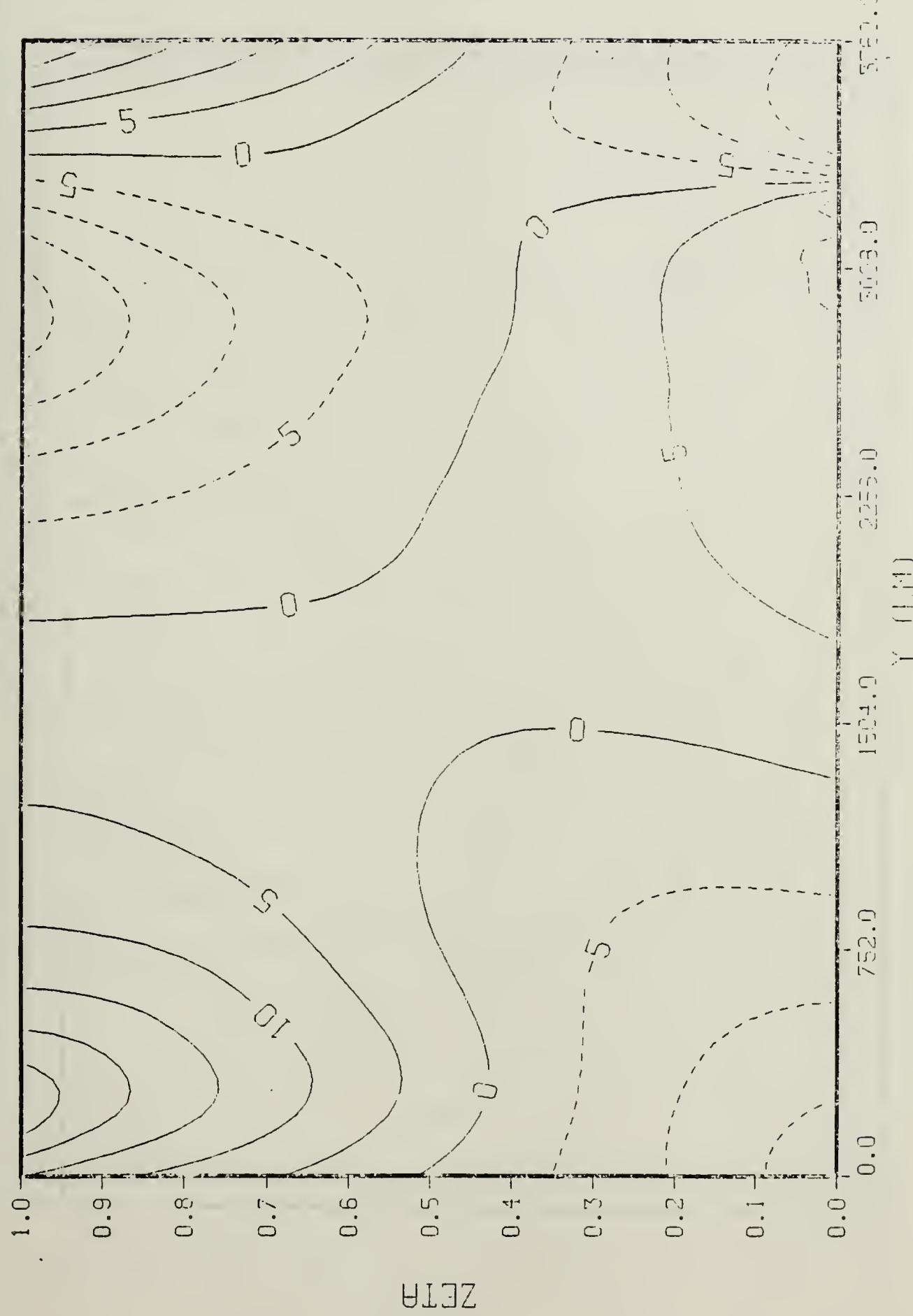
Fig. 31. u (m/sec). 48 hours. Deformation and mountain

Fig. 32. v (m/sec). 48 hours. Deformation and mountain

62
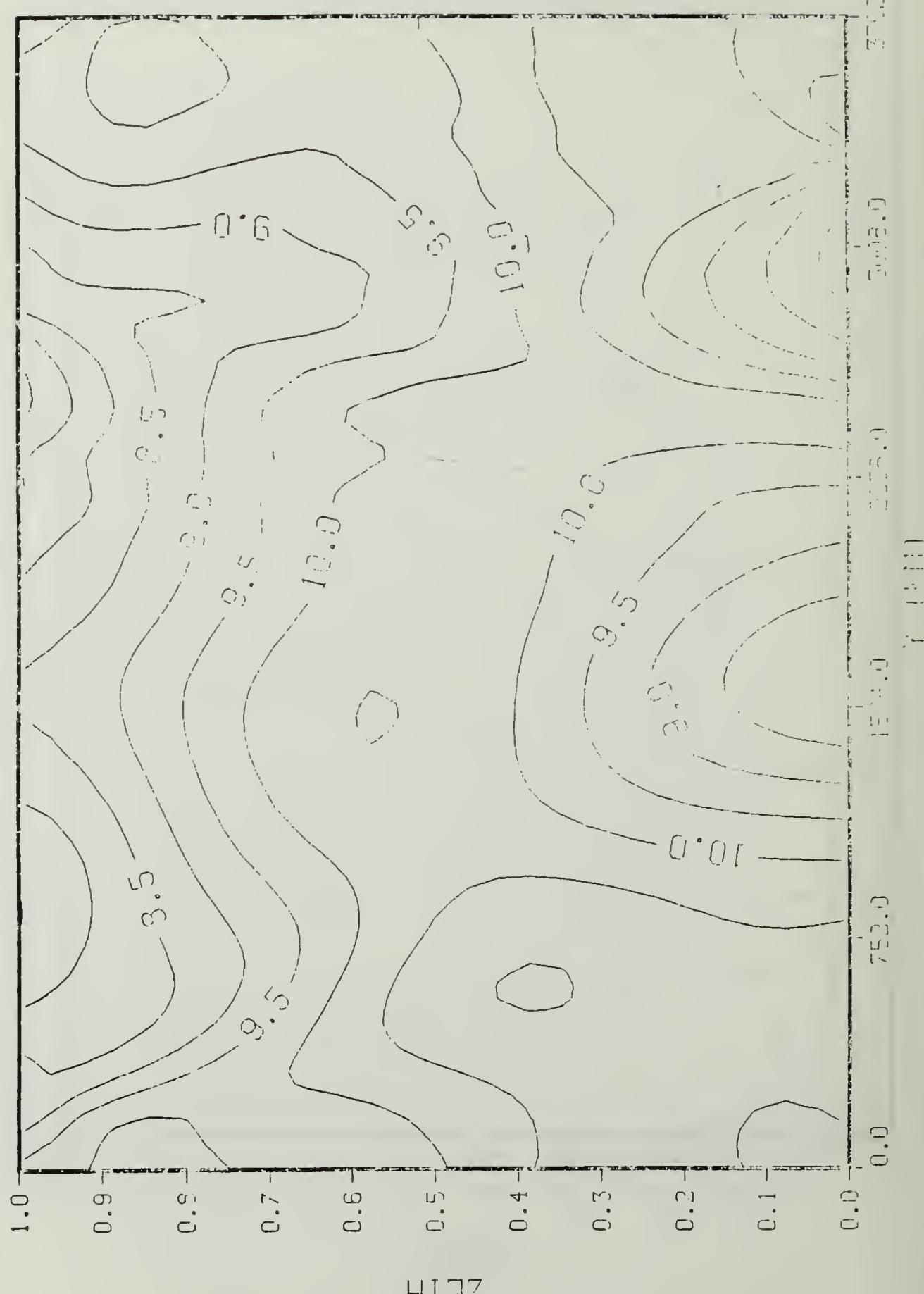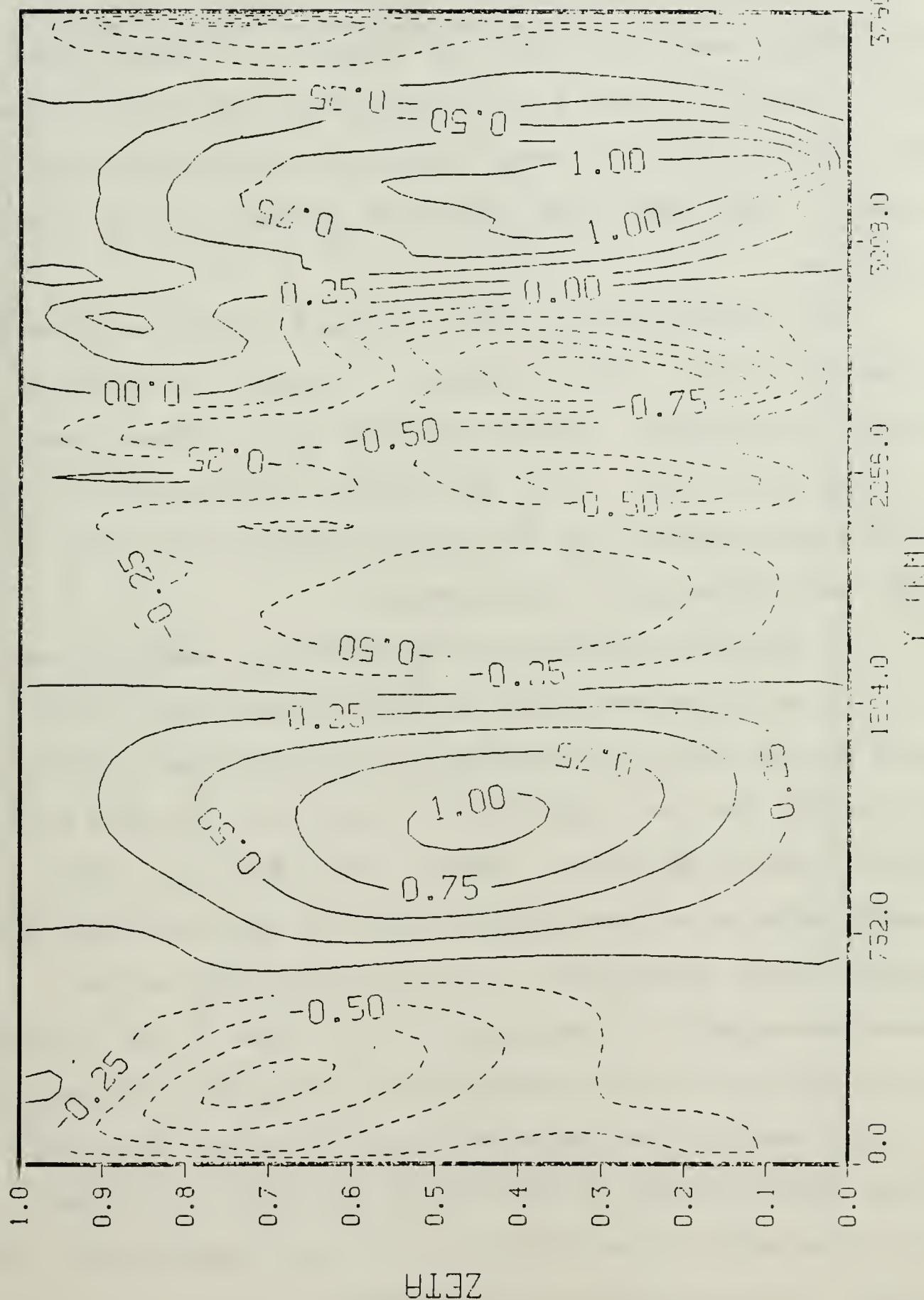
Fig. 33. $\dot{\zeta}$ ($\times 10^{-6}$ sec^{-1}). 48 hours. Deformation and mountain

63

1. Maximum Deformation over the Valley

The initial deformation is shown in Fig. 15. As in the previous cases, the front has formed by 24 hours (Figs. 34-37). There is a small tilt toward the colder air in the north and the front has moved farther up the mountain than in Case C. The upper level front has passed over the mountain ridge.

As the deformation flow continues to move northward, so does the front. During the next 24 hours, the speed of the front slows down, but the gradient in the temperature field tightens (Figs. 38-41) and forms a discontinuity. The cyclonic shear around the front has increased and there is strong vertical motion in that region.

A careful comparison of the potential temperatures at t = 24 hours between Figs. 24 and 34 shows very little change between the flat experiment and the mountain experiment, except for the translation in Fig. 34. The same conclusion holds at 48 hours. Bannon (1983,1984) has shown that mountain effects on frontogenesis will be important when the mountain forced convergence is of the same order as the frontal convergence. Comparison of v in Figs. 6 and 18 shows that the mountain forced convergence is only about 25 percent of the mountain forced convergence at 24 hours. This ratio is even smaller later in the frontal evolution. With the large scale mountain used in this and later experiments, the effects of the topography are unimportant.
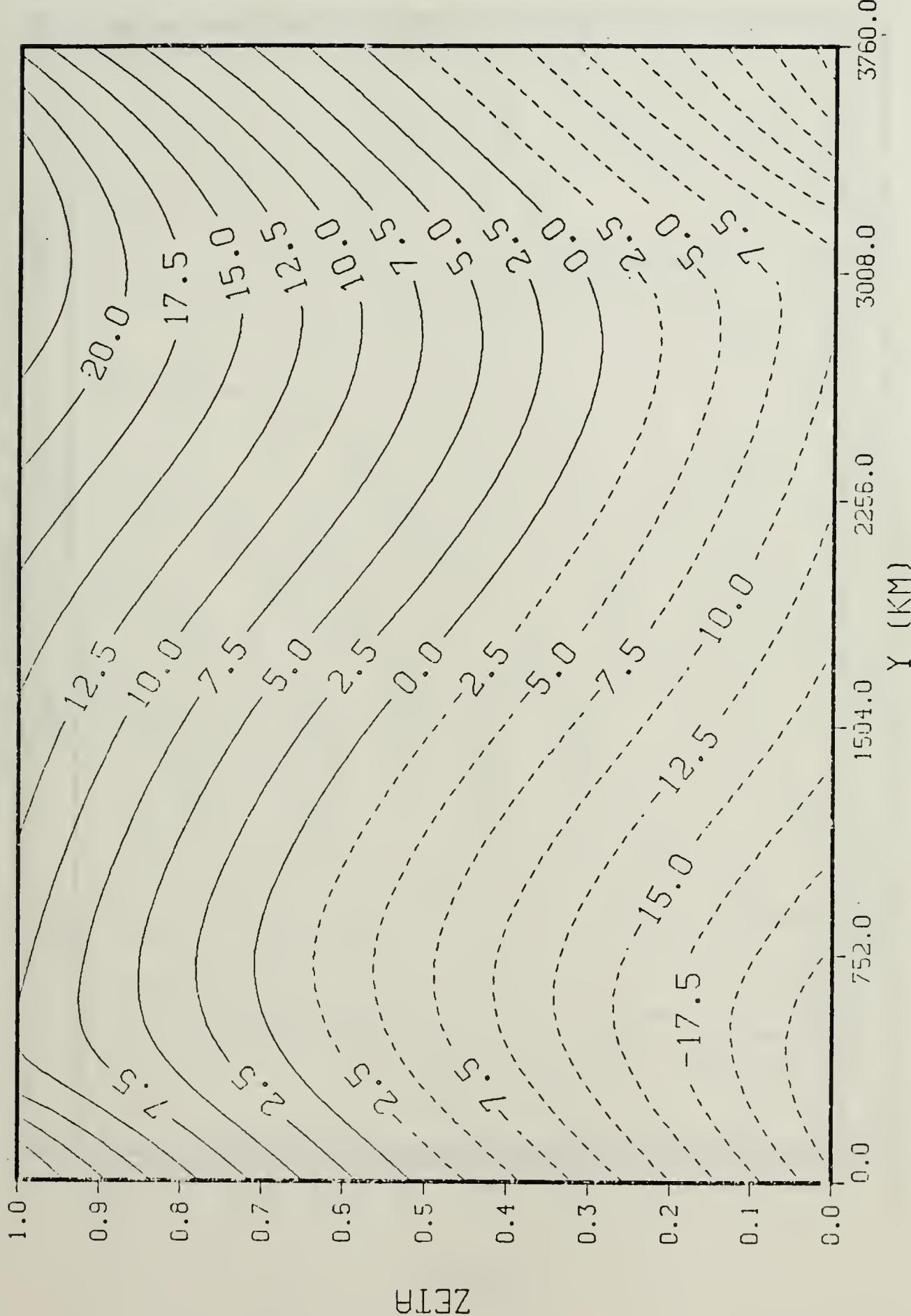
Fig. 34. θ(K). 24 hours. Maximum deformation over valley
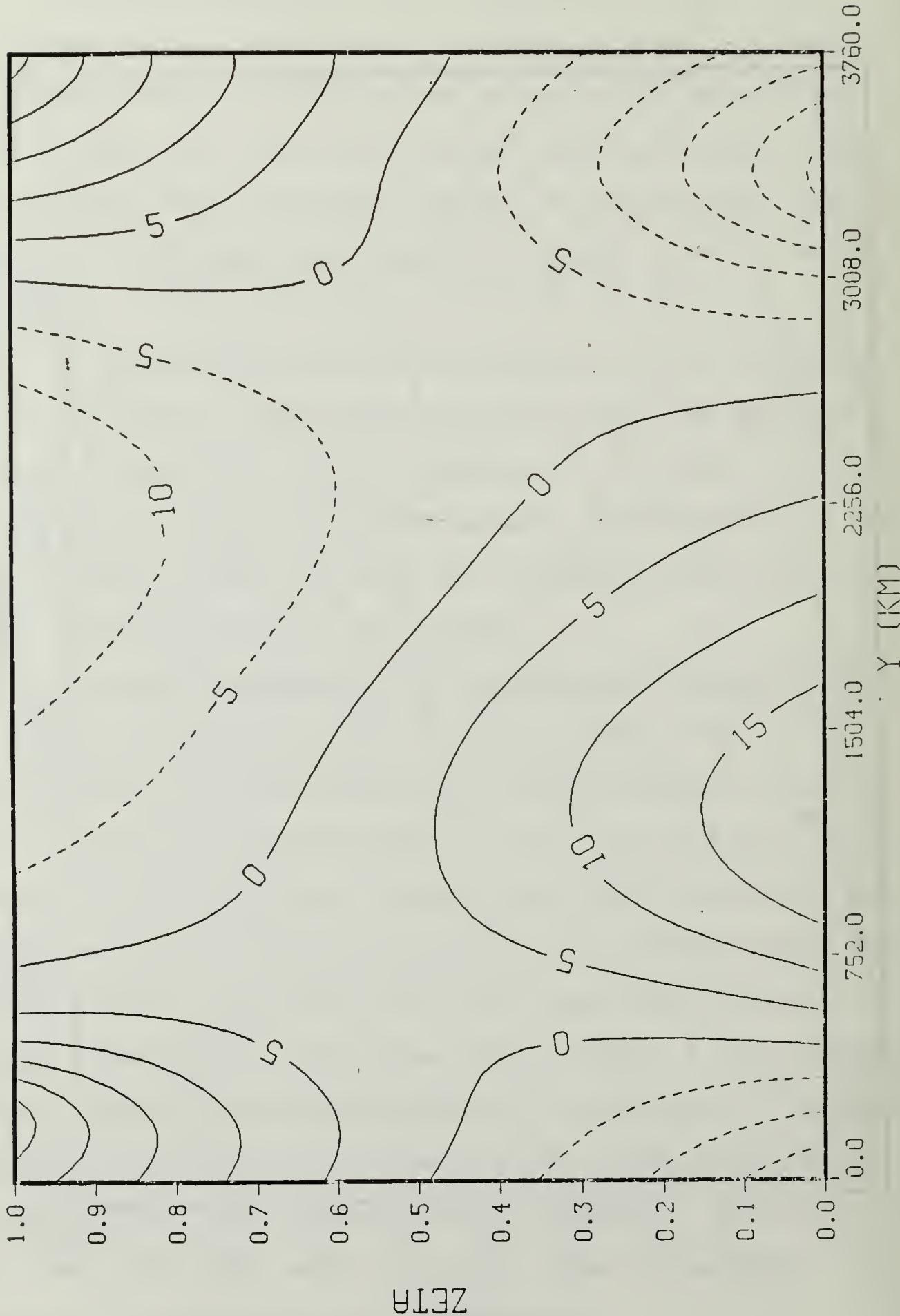
Fig. 35.   u (m/sec).   24 hours.   Maximum deformation over valley

66
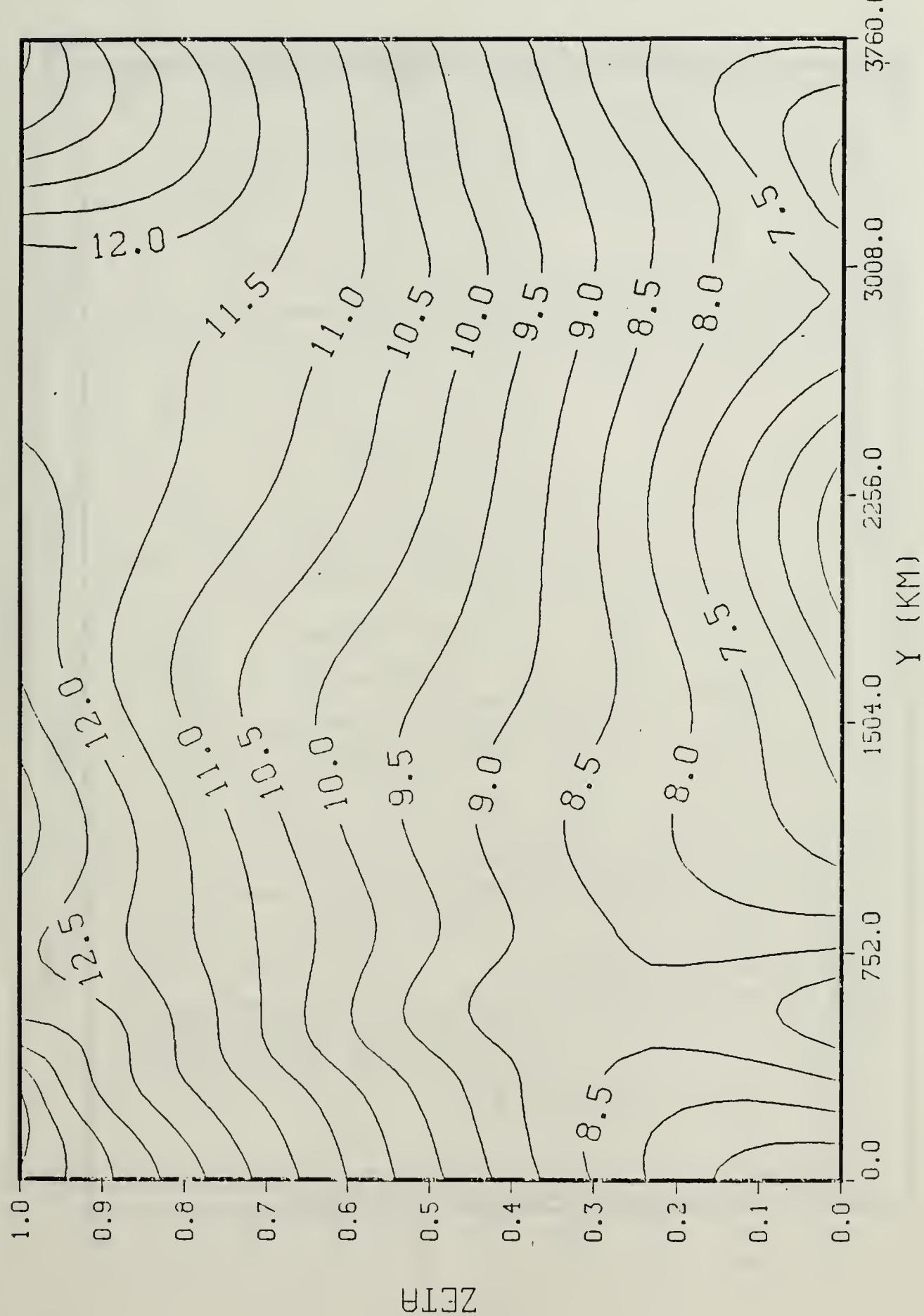
Fig. 36. v (m/sec). 24 hours. Maximum deformation over valley

67
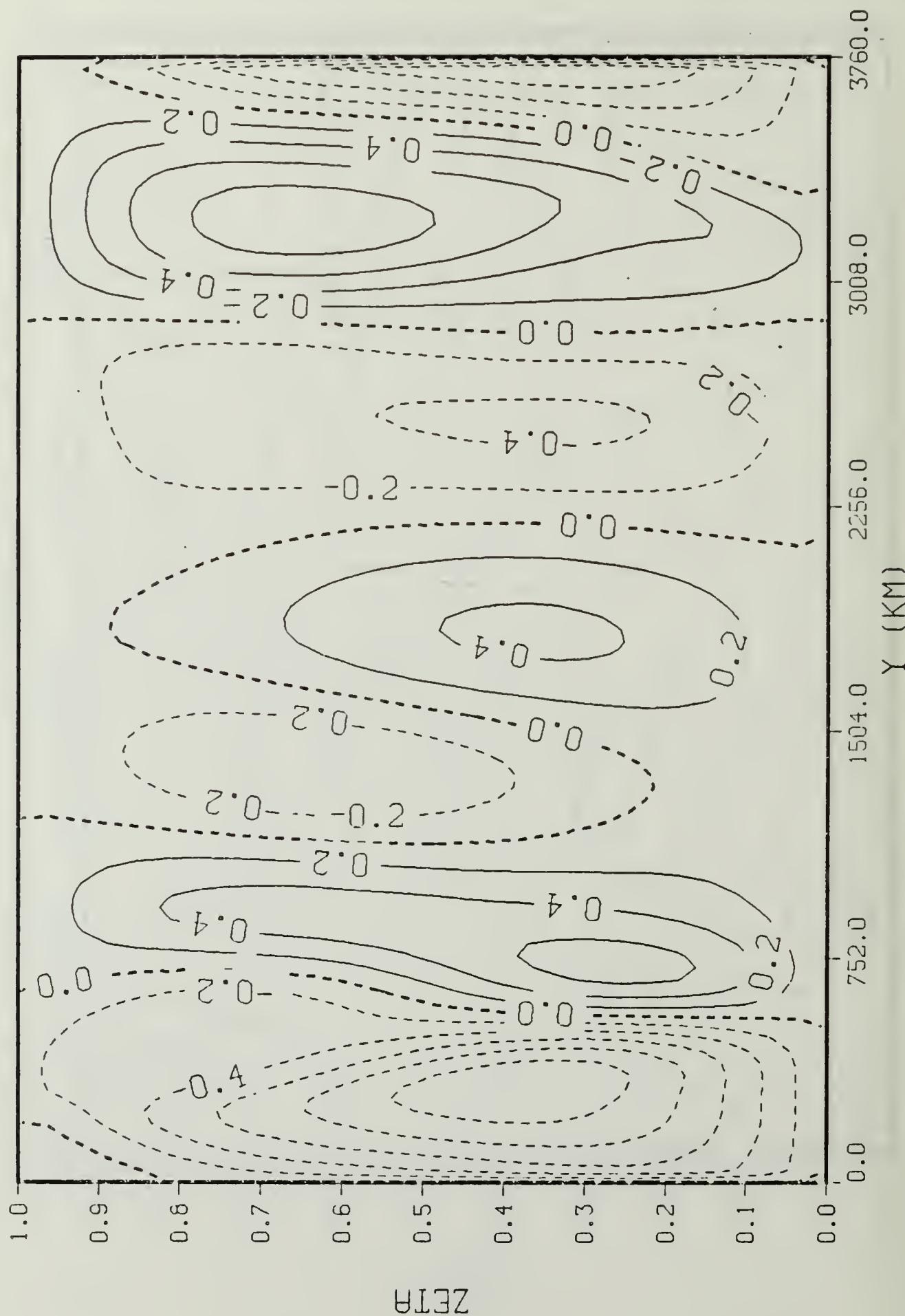
Fig. 37. $\dot{\zeta}$ ($\times 10^{-6}$ sec^{-1}). 24 hours. Maximum deformation over valley

68
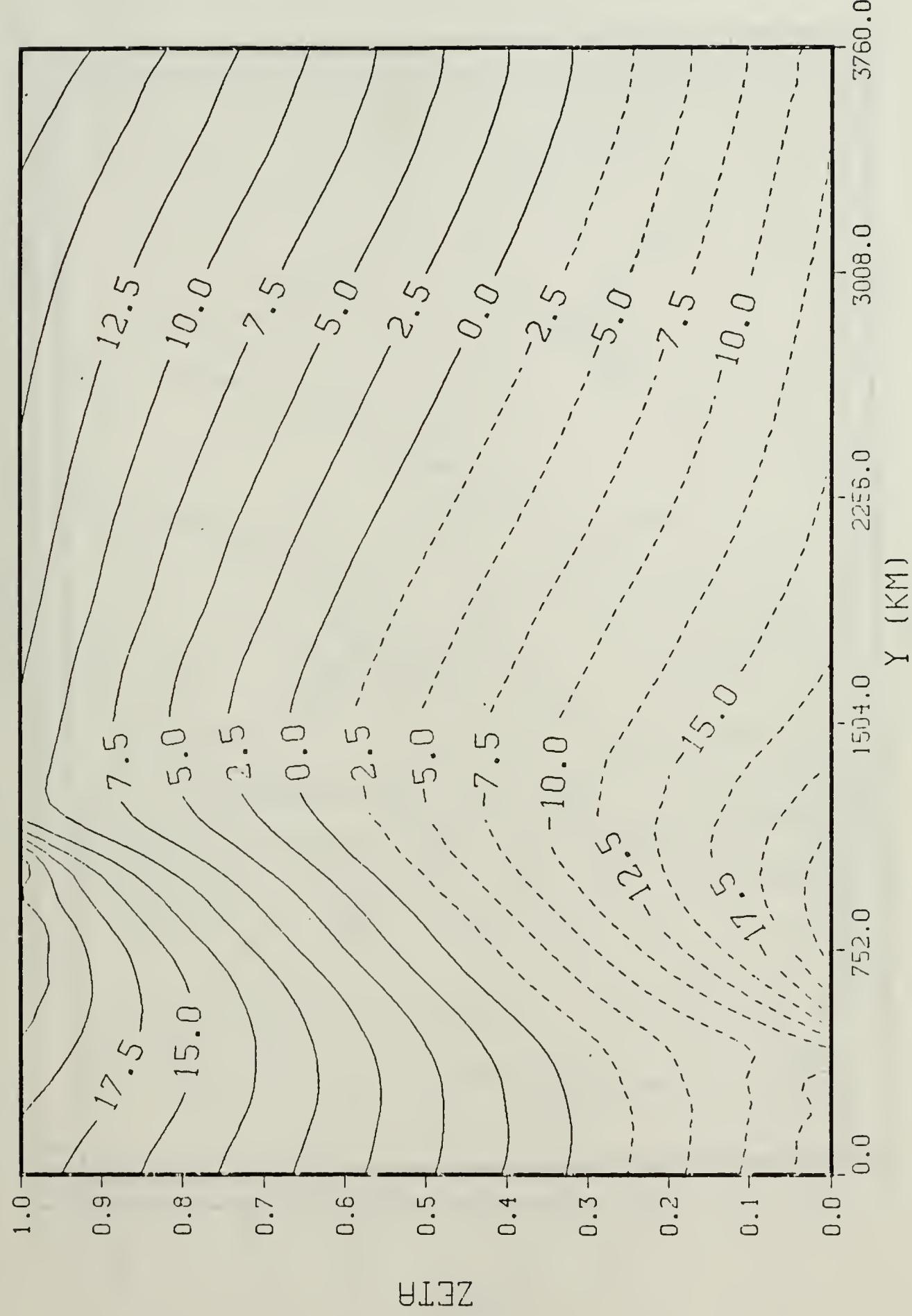
Fig. 38. θ(K). 48 hours. Maximum deformation over valley

69
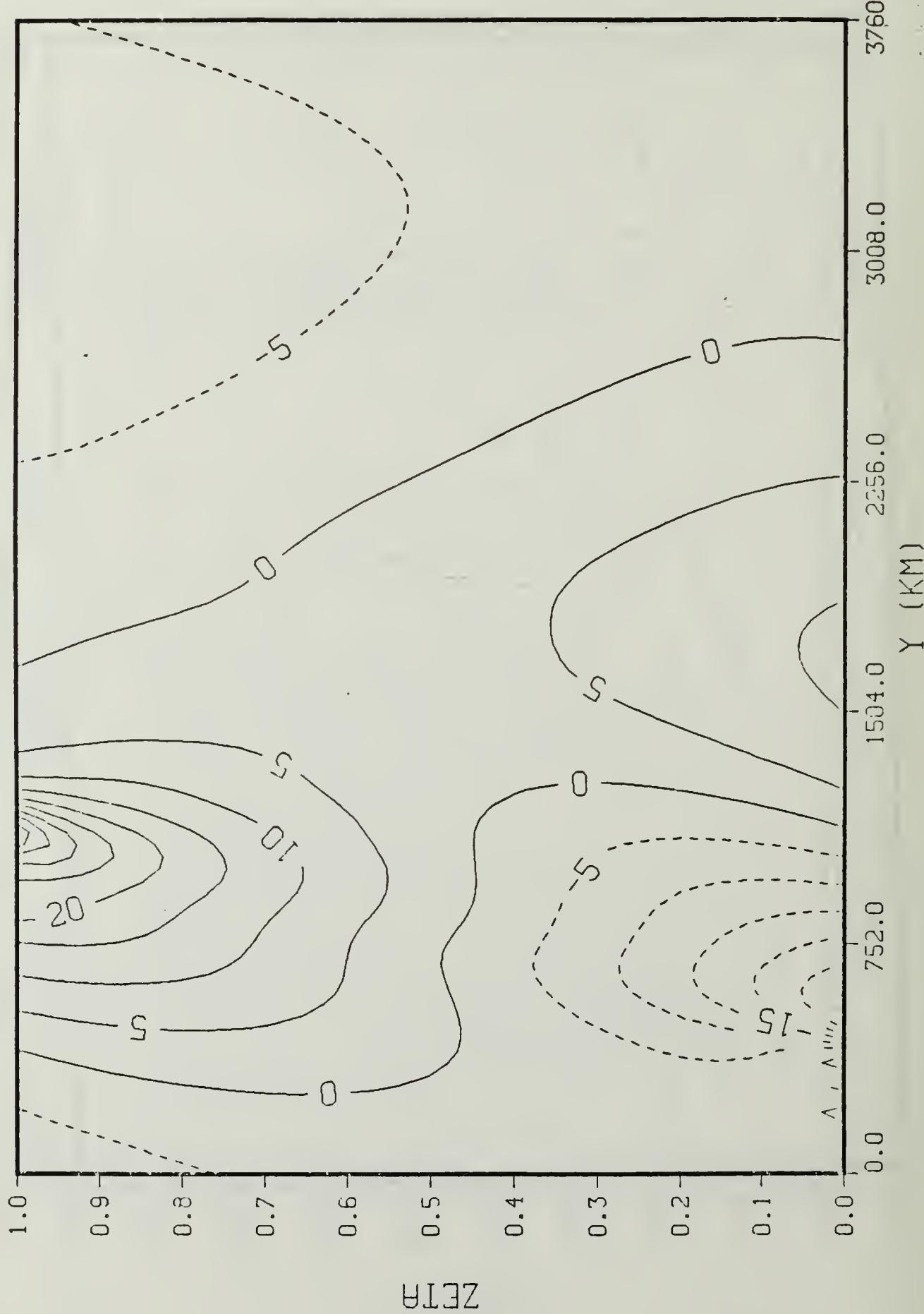
Fig. 39. u (m/sec). 48 hours. Maximum deformation over valley

70
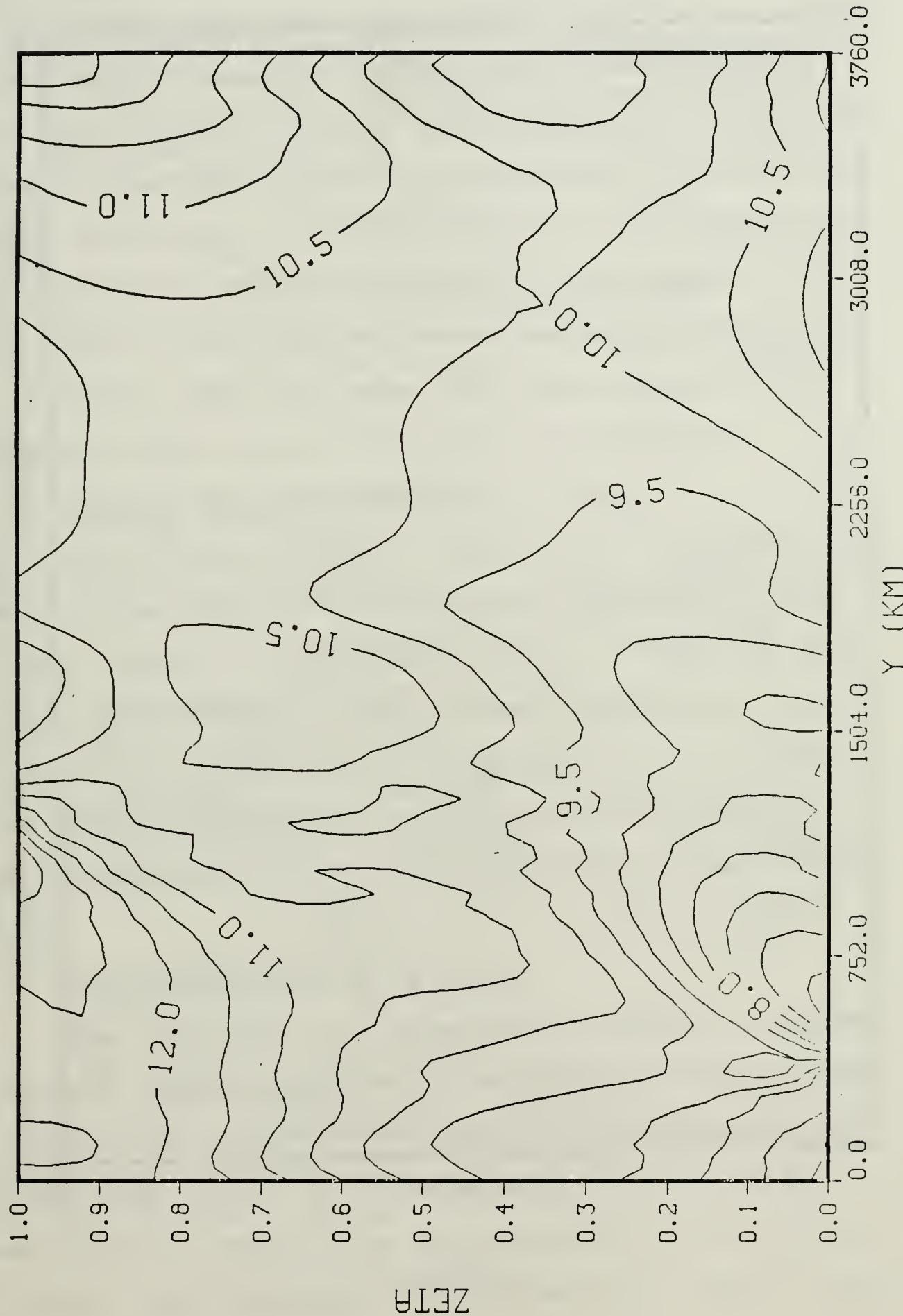
Fig. 40. v (m/sec). 48 hours. Maximum deformation over valley

71
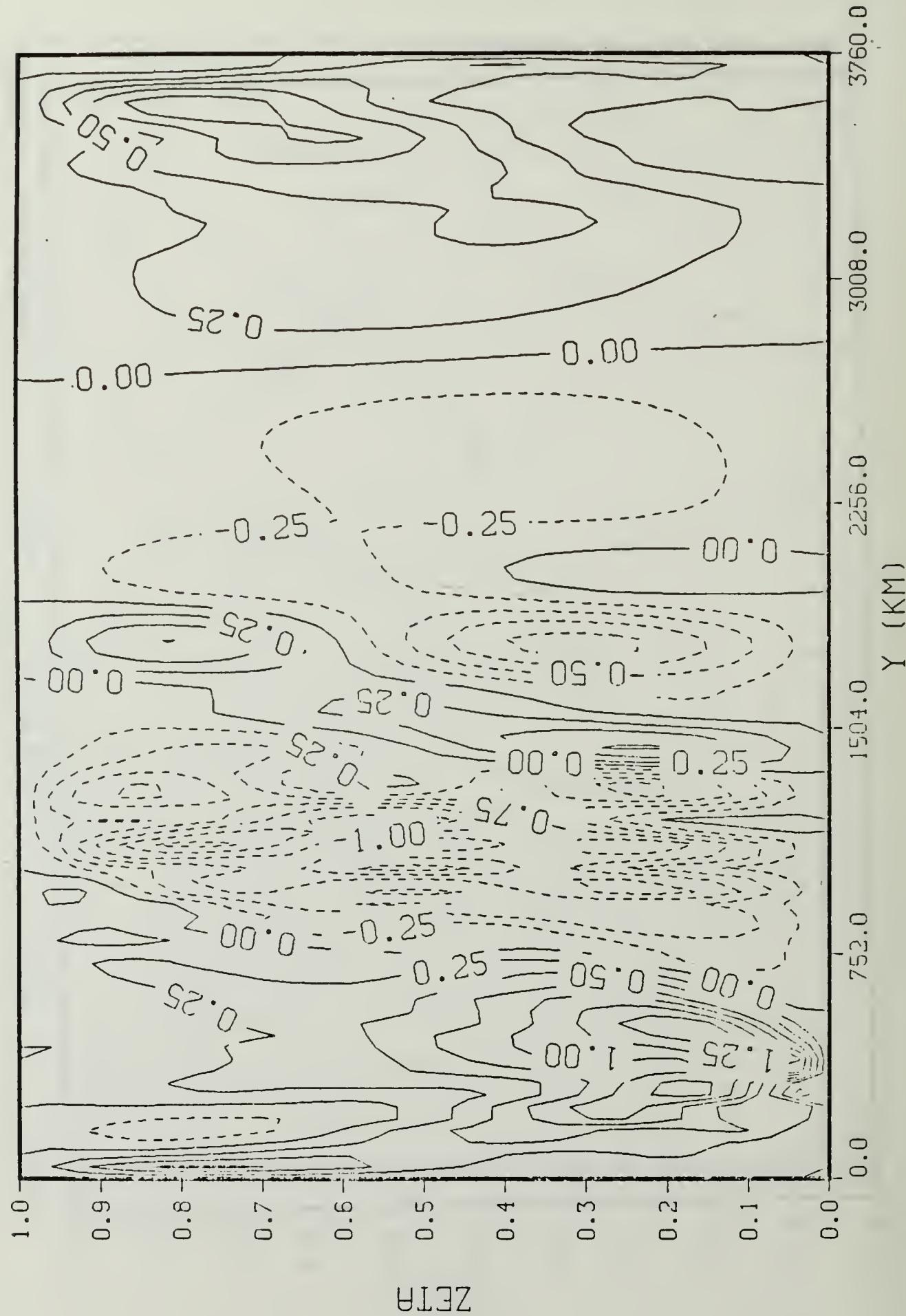
Fig. 41. $\dot{\zeta}$ ($\times 10^{-6}$ sec^{-1}). 48 hours. Maximum deformation over valley

72

2. Deformation Shifted One-Quarter Wavelength

In this experiment, the deformation field is shifted one-quarter of a wavelength to the north with respect to the initial fields (Fig. 42). The topography is also unimportant in this experiment. At t = 24 hours, there is only a slight indication of frontal formation in the temperature field, but a much stronger suggestion of the front in the u field. The u field, however, shows little tilt (Figs. 43-46). Williams (1968) has shown that this phasing of the deformation field is inefficient for frontogenesis.

3. Reversed Deformation Field

As is shown in Fig. 47, the initial deformation flow is in opposite phase with the original deformation field. The front can be seen at 24 hours in Figs. 48-51. As with previous cases, the front tilts toward the cold air, but in this case, the tilt is toward the south. This is a result of the reversed deformation field. The fields are mirror images of the fields in the basic experiment except for the shift.

4. Deformation Reverse of Case 2

The last case to be considered is the one in which the maximum deformation flow is the reverse of Case 2 (Fig. 52). The first indication of frontal activity can be seen 24 hours later (Figs. 53-56) especially in the u field. Strong cyclonic activity can be seen here with no evidence of a tilt. The temperature field shows only a small tightening
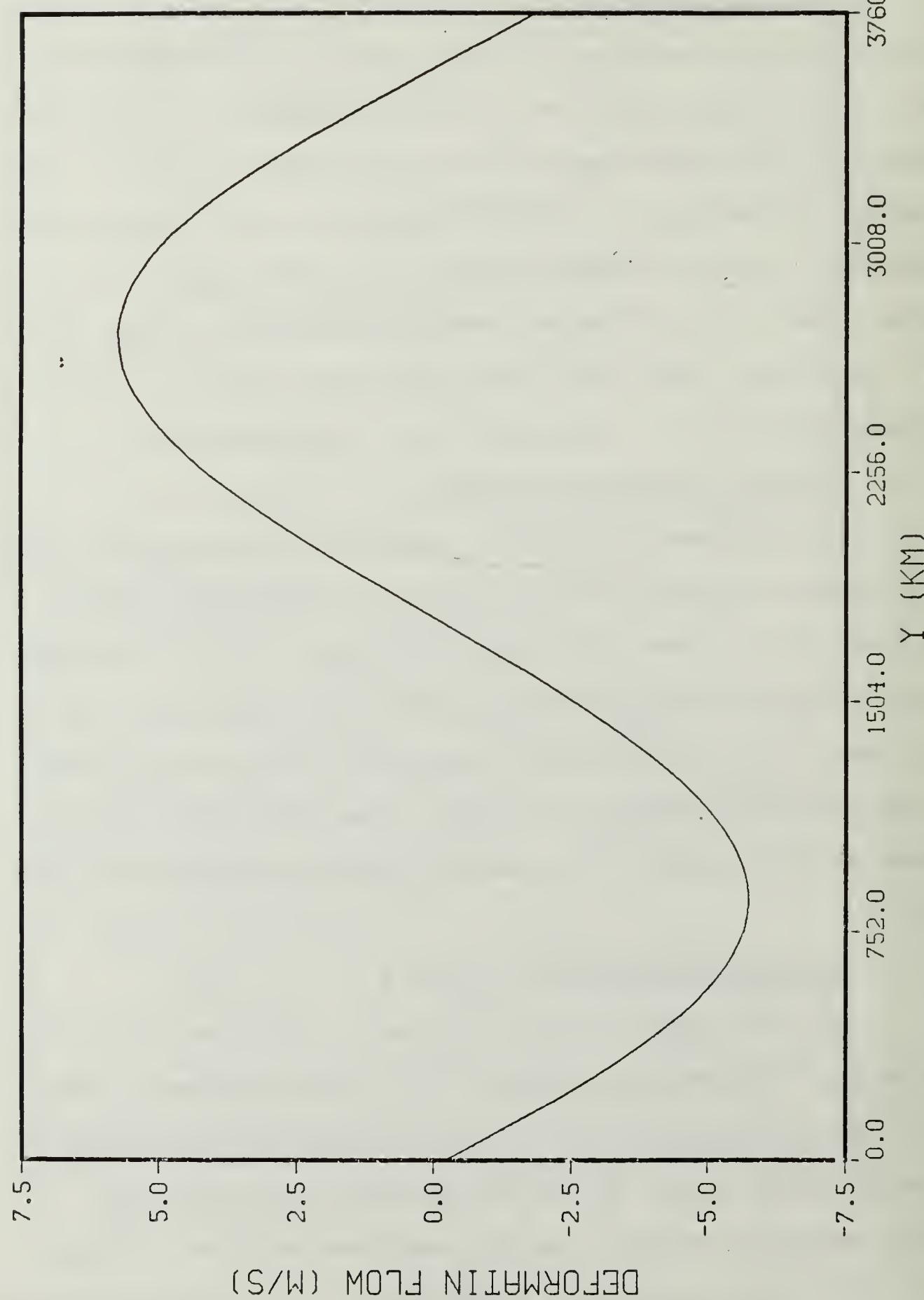
Fig. 42. Deformation when maximum is on the upslope side of the mountain.

74
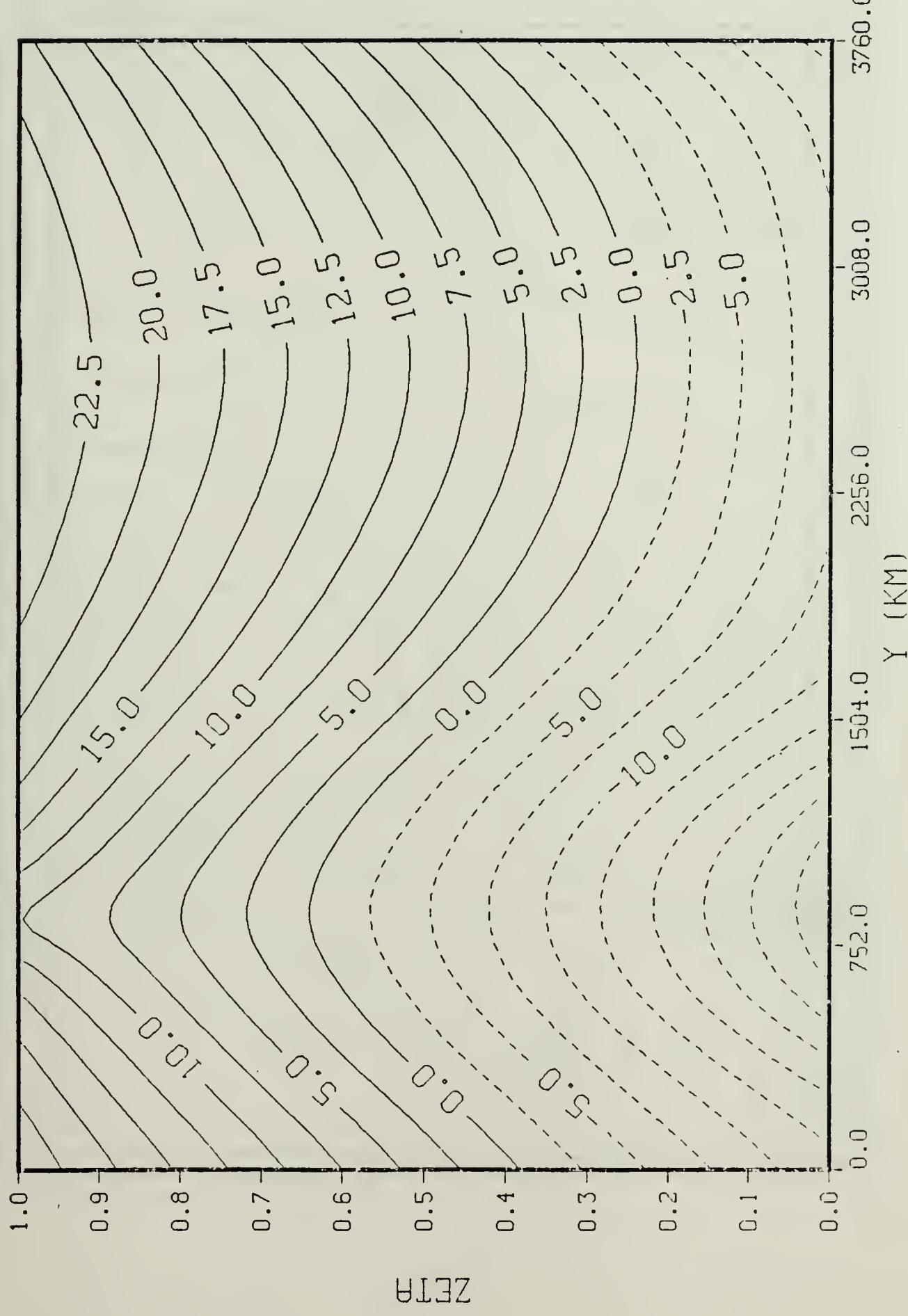
Fig. 43. θ(K). 24 hours. Deformation shifted 1/4 wavelength
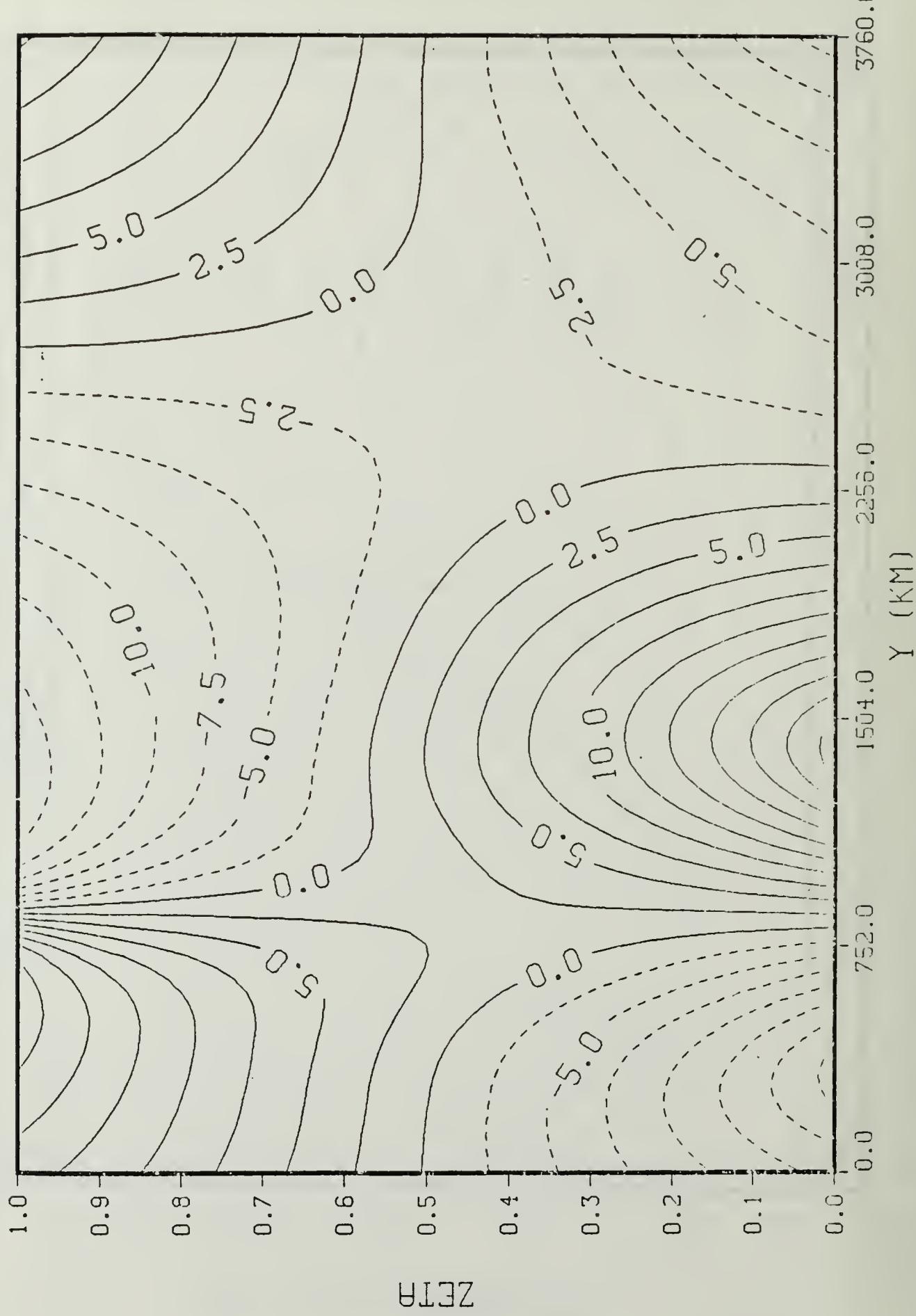
Fig. 44. u (m/sec). 24 hours. Deformation shifted 1/4 wavelength

76
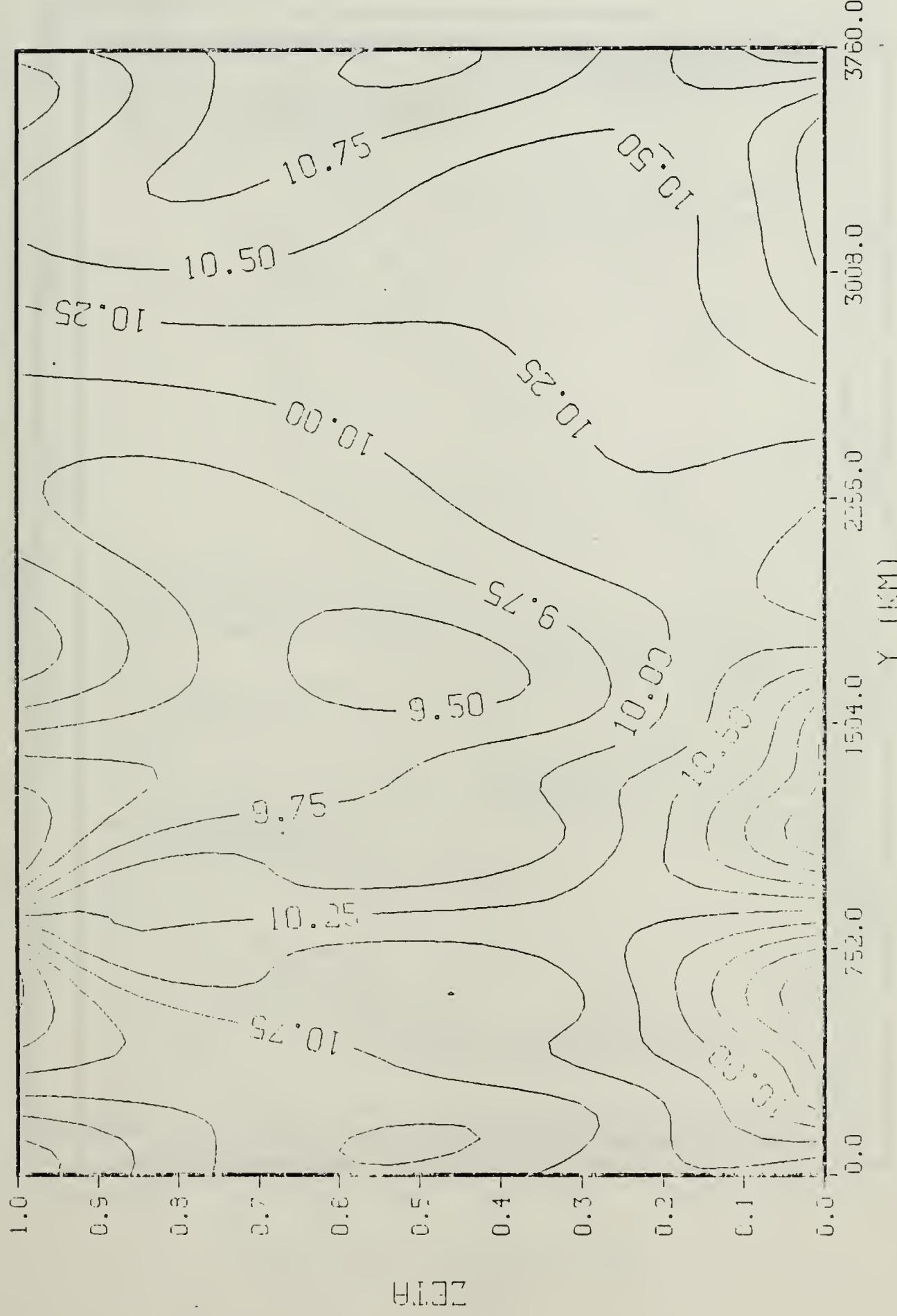
Fig. 45.   v (m/sec).   24 hours.   Deformation shifted 1/4 wavelength

77
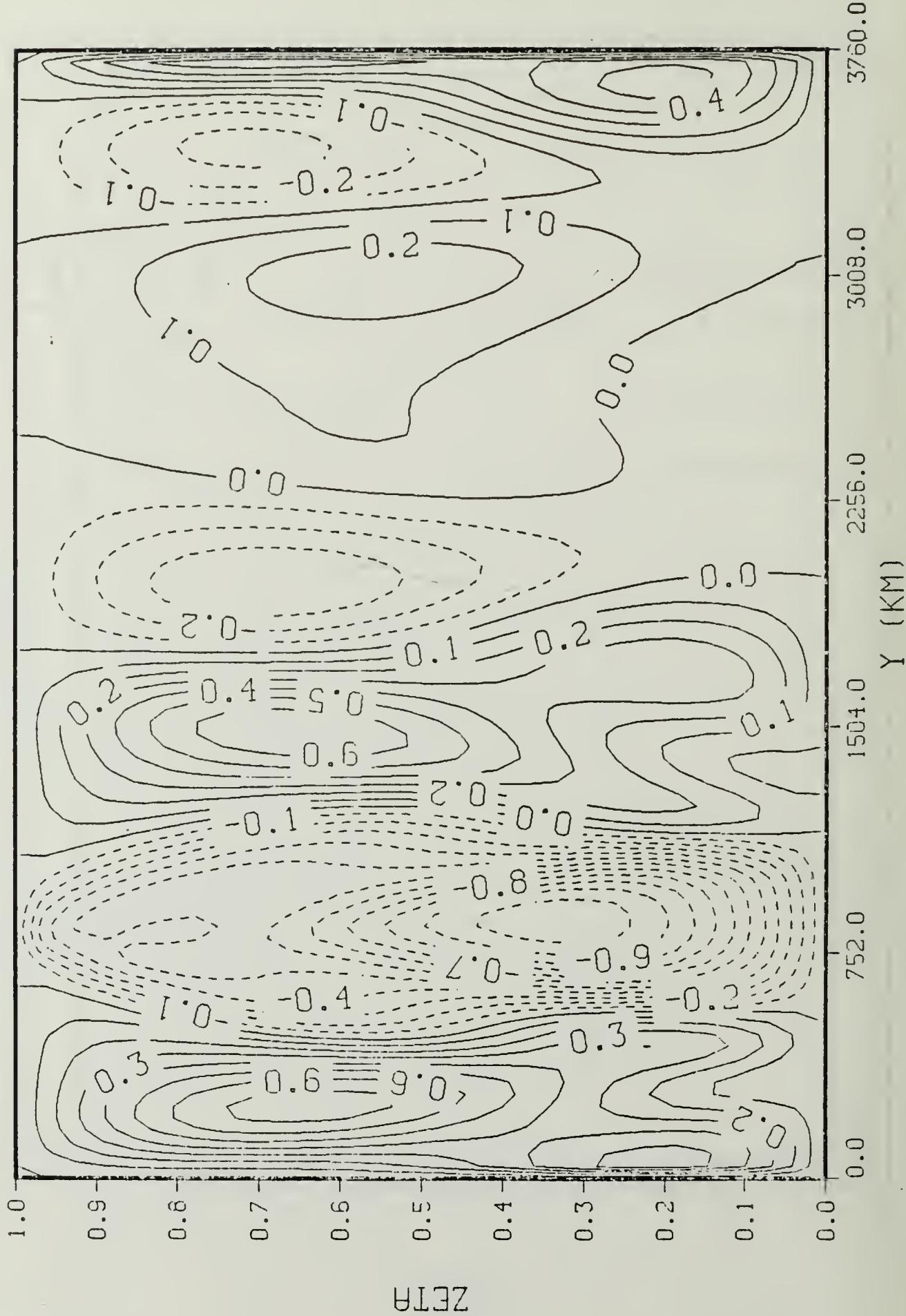
Fig. 46. $\dot{\zeta}$ ($\times 10^{-6}$ sec^{-1}). 24 hours. Deformation shifted 1/4 wavelength.

78
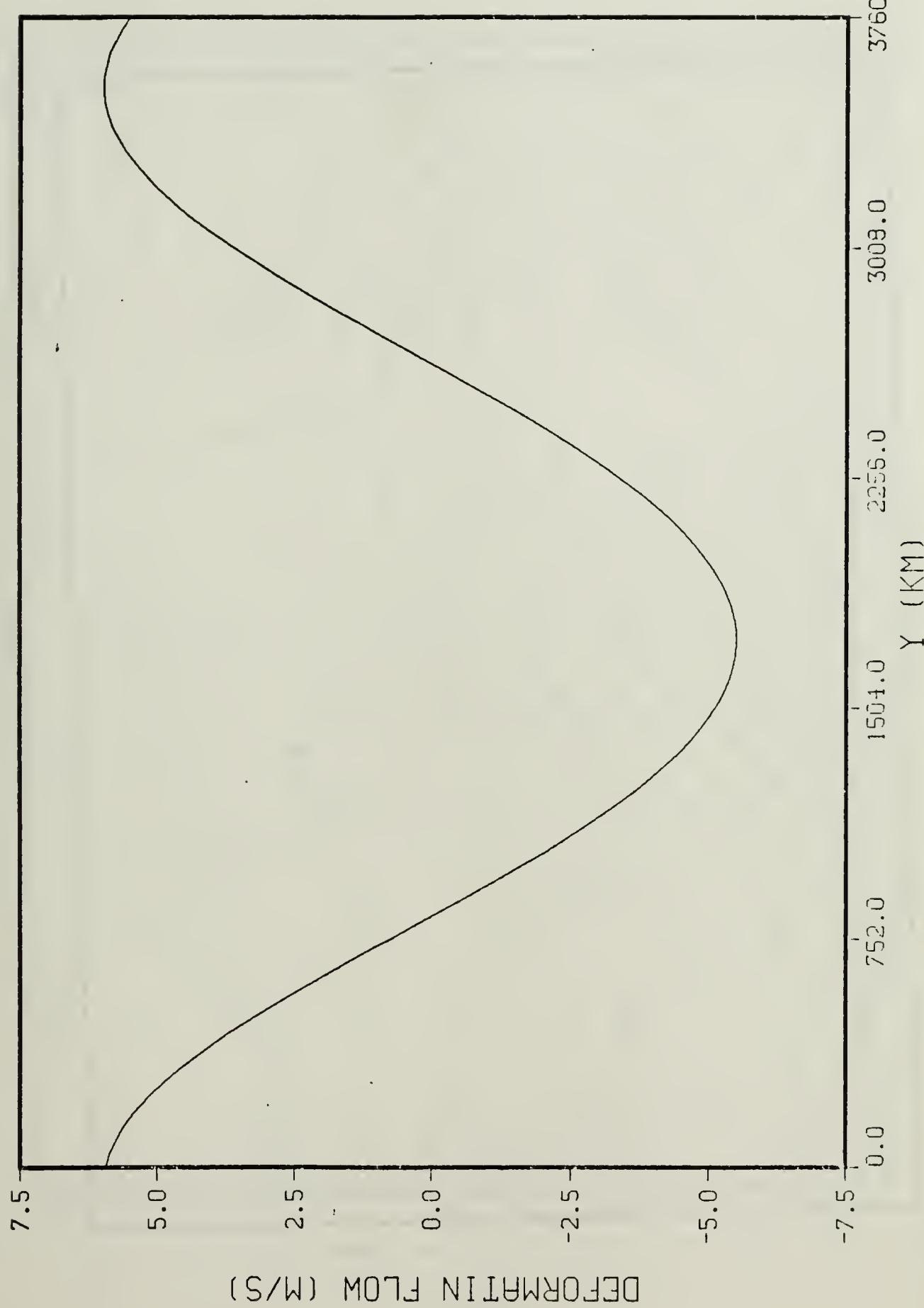
Fig. 47. Deformation flow when maximum is over the ridge

79
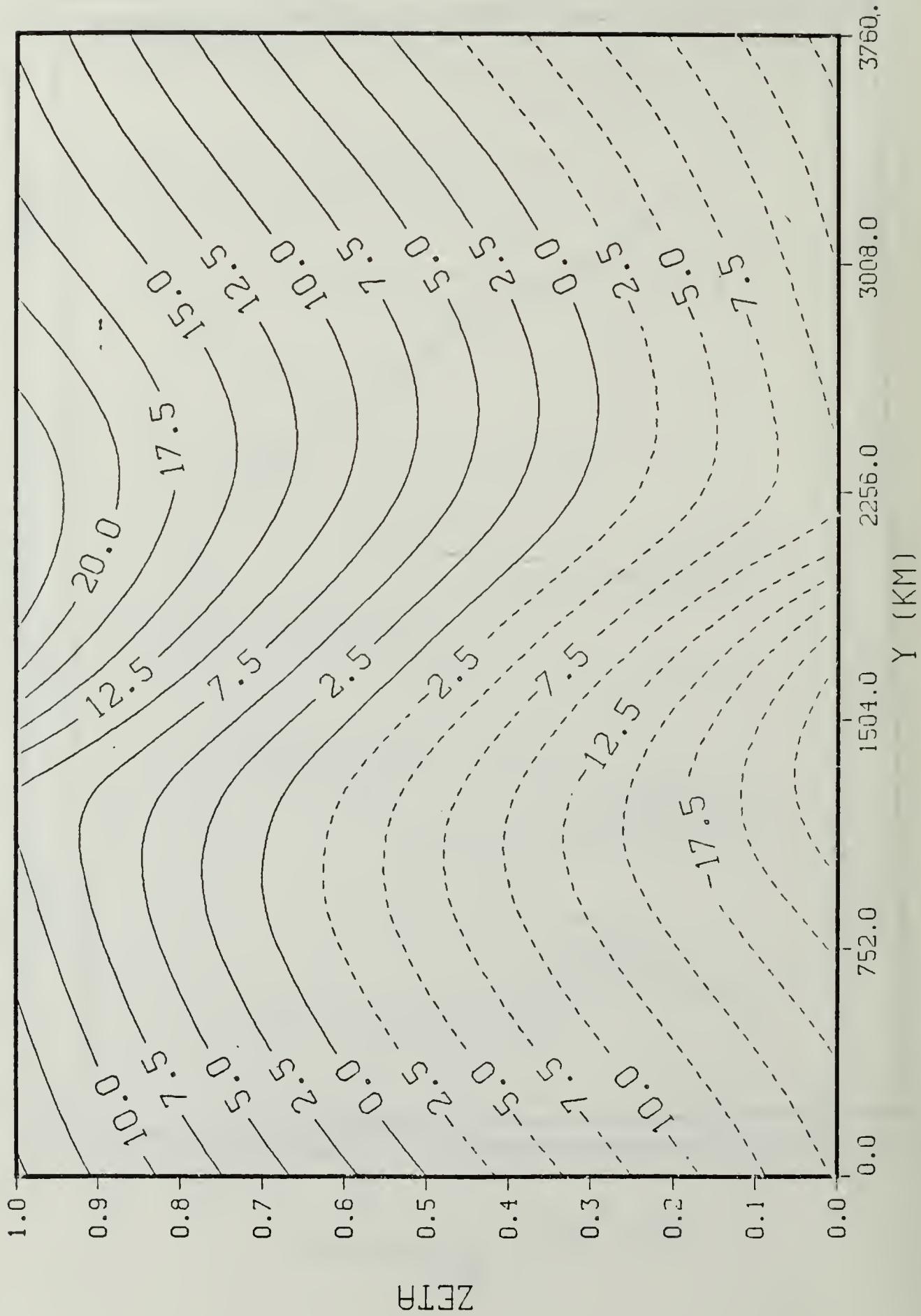
Fig. 48. θ(K). 24 hours. Reversed deformation field
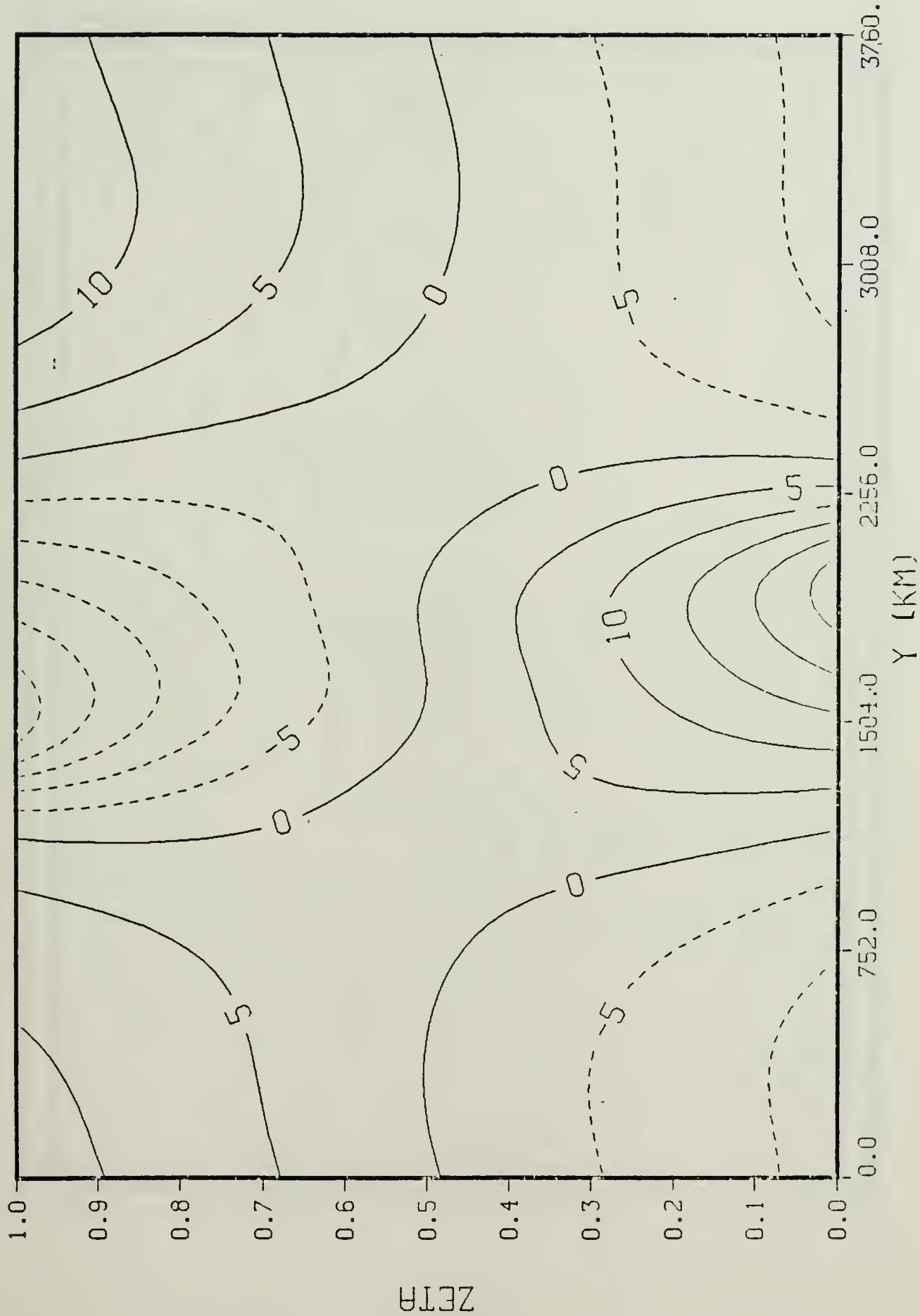
Fig. 49. u (m/sec). 24 hours. Reversed deformation field

81
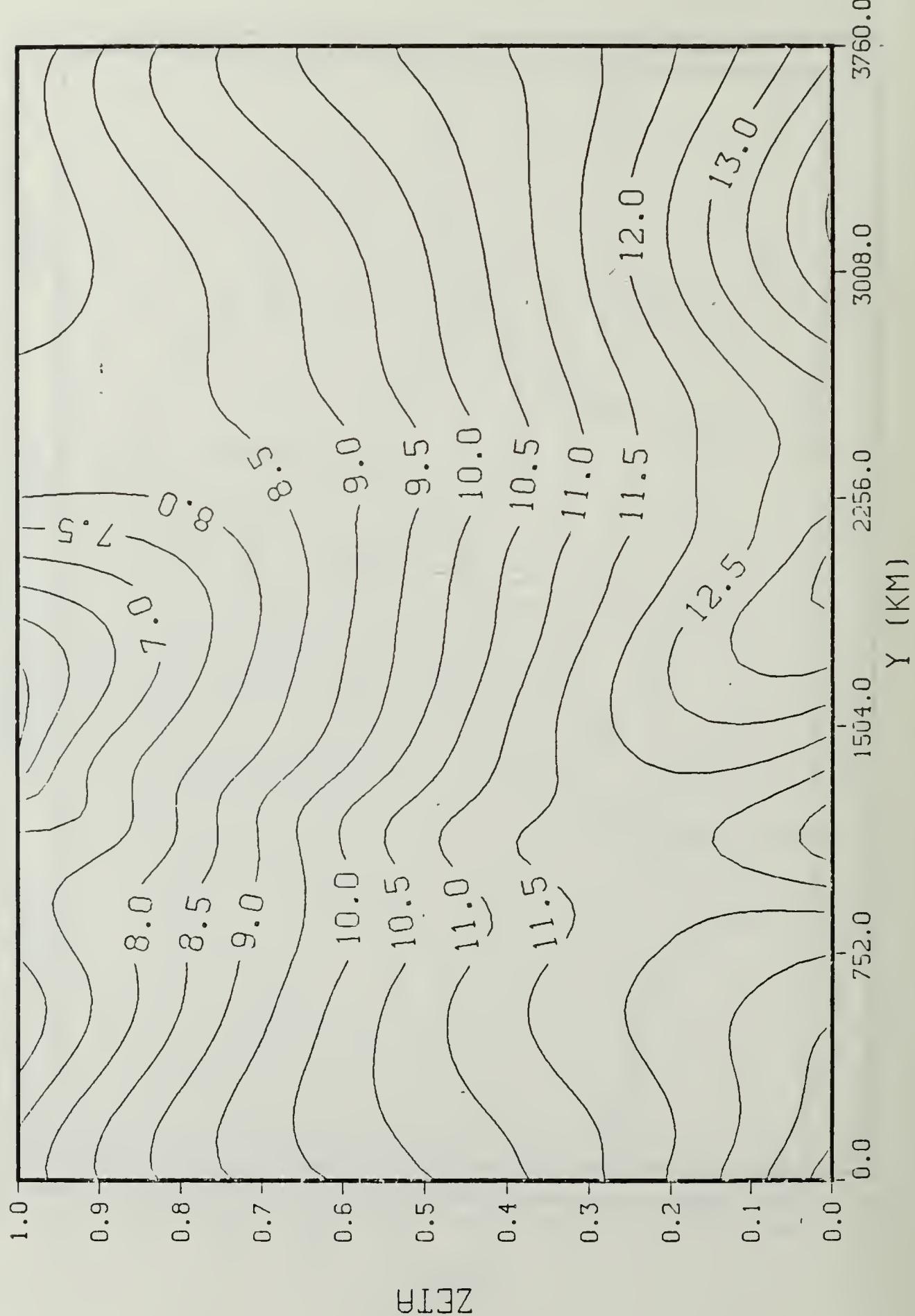
Fig. 50. v (m/sec). 24 hours. Reversed deformation field

82
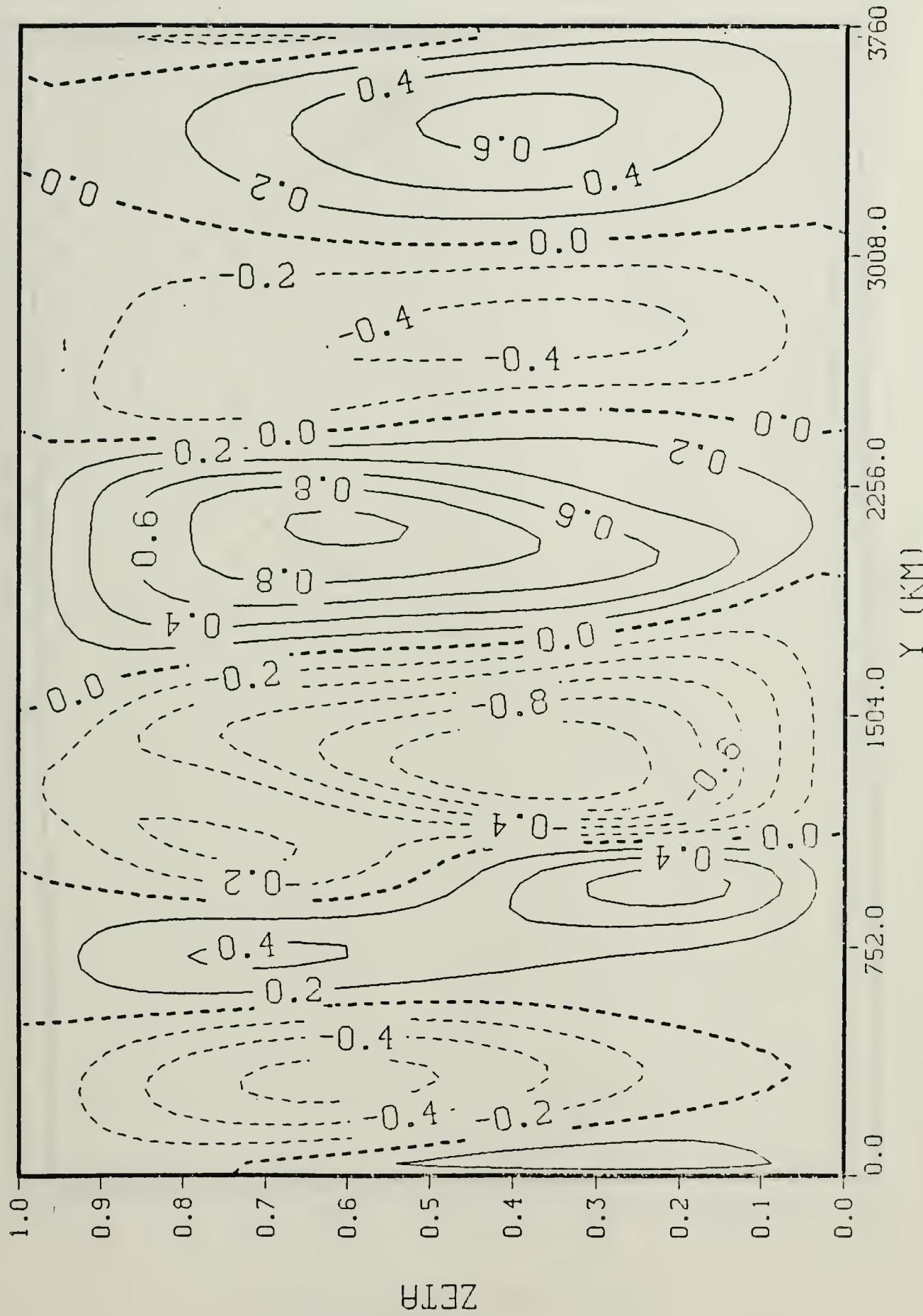
Fig. 51. $\dot{\zeta}$ ($\times 10^{-6}$ sec^{-1}). 24 hours. Reversed deformation field

83
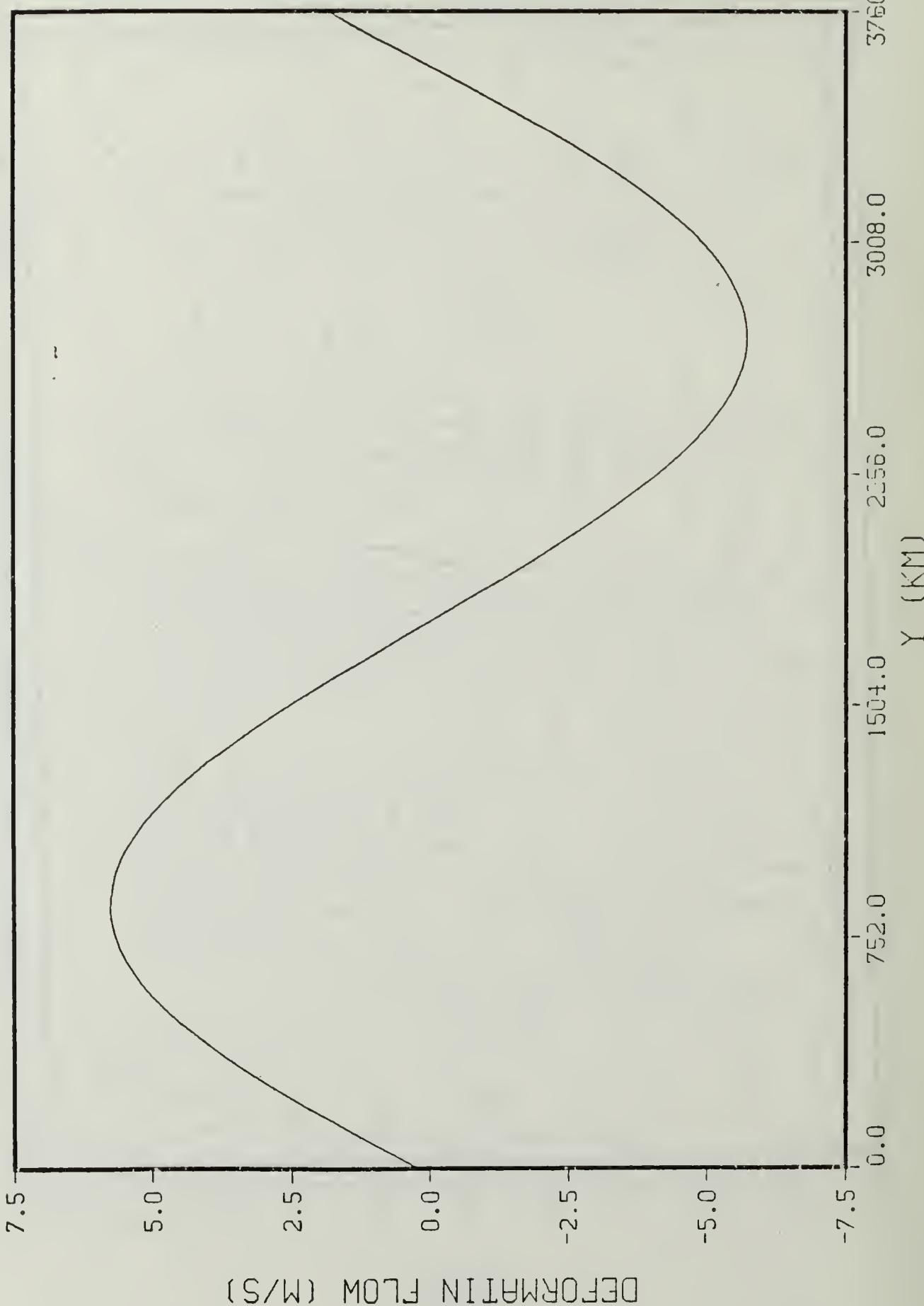
Fig. 52.   Deformation when maximum is on the downslope side of the mountain

84
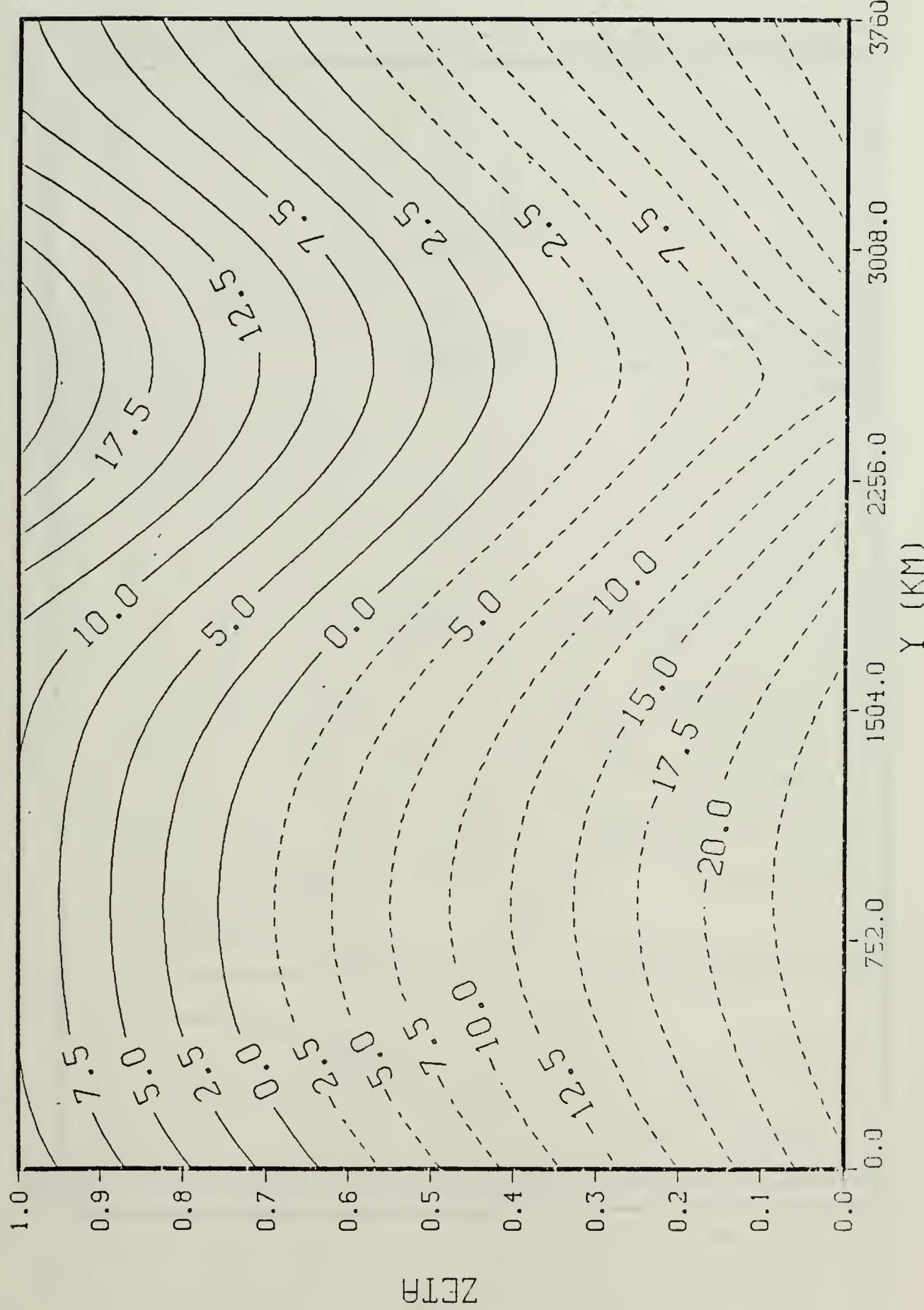
Fig. 53. $\theta(K)$. 24 hours. Deformation reverse of case 2
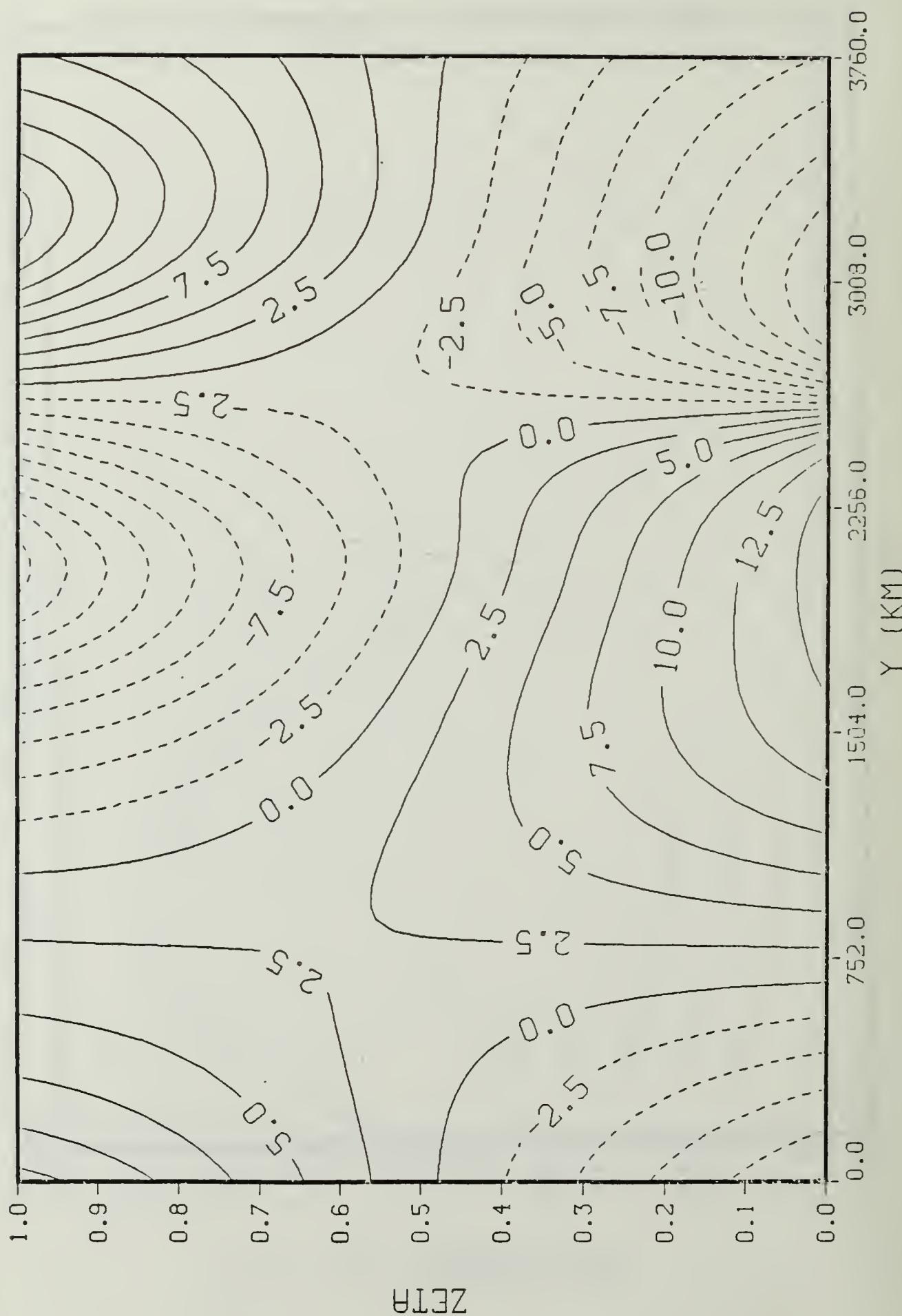
Fig. 54. u (m/sec). 24 hours. Deformation reverse of case 2
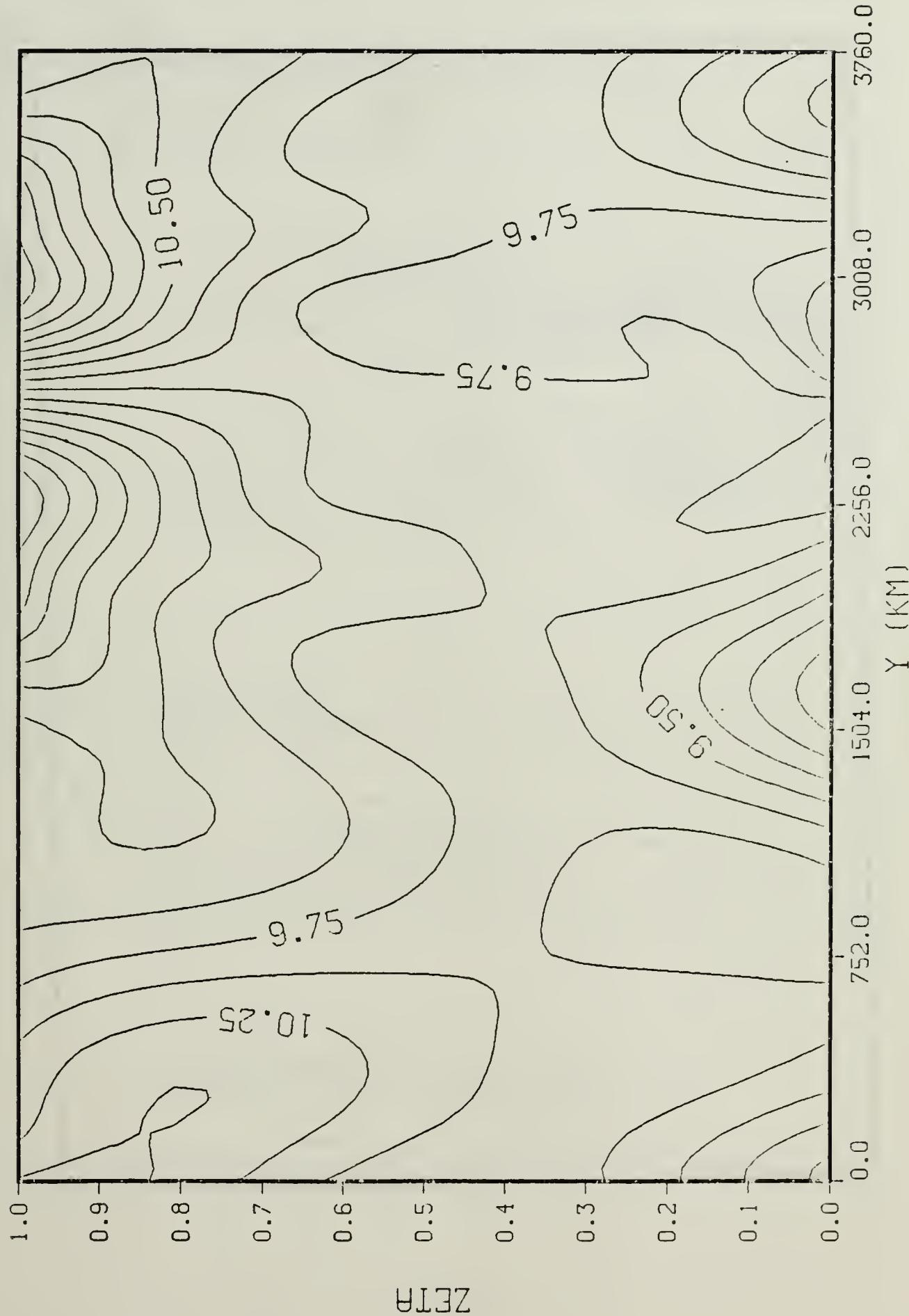
Fig. 55.   v (m/sec).   24 hours.   Deformation reverse of case 2

87
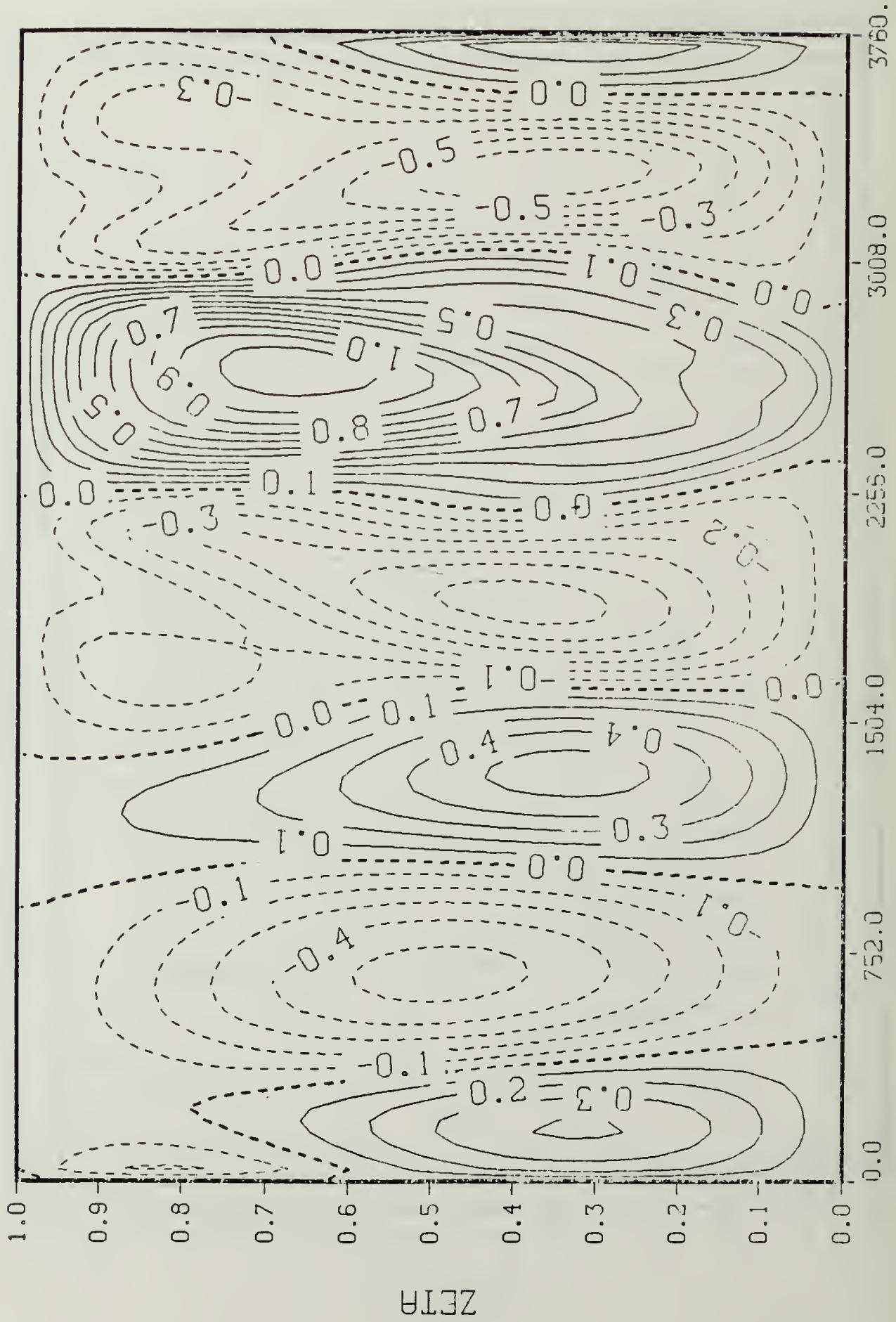
Fig. 56. $\dot{\zeta}$ ($\times 10^{-6}$ sec^{-1}). 24 hours. Deformation reverse of case 2

88

of the gradient from the initial conditions. This is very
similar to Case 2, but the maximum shear is at the lower
boundary.

V. <u>CONCLUSIONS AND RECOMMENDATIONS</u>

In this study, a numerical model of frontogenesis was constructed which included surface topography. Periodic boundary conditions were included and a periodic deformation field was introduced. The model was successfully tested with frontogenesis with no topography and for stratified flow over a mountain with no deformation field. Combined experiments with topography and a moving deformation field were carried out. The experiments showed negligible effects on frontogenesis by the topography.

The next step in this research is to introduce smaller scale topography which should lead to a noticeable effect as suggested by the frontogenesis theories of Bannon (1983, 1984). Other effects including vertical wind shear could be included later.

LIST OF REFERENCES

Bannon, P. J., 1983: Quasi-geostrophic frontogenesis over topography. J. Atmos. Sci., 40, 2266-2277.

_____, 1984: A semi-geostrophic model of frontogenesis over topography. Beitr. Phys. Atmosph., 57, 393-408.

DeBoer, J. K., 1970: Numerical Simulation of Atmospheric Flow over an Idealized Mountain. MS Thesis, Department of Meteorology, Naval Postgraduate School, 50 pp.

Haltiner, G. J. and R. T. Williams, 1980: Numerical Prediction and Dynamic Meteorology, John Wiley and Sons, 477 pp.

Hoskins, B. J. and F. P. Bretherton, 1972: Atmospheric frontogenesis models: Mathematical formulations and solution. J. Atmos. Sci., 29, 11-37.

Ogura, Y. and Phillips, N. A., 1962: Scale analyses of deep or shallow convection in the atmosphere. J. Atmos. Sci., 19, 173-179.

Phillips, N. A., 1957: A coordinate system having some special advantages for numerical forecasting. J. Meteor., 24, 184-185.

Stone, P. H., 1966: Frontogenesis by horizontal wind deformation fields. J. Atmos. Sci., 23, 455-565.

Walton, J. R., 1968: The Validity of Using Smoothed Topography for Numerical Weather Prediction. MS Thesis, Department of Meteorology, Univ. of Utah, 21 pp.

Williams, R. T., 1968: A note on quasi-geostrophic frontogenesis. J. Atmos. Sci., 25, 1157-1159.

_____, 1972: Quasi-geostrophic versus non-geostrophic frontogenesis. J. Atmos. Sci., 29, 3-10.

_____, and J. Plotkin, 1968: Quasi-geostrophic frontogenesis, J. Atmos. Sci., 25, 201-206.

INITIAL DISTRIBUTION LIST

No. Copies

1. Defense Technical Information Center   2
   Cameron Station
   Alexandria, Virginia   22306-6145

2. Library, Code 0142   2
   Naval Postgraduate School
   Monterey, California   93943-5100

3. Meteorology Reference Center, Code 63   1
   Department of Meteorology
   Naval Postgraduate School
   Monterey, California   93943-5100

4. Chairman, Code 63Rd   1
   Department of Meteorology
   Naval Postgraduate School
   Monterey, California   93943-5100

5. Chairman, Code 68Mr   1
   Department of Oceanography
   Naval Postgraduate School
   Monterey, California   93943-5100

6. Dr. Roger T. Williams   2
   Department of Meteorology
   Naval Postgraduate School
   Monterey, California   93943-5100

7. Director   1
   Naval Oceanography Division
   Naval Observatory
   34th and Massachusetts Avenue NW
   Washington, D.C.   20390

8. Commander   1
   Naval Oceanography Command
   NSTL Station
   Bay St. Louis, Missouri   39522

9. Commanding Officer   1
   Naval Oceanographic Office
   NSTL Station
   Bay St. Louis, Missouri   39522

10. Commanding Officer   1
     Fleet Numerical Oceanography Center
     Monterey, California 93943-5100

11. Commanding Officer   1
     Naval Ocean Research and
        Development Activity
     NSTL Station
     Bay St. Louis, Missouri 39522

12. Commanding Officer   1
     Naval Environmental Prediction
        Research Facility
     Monterey, California 93943-5100

13. Chairman, Oceanography Department   1
     U.S. Naval Academy
     Annapolis, Maryland 21402

14. Chief of Naval Research   1
     800 N. Quincy Street
     Arlington, Virginia 22217

15. Office of Naval Research, Code 420   1
     Naval Ocean Research and Development
        Activity
     NSTL Station
     Bay St. Louis, Missouri 39522

16. Commander (Air-370)   1
     Naval Air Systems Command
     Washington, D.C. 20360

17. LT Deborah Ann Zankofski   2
     USS Lexington (AVT 16)
     Naval Air Station
     Pensacola, Florida 32508

18. Dr. C.-P Chang, Code 63Cp   1
     Department of Meteorology
     Naval Postgraduate School
     Monterey, California 93943-5100

19. Dr. R. L. Elsberry, Code 63Es   1
     Department of Meteorology
     Naval Postgraduate School
     Monterey, California 93943-5100

20. Dr. R. L. Haney, Code 63Hy   1
     Department of Meteorology
     Naval Postgraduate School
     Monterey, California 93943-5100

21. Dr. B. J. Hoskins   1
     Department of Geophysics
     University of Reading
     Reading, United Kingdom

22. Dr. E. C. Nickerson   1
     NOAA, Atmospheric Physics &
        Chemistry Laboratory
     Boulder, Colorado 80302

23. Dr. C. H. Wash, Code 63   1
     Naval Postgraduate School
     Monterey, California 93943-5100

24. Dr. Andrew Staniforth   1
     Recherce en Prevsion Numerique
     West Isle Office Tower, 5 ieme etage
     2121 route Trans-Canada
     Dorval, Quebec H9P1J3, Canada

25. Dr. J. Hovermale   1
     Naval Environmental Prediction
        Research Facility
     Monterey, California 93943

26. Dr. R. T. Pierrehumert   1
     Geophysical Fluid Dynamics Lab/NOAA
     P.O. Box 308
     Princeton, New Jersey 08540

27. W. Blumen   1
     Campus Box 391
     University of Colorado
     Boulder, Colorado 80309

28. Dr. M. A. Rennick   1
     Department of Meteorology
     Naval Postgraduate School
     Monterey, California 93943-5100

29. Dr. M. Peng   1
     Department of Meteorology
     Naval Postgraduate School
     Monterey, California 93943-5100

30. Dr. C.-S. Liou, Code 63   1
     Naval Postgraduate School
     Monterey, California 93943-5100

31. Dr. David Adamec, Code 63   1
     Naval Postgraduate School
     Monterey, California 93943-5100

32. Dr. R. B. Smith   1
    Department of Geology and Geophysics
    Yale University
    P.O. Box 6666
    New Haven, Connecticut 06511

33. Dr. Peter Bannon   1
    Department of Geophysical Sciences
    University of Chicago
    Chicago, Illinois 60637

34. Dr. R. Gall, Code 63   1
    Department of Meteorology
    Naval Postgraduate School
    Monterey, California 93943-5100

35. Mr. Lang C. Chou, Code 63   1
    Department of Meteorolgy
    Naval Postgraduate School
    Monterey, California 93943-5100